

MAGYAR ÁLLAMI
EÖTVÖS LORÁND
GEOFIZIKAI INTÉZET

GEOFIZIKAI
KÖZLEMÉNYEK

ВЕНГЕРСКИЙ
ГЕОФИЗИЧЕСКИЙ
ИНСТИТУТ
ИМ Л. ЭТВЕША

ГЕОФИЗИЧЕСКИЙ
БЮЛЛЕТЕНЬ



BUDAPEST

EÖTVÖS LORÁND
GEOPHYSICAL INSTITUTE
OF HUNGARY

GEOPHYSICAL TRANSACTIONS

CONTENTS

- | | | |
|---|--|-----|
| Focusing aspects of zero-offset migration | <i>E. Maeland</i> | 145 |
| Electromagnetic parameters at the surface of a conductive halfspace in terms of the subsurface current distribution | <i>L. Szarka
G. Fischer</i> | 157 |
| Direct interpretation of magnetic anomalies due to spherical sources – a Hilbert transform method | <i>N. Sundararajan
B. Umashankar
N. L. Mohan
S. V. Seshagiri
Rao</i> | 173 |
| Magnetic susceptibility anisotropy measurements on Miocene ignimbrites from Bükkalja, Hungary | <i>R. Bordás</i> | 185 |
| The propagation of channel waves in a coal seam with horizontal and vertical inhomogeneities | <i>V. N. Danilov
M. Dobróka
V. Sz. Yamshikov</i> | 199 |
| Parameter sensitivity of underground dc measurements | <i>Á. Gyulai</i> | 209 |

VOL. 35. NO. 3. APRIL 1990 ISSN (0016-7177)

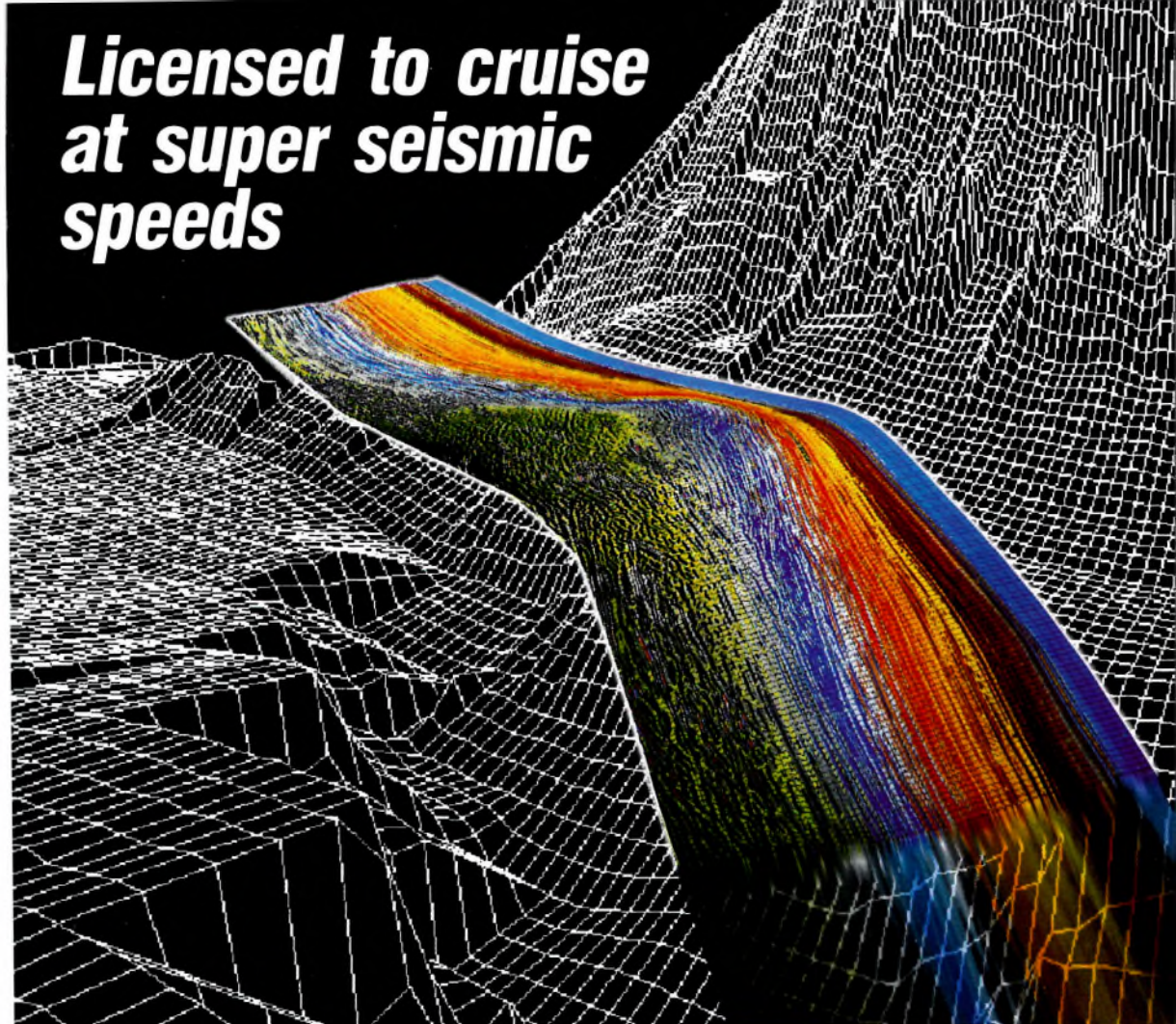
TARTALOMJEGYZÉK

A $t(0)$ időszelvény migrációjának fókuszáló hatásai	<i>E. Maeland</i>	156
Elektromágneses paraméterek vezető féltér felszínén, a vezetőn belüli árameloszlás függvényében	<i>Szarka L. G. Fischer</i>	172
Gömb alakú hatók okozta mágneses anomáliák értelmezése — egy Hilbert transzformációs módszer	<i>N. Sundararajan B. Umashankar N. L. Mohan S. V. Seshagiri Rao</i>	183
Mágneses szuszceptibilitás anizotrópia mérések bükkaljai miocén ignimbriteken	<i>Bordás R.</i>	197
A csatornahullámok terjedése horizontálisan és vertikálisan inhomogén köszéntelepben	<i>V. N. Danilov Dobróka M. V. Sz. Yamshikov</i>	208
Földalatti egyenáramú mérések paraméterérzékenysége	<i>Gyulai Á.</i>	225

СОДЕРЖАНИЕ

Фокусирующие эффекты миграции временного профиля $t(0)$	<i>Э. Мейланд</i>	156
Электромагнитные параметры на поверхности проводящей полусферы в зависимости от распределения тока по проводнику	<i>Л. Сарка Г. Фишер</i>	172
Интерпретация магнитных аномалий, вызванных сферическими возмущающими силами, методом трансформации Гильберта	<i>Х Сундарараджан Б. Умашанкар Н. Л. Мохан С. В. Сесхагири Рао</i>	183
Измерения анизотропии магнитной восприимчивости миоценовой игнимбритов в Бюккалья	<i>Р. Бордаш</i>	197
Распознавание канальных волн в неоднородном по горизонтали и вертикали угольном пласте	<i>В. Н. Данилов М. Доброка В. С. Ямщиков</i>	208
Чувствительность параметров пласта при зондированиях методом потоянного тока в подземных условиях	<i>А. Дьюлаи</i>	225

Licensed to cruise at super seismic speeds



If your seismic data processing gets stuck in first gear when entering complex geological zones, consider licensing seismic processing software from Western Geophysical.

Western software is being used to process data from geologic provinces throughout the world. In fact, more miles of seismic data are processed with Western software, at the highest efficiency level, than any other software.

Western seismic processing software operates on vector supercomputers as well as scalar mainframes and departmental minicomputers. Every user has access to Western's comprehensive program library designed for effective and efficient processing of 2-D and 3-D surveys on land, at sea, and across shallow-water transition zones.

The latest software enhancements, released on a continuous basis by Western's R&D and Computer Science departments, are available through the Software Subscription Service. If you run into a

problem, our Rapid Response teams are on alert to clear any processing flightpaths.

Whether you need a basic processing package or full facility management, call Western Geophysical and shift your seismic center into high gear.



WESTERN GEOPHYSICAL

Wesgeco House
PO Box 18
455 London Road
Isleworth, Middlesex
England TW7 5AB
(081) 560 3160
Fax (081) 847 3131

Houston	(713) 789 9600
Denver	(303) 770 8660
Calgary	(403) 291 8100
Singapore	65-258 3455
Caracas	58-2-262 0272
Bogota	57-1-267 6199
Rio de Janeiro	55-21-541-1599



EÖTVÖS L. GEOPHYSICAL INSTITUTE OF HUNGARY

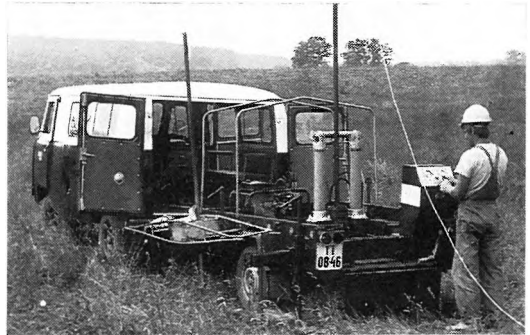
THE OLDEST INSTITUTION FOR APPLIED GEOPHYSICS
OFFERS THE LATEST ACHIEVEMENTS FOR
GROUND-WATER PROSPECTING
and
ENVIRONMENTAL PROTECTION

The most often occurring demands:

- local geophysical measurements for the water supply of small communities by a few wells
- regional geophysical mapping to determine hydrological conditions for irrigation, regional agricultural development,
- large-scale exploration for the water supply of towns, extended areas i.e. regional waterworks,
- determination of bank storage of river terraces, planning of bank filtered well systems,
- thermal water exploration for use as an energy source, agricultural use or community utilization,
- cold and warm karst water prospecting,
- water engineering problems, water construction works



The Maxi-Probe electromagnetic sounding and mapping system – produced under licence by Geoprobe Ltd. Canada – is an ideal tool for shallow depths, especially in areas where seismic results are poor or unobtainable



ELGI has a vast experience in solving problems of environmental protection such as control of surface waters, reservoir construction, industrial and communal waste disposal, protection of surface and ground water etc. ELGI's penetrometer provides in-situ information – up to a maximum depth of 30 m – on the strength, sand/shale ratio and density without costly drilling.



Field work with ELGI's 24-channel portable seismograph

ELGI offers contracts with co-operating partners to participate in the whole complex process of exploration–drilling–production.

For further information ask for our booklets on instruments and applications. Let us know your problem and we will select the appropriate method and the best instrument for your purpose.

*Our address: ELGI POB 35. Budapest,
H-1440. HUNGARY
Telex: 22-6194 elgi h*

FOCUSING ASPECTS OF ZERO-OFFSET MIGRATION

Einar MAELAND*

Migration with an erroneous velocity gives a 'smile' or curve along which the energy is smeared. Associated with the 'smile' is another curve, the caustic or edge of regression, enveloped by the normal rays. Computation of this curve reveals that it is cusped. Migration of zero-offset data with an erroneous velocity can give a 'focus' only if the imaging principle is modified according to the position of the cusp. Within the paraxial approximation of the wave equation, the focus is cusped whether or not the correct velocity is used.

Keywords: seismic diffraction, data processing, wave equation, migration, velocity, geometrical optics, paraxial approximation, caustic

1. Introduction

Migration of zero-offset data will in general suffer from velocity errors, and the migrated output will be contaminated by focusing errors. If zero-offset data from a single point diffractor is considered, the result of migration with an erroneous velocity is a 'smile'. In zero-offset migration, the data is extrapolated by some suitable operator to a certain depth, at which an imaging principle is applied. Much effort has been devoted to the construction of extrapolation operators, but only a few have studied the effect of varying the imaging principle. The reason is that migration of zero-offset data is based upon the exploding reflector model as described by LOEWENTHAL, LU, ROBERSON and SHERWOOD [1976].

If the data is migrated with an erroneous velocity, the 'image' is blurred and there is a loss of resolution. Still a 'focus' may exist if only the imaging principle is modified. This has to some extent been discussed by DE VRIES and BERKHOUT [1984], a discussion which was based on the paraxial approximation of the wave equation. In order to gain insight into the focusing aspects of migration, an alternative investigation within the framework of geometrical optics or ray theory will be carried out.

In ray theory what matters is not the individual rays, but rather a family of rays. Associated with a family of rays is the possibility of focal regions or caustics, which occur on contact with neighbouring rays. So at a caustic two or more rays become parallel. Outside the caustic there is only one ray through

* Seismological Observatory, University of Bergen, Allegt. 41, N-5007 Bergen, Norway
Manuscript received (revised version): 25 May, 1989

each point. On the caustic curve, rays touch in pairs, while if three rays touch, the caustic is cusped. Consequently, as far as the amplitude of the wave field is concerned, it must be significant on a caustic, and exceptional at a cusp. Hence, the possibility of a cusp becomes important, and if one exists, it will be used to modify the imaging principle so as to produce a focus when zero-offset data is migrated with an erroneous velocity.

Strictly speaking, ray theory cannot account for diffraction and focusing phenomena. Nevertheless, certain approximative methods can be applied successfully to evaluate the seismic wave field close to a caustic. CARTER and FRAZER [1982] reported a net phase-shift within the 'smile'. The phase-shift is in accordance with the approximations of geometrical optics. Within the paraxial approximation of the wave equation, a true focus cannot be realized, even if the correct velocity is applied. The caustic represents the concentration of energy, and can be considered as the aberrated image of a point source. The caustic is cusped, and the cusp replaces the true focus.

2. Over- and undermigration

Let cartesian coordinates (x, z) be defined with x in the horizontal and z in the vertical direction, respectively. Without any loss of generality, only the two-dimensional problem will be studied. Assume that a point diffractor is located at the position $(0, z_*)$. The travel time t_0 recorded at a point x_0 on the x -axis is given by

$$(c_0 t_0)^2 = x_0^2 + z_*^2, \quad (1)$$

where c_0 is the (true) velocity in the medium. The kinematic part of migration is the construction of an envelope of (spherical) waves with radius $r_0 = c_0 t_0$ and the origin at the position x_0 on the x -axis. In order to study the effects of over- and undermigration, an erroneous velocity $c \neq c_0$ will be used, so that the radius is equal to $r = ct_0$. Let (x, z) be a point on the wave surface

$$(x - x_0)^2 + z^2 = \gamma^2 (c_0 t_0)^2, \quad (2)$$

where $\gamma = c/c_0$ is the velocity ratio. The two equations can be put in the form $F(x, z, x_0) = 0$, where x_0 is a free parameter. To obtain the envelope [SNEDDON 1957], the parameter x_0 must be eliminated between the two equations $F(x, z, x_0) = 0$ and $\partial F(x, z, x_0)/\partial x_0 = 0$. The result is

$$x^2/(\gamma^2 - 1) + z^2/\gamma^2 = z_*^2, \quad (3)$$

which describes an elliptic or hyperbolic 'smile' according to $\gamma > 1$ or $\gamma < 1$, respectively. This is the so-called 'zero-distance phase front of refraction' [CORNBLEET 1984], since the 'optical distance' between a point (x, z) on this surface in a medium with velocity c , and the point $(0, z_*)$ in a medium with velocity c_0 , is zero. In the terminology of optics, the zero-distance phase front of refraction is the 'virtual image' of the point source.

The effect of an erroneous velocity is a blurring of the focus. As far as the focusing aspects of zero-offset migration is concerned, the imaging principle is applied too late when $\gamma > 1$, or too early when $\gamma < 1$, so a focus (if any) can only be achieved by a modification of the imaging principle. With a radius $r = ct_0$, only the phase front of zero-distance ($ct = 0$) can be constructed, but with a radius $r = c|t_0 - t|$, the envelope is a parallel wavefront according to Huygens' construction. When the velocity is correct, but the imaging principle is applied at a time $t > 0$, the result is in some sense similar (but not identical) to a case with a velocity $c < c_0$ and imaging at $t = 0$. On the other hand, if the imaging is applied at a time $t < 0$, the result is in some sense similar to a case with a velocity $c > c_0$ and imaging at $t = 0$.

If a radius $r = c|t_0 - t|$ is utilized, the equations can be represented by the one-parameter system of surfaces $F(x, z, t, x_0) = 0$. From a mathematical point of view, it may be more adequate to consider a characteristic curve on this surface [SNEDDON 1957], i.e., a solution of $F = 0$ and $\partial F / \partial x_0 = 0$ (for any fixed x_0). As x_0 can take any value on the x -axis, a locus of the intersection of different characteristic curves can be constructed. The locus is a solution of $F = \partial F / \partial x_0 = \partial^2 F / \partial x_0^2 = 0$, giving the caustic or edge of regression of the envelope of the surface $F = 0$. The result is a curve given by a set of parametric equations $x(x_0)$, $z(x_0)$ and $t(x_0)$, say. This is the simplest way to compute the caustic, but it is much more instructive to construct a family of rays of the zero-distance phase front, and then compute the envelope of the ray family. The results are of course identical, as the methods only differ in their mathematical formulation.

3. The caustic

The definition of a caustic is a curve enveloped by the normal rays which have their origin at the zero-distance phase front, which by itself is an envelope of the one-parameter system of curves $F(x, z, x_0) = 0$. Let the angle between the horizontal x -axis and the normal from a point (x, z) on the (elliptic or hyperbolic) zero-distance phase front be denoted by β . Assume that $x = f(u)$ and $z = g(u)$ is a parametric description of the wavefront at time $t = 0$. A parallel wavefront at a distance $d = ct$ is defined by a set of parametric equations $x = X(t, u)$ and $z = Z(t, u)$

$$\begin{aligned} X(t, u) &= f(u) + ct \cdot \cos(\beta), \\ Z(t, u) &= g(u) + ct \cdot \sin(\beta). \end{aligned} \tag{4}$$

The tangent of the zero-distance phase front has a direction given by dg/df . The direction of the normal (ray) is $\tan(\beta) = -df/dg$. It follows that $\cos(\beta) = g'(u)/D(u)$ and $\sin(\beta) = -f'(u)/D(u)$, where $f'(u) = df/du$, $g'(u) = dg/du$ and $D^2 = (df/du)^2 + (dg/du)^2$. Moreover, by eliminating the time (t), a system of curves $x = \xi$ and $z = \zeta$ are obtained, given here by

$$[\zeta - g(u)] = \tan(\beta) \cdot [\xi - f(u)]. \tag{5}$$

For each value of the parameter u , this equation defines a straight line in the x - z plane, that is, a normal ray. The equation can be put in the form $G(\xi, \zeta, u) = 0$, from which the envelope of the family of rays can be calculated. The results is

$$\begin{aligned}\xi(u) &= f(u) - \frac{g'(u) \cdot R(u)}{D(u)}, \\ \zeta(u) &= g(u) + \frac{f'(u) \cdot R(u)}{D(u)},\end{aligned}\quad (6)$$

where $R(u)$ is the radius of curvature of the zero-distance phase front. Hence, with $ct = -R(u)$, this construction reveals that the caustic is the locus of the centers of curvature of the zero-distance phase front. This locus is also known as the 'evolute' [CORNBLEET 1984].

The set of parametric equations $x = f(u)$ and $z = g(u)$ are not unique, so it is possible to choose a suitable set at will. Let $\Gamma > 0$ be defined by $\Gamma^2 = |\gamma^2 - 1|$. When $\gamma > 1$ (overmigration), a suitable set of parametric equations are

$$\frac{x}{z_*} = \Gamma \cdot \sin(u) \quad \text{and} \quad \frac{z}{z_*} = \gamma \cdot \cos(u), \quad (7)$$

where $|u| \leq \frac{\pi}{2}$, while if $\gamma < 1$ (undermigration)

$$\frac{x}{z_*} = \Gamma \cdot \sinh(u) \quad \text{and} \quad \frac{z}{z_*} = \gamma \cdot \cosh(u), \quad (8)$$

where $-\infty < u < +\infty$. The computations will be simplified by defining $x/z_* = \Gamma \cdot S(u)$ and $z/z_* = \gamma \cdot C(u)$, where $S(u)$ and $C(u)$ are the circular or hyperbolic sine and cosine functions, according to $\gamma > 1$ or $\gamma < 1$, respectively.

4. The cusp

In the terminology of geometrical optics, a caustic is a curve enveloped by reflection or refraction of light from a curved surface [CORNBLEET 1984]. The caustic may be cusped, i.e., there may be a point at which two branches of the caustic have a common tangent. The geometry of the present problem allows an explicit parametric representation of the parallel wavefronts and the caustic, hence, the possibility and the position of a cusp can easily be attained. With the (elliptic or hyperbolic) zero-distance phase front defined by $f(u) = z_* \Gamma \cdot S(u)$ and $g(u) = z_* \gamma \cdot C(u)$, a parallel wavefront may be written

$$\begin{aligned} X(t, u) &= z_* S(u) \cdot \left[\Gamma \pm \frac{\gamma^2 c_0 t}{z_* D(u)} \right], \\ Z(t, u) &= z_* C(u) \cdot \left[\gamma - \frac{\gamma \Gamma c_0 t}{z_* D(u)} \right], \end{aligned} \quad (9)$$

where $D^2 = \Gamma^2 + S^2$. The upper sign is used when $\gamma < 1$ and the lower sign when $\gamma > 1$. The parameter t labels the wavefronts, while the parameter u labels the rays. The caustic (evolute) is given by

$$\Gamma \cdot \xi(u) = -z_* [S(u)]^3, \quad \gamma \cdot \zeta(u) = z_* [C(u)]^3. \quad (10)$$

It is worthwhile giving this particular curve a name. When $\gamma > 1$, the parametric equations represent an 'astroid' [CORNBLEET 1984]. Hence, the phrase elliptic or hyperbolic astroid, according to $\gamma > 1$ or $\gamma < 1$, respectively, will be used. Moreover, associated with the caustic is the time $ct = -R(u)$, or $t = \tau(u)$, which can be written

$$\frac{c_0 \tau}{z_*} = \frac{\gamma^2 - 1}{\gamma^2} \cdot \left[1 + \left(\frac{S}{\Gamma} \right)^2 \right]^{\frac{3}{2}}. \quad (11)$$

The astroid is cusped at the points where $|\partial \zeta / \partial \xi| \rightarrow \infty$ or $|d\zeta/d\xi| \rightarrow 0$, i.e., at $u = 0$, giving $\xi_C = 0$ and $\zeta_C = z_*/\gamma$. If $\gamma > 1$, it is also cusped at the position $\pm(x_A, 0)$, where $x_A = z_*/\Gamma$. If $|x_0| \geq x_A$, the point x_0 lies within the 'shadow region' of geometrical optics.

Associated with the cusp (ξ_C, ζ_C) is the time $\tau_C = \tau(0)$, given by $c_0 \tau_C / z_* = (\gamma^2 - 1) / \gamma^2$. With respect to the focusing aspects of zero-offset migration with an erroneous velocity, imaging at time $t = 0$ cannot yield a focus. If the imaging principle is modified according to $t = \tau_C$, the focus is forced to coincide with the position of the cusp. However, the vertical position of the cusp is $\zeta_C \neq z_*$, so the penalty is a position error. On the other hand, the gain is that the amplitude, and hence the phase information of the migrated output, may be easy to attain. The phase information may be used to modify the imaging principle or the velocity so as to improve the quality of the migrated output at time $t = 0$.

Figures 1a, b display a family of normal rays from the elliptic or hyperbolic zero-distance phase front, according to $\gamma > 1$ or $\gamma < 1$, respectively. The approximate position of the caustic can readily be identified. Figures 2a, b display the exact positions of the caustics. Also shown are examples of parallel wavefronts close to the characteristic cusp at which the two branches of the caustic meet. Beyond the cusp and between the two branches, the wavefront has a folded form, so the wavefront also has a cusp at the point where it touches the caustic. Figures 3a, b show the results of migration by the phase-shift method [GAZDAG 1978], but with the modified imaging principle according to $t = \tau_C$. The input signal is a zero-phase Ricker wavelet, i.e., the second derivative of the function $\exp[-2(t/t_0)^2]$, with $t_0 = 0.05$ sec. The extrapolation step is

$\Delta z = 0.01$ km, the velocity is $c_0 = 1$ km/sec, with the point diffractor located at depth $z_* = 1.0$ km ($x_* = 1.5$ km). Although the position of the cusp is well defined, the migrated output from the phase-shift method still shows an indica-

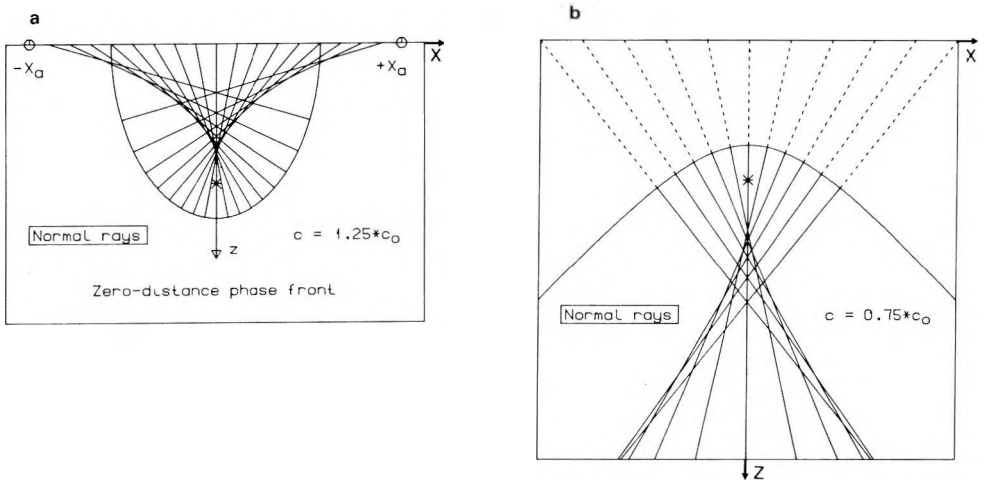


Fig. 1. The zero-distance phase front and the ray paths (normal incidence). The asterisk marks the point diffractor

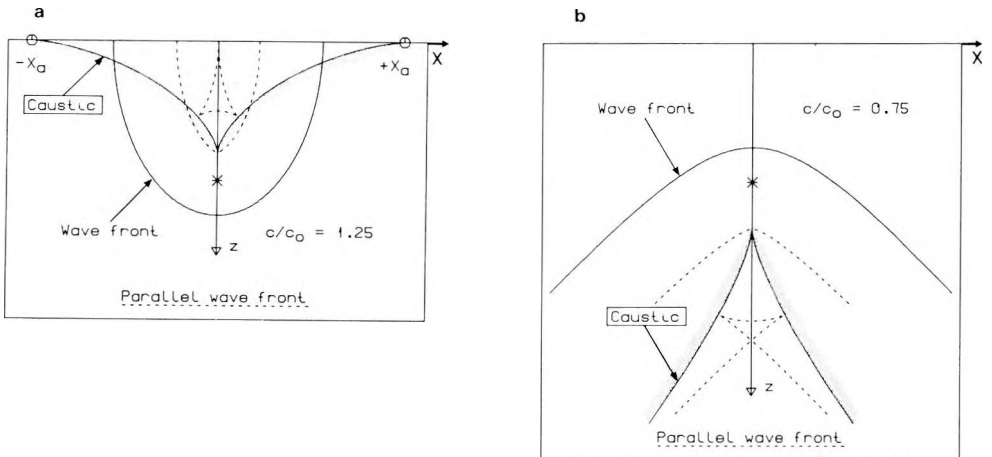
a) Overmigration, $c/c_0 = 1.25$ b) Undermigration, $c/c_0 = 0.75$

1. ábra. A diffraktálopont (csillag) virtuális képe (elliptikus fázis front) és a normál beesésű sugarak

a) Túlmigrálás esete, $c/c_0 = 1,25$ b) Alulmigrálás esete, $c/c_0 = 0,75$

Рис. 1. Кажущаяся картина (эллиптический фазовый фронт) дифракционной точки (звездочка) и лучи нормального падения

a) случай сверхмиграции $c/c_0 = 1,25$ б) случай недостаточной миграции $c/c_0 = 0,75$.



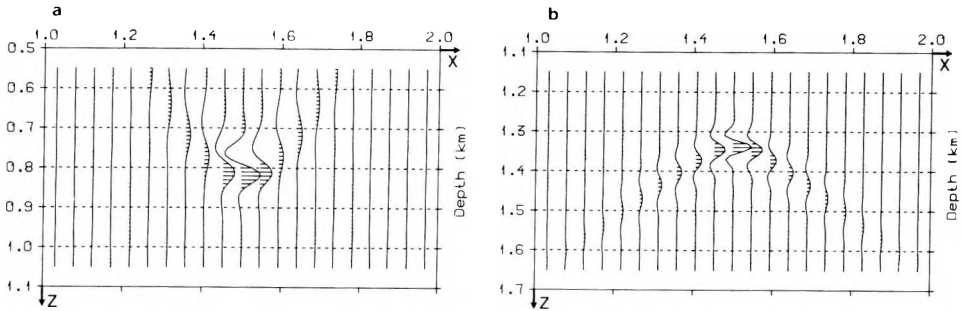


Fig. 3. Migrated data with the phase shift method. Parameter values are $z_* = 1$ km, $c_0 = 1$ km/sec
 a) Overmigration, $c/c_0 = 1.25$ and imaging applied at $t = \tau_c > 0$
 b) Undermigration, $c/c_0 = 0.75$ and imaging applied at $t = \tau_c < 0$

3. ábra. Fázistolás eljárással migrált adatok. Modellparaméterek: $z_* = 1$ km, $c_0 = 1$ km/sec
 a) Túlmigrálás esete, $c/c_0 = 1,25$ és a leképezés $t = \tau_c > 0$ időre történt
 b) Alulmigrálás esete, $c/c_0 = 0,75$ és a leképezés $t = \tau_c < 0$ időre történt

Рис. 3. Данные, мигрированные методом фазового сдвига. Модельные параметры:
 $z_* = 1$ км, $c_0 = 1$ км/сек

- a) случай сверхмиграции, $c/c_0 = 1,25$ и отражение происходит при $t = \tau_c > 0$
 б) случай недостаточной миграции, $c/c_0 = 0,75$ и отражение происходит при $t = \tau_c < 0$.

Fig. 2. The caustic (elliptic astroid) and the parallel wavefronts (dashed)
 a) Overmigration b) Undermigration

2. ábra. A kausztika (elliptikus asztroid) és a párhuzamos hullámfrontok (szaggatott vonallal jelölve)
 a) Túlmigrálás esetén b) Alulmigrálás esetén

Рис. 2. Каустика (эллиптический астронд) и параллельные фронты волны (обозначены прерывистой линией)
 а) в случае сверхмиграции б) в случае недостаточной миграции.

tion of the 'smile'. This is reminiscent of the wavefront at time $t = \tau_c$. The position of the apex of the wavefront coincides with the position of the cusp. The migrated output is a 'snapshot' of the wave field, and the amplitude maxima of the migrated output are close to the actual position of the caustic.

A more or less well defined 'focus' is attained, but the phase of the migrated output are not identical according to $\gamma > 1$ or $\gamma < 1$, respectively. Ray theory gives excellent information about the travel time of individual rays, but suffers from giving little reliable information about the amplitudes (caused by the vanishing of ray-tube area in the caustic region). A net phase-shift of $\pi/2$ in overmigration as compared with undermigration was reported by CARTER and FRAZER [1982]. A phase-shift of $\pi/2$ every time a ray passes through a caustic is consistent with the approximation of geometrical optics, i.e., the amplitude varies inversely with the square-root of ray-tube area. Inspection on figures 1a, b reveals that the normal rays touch the caustic en route from the zero-distance phase front to a point on the x -axis only when $\gamma > 1$. This is a logical explanation of the fact that the phase experiences a net phase-shift of $\pi/2$ in overmigration as compared to undermigration.

5. The paraxial approximation

Much effort has been devoted to the construction of an extrapolation operator within the paraxial approximation of the wave equation. This approximation has a long history, related to the FRESNEL approximation in optical literature, or the 15° -approximation in seismic literature [CLAERBOUT 1985]. One of the most important implications of this approximation is anisotropy, but the kinematic part of migration is still a construction of the envelope of the secondary wavelets according to the theorem of Huygens. However, the surface of the secondary wavelets are no longer spherical, but rather elliptical

$$(x - x_0)^2 + 2z^2 = 2\gamma z c_0 t_0, \quad (12)$$

Where $\gamma = c/c_0$ is the velocity ratio. The particular form of the wavelets follows from the dispersion relation and evaluation of the group velocity and the related wavesurface [CLAERBOUT 1985]. In order to compute the envelope, the travel time curve and the latter equation are put in the form $F(x, z, x_0) = 0$, and the envelope represented by a set of parametric equations $x = f(x_0)$ and $z = g(x_0)$. Although it is only a minor point, x_0 is not the most suitable parameter to be used. Since the travel time curve is a hyperbola, the actual computations will be simplified by utilizing

$$\frac{x_0}{z_*} = \sinh(v) = S, \quad \frac{c_0 t_0}{z_*} = \cosh(v) = C, \quad (13)$$

where $-\infty < v < +\infty$. After some simple algebra, the result is a set of parametric equations

$$\frac{f(v)}{z_*} = \frac{S \cdot [2(1 - \gamma^2) + (\gamma T)^2]}{2 + (\gamma T)^2}, \quad (14)$$

$$\frac{g(v)}{z_*} = \frac{2\gamma C}{2 + (\gamma T)^2}, \quad T = \tanh(v).$$

It is not possible to solve this problem in a closed form (in terms of a simple functional relation between x and z), but this is not essential, as the equations are well suited for computational methods.

Let a family of rays be constructed according to eq. (5). Due to the anisotropy, the rays are not orthogonal to the plane waves, so the caustic is not the locus of the centers of curvature of the zero-distance phase front. It follows that the angle β cannot be deduced from the derivative (dg/df) of the set of parametric equations, but only from

$$\cot(\beta) = \frac{x_0 - f(v)}{g(v)}, \quad (15)$$

which, upon substituting from eq. (14), can be written

$$\cot(\beta) = \gamma \cdot \tanh(v). \quad (16)$$

The (maximum) ray-angle is related to the aperture of the extrapolation operator. It follows that the aperture within the paraxial approximation of the wave equation is always less than $\pi/2$, irrespective of the actual value of the velocity ratio.

The construction of the caustic enveloped by the rays is straightforward. The parametric equations are

$$\xi(v) = -z_*[S(v)]^3, \quad \gamma \cdot \zeta(v) = z_*[C(v)]^3, \quad (17)$$

while the corresponding time $t = \tau(v)$ is

$$\frac{c_0 \tau}{z_*} = C \cdot \frac{2(\gamma^2 - 1) + (2 + \gamma^2)S^2}{2\gamma^2}. \quad (18)$$

The caustic is a hyperbolic astroid, irrespective of the actual value of the velocity ratio. A cusp occurs for $v = 0$, so the conclusion is that the position of the focus (ξ_C, ζ_C), and the modified imaging principle ($t = \tau_C$), are not given any new values within the paraxial approximation. Thus, with respect to the focusing aspects of zero-offset migration, migration within the paraxial approximation is in some sense similar (but not identical) to undermigration with the exact wave equation. It follows that the qualitative results of migration with $\gamma = 1$ are inherent for any $\gamma \neq 1$. Consequently, only the case $\gamma = 1$ will be discussed.

Let a parallel wavefront $x = X(t, v)$ and $z = Z(t, v)$ be constructed at a distance $d = c_g t$, where c_g is the group-velocity. The group-velocity $c_g = c_g(v)$ is defined by

$$[t_0 c_g(v)]^2 = [x_0 - f(v)]^2 + [g(v)]^2, \quad (19)$$

which yields the relation

$$c_g(v) = 2c \sqrt{\frac{1+T^2}{2+T^2}}. \quad (20)$$

It follows that a parallel wavefront is given by

$$X(t, v) = \frac{Tz_* \left(ST + \frac{2ct}{z_*} \right)}{2+T^2}, \quad (21)$$

$$Z(t, v) = \frac{2z_* \left(C - \frac{ct}{z_*} \right)}{2+T^2}.$$

Figure 4a displays the caustic with the characteristic cusp. Also shown are different wavefronts (dashed) when the imaging principle is applied at times $t > 0$ and $t < 0$, respectively. In the latter case the wavefronts are folded and touch the caustic at a cusp. A 'focus' at the correct position, $\zeta = z_*$, can only be achieved if $\gamma = 1$, and if the imaging principle is applied at time $t = \tau_c = 0$. Figure 4b displays the result of migration with the phase-shift method [GAZDAG 1978]. The signal and other input parameters are the same as used in Figure 3b. The phase of the migrated output has not been changed, which can be explained by the hyperbolic shape of the astroid.

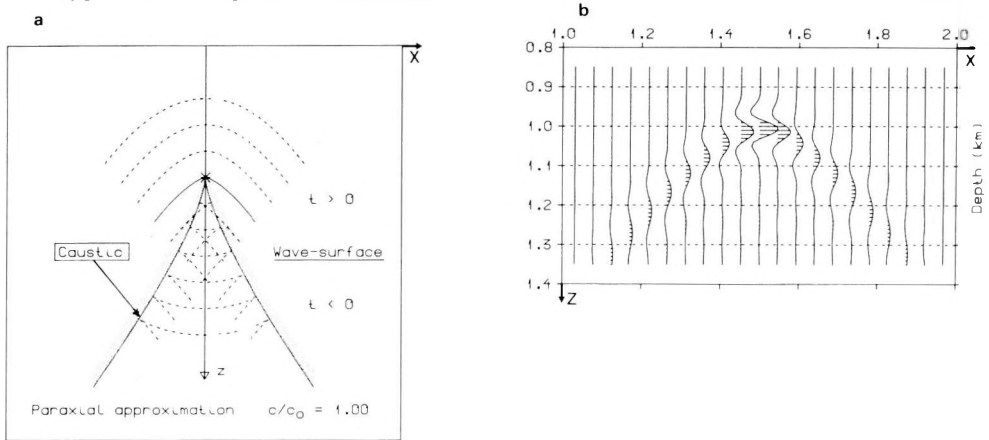


Fig. 4. Paraxial approximation with correct velocity. Parameter values: $z_* = 1$ km, $c_0 = 1$ km/sec
 a) Parallel wavefronts (dashed) and the caustic (hyperbolic astroid) b) Migrated data

4. ábra. Paraxiális közelítés pontos sebességgel. Paraméterértékek: $z_* = 1$ km, $c_0 = 1$ km/sec
 a) Párhuzamos hullámfrontok (szaggatott vonal) és a kauszтика (hiperbolikus aszteroid)
 b) Migrált adatok

Рис. 4. Параксальное приближение при точной скорости. Значения параметров: $z_* = 1$ км, $c_0 = 1$ км/сек.

- a) Параллельные волновые фронты (прерывистая линия) и каустика (гиперболический астероид) b) Мигрированные данные.

6. Conclusion

The focusing aspects of zero-offset migration within the framework of geometrical optics or ray theory has been examined. Although this theory cannot give the correct amplitude and phase of the migrated data, some results from this theory are still of interest. The kinematic part of zero-offset migration is based on Huygens construction of a wavefront as the envelope of secondary wavelets. With no velocity errors ($c = c_0$), this construction will give the correct position of the point diffractor (focus). However, if velocity errors are present ($c \neq c_0$), the envelope will be a hyperbolic or elliptic 'smile'. According to the definition of 'optical distances', the optical distance between this curve (in a medium with velocity c) and the point source (in a medium with velocity c_0), is zero. Consequently, in the terminology of optics, this curve has been denoted the 'zero-distance phase front of refraction', or the 'virtual image' of the true point source. The conclusion is that migration with an erroneous velocity (and imaging at time $t=0$), will always give the zero-distance phase front of refraction.

The result of migration with an erroneous velocity is a blurring or smearing of the focus. Construction of a family of rays and the caustic enveloped by the rays, reveals that a 'focus' may still be defined if the caustic by itself is cusped. However, this new 'focus' cannot emerge as a result of migration unless the imaging principle is modified. The construction of the caustic gives insight into the focusing aspects of zero-offset migration. An analysis of the focusing aspects within the paraxial approximation of the wave equation reveals that neither the position of the focus, nor the modified imaging principle are given any new values as a consequence of this approximation.

Within the paraxial approximation of the wave equation, ray theory seems to give reliable results, irrespective of the actual value of the velocity ratio. If the velocity ratio $c/c_0 = \gamma \rightarrow 1$, a focus can be defined at the cusp of the caustic. On the other hand, if the exact wave equation is considered, ray theory suffers from giving reliable results in the limit $\gamma \rightarrow 1$. This is caused by the elliptic or hyperbolic shape of the caustic when $\gamma > 1$ or $\gamma < 1$, respectively. Consequently, while the position of the cusp is defined, the orientation (up or down) of the cusp is not defined in this limit. The conclusion is that in this particular case, ray theory seems to be inadequate.

REFERENCES

- CARTER J.A. and FRAZER L.N. 1982: Rapid F-K migration of zero offset marine reflection data. *Journal of Geophysical Research* **87** (B11), pp. 9365–9373
- CLAERBOUT J.F. 1985: *Imaging the Earth's Interior*. Blackwell Scientific Publications, 398 p.
- CORNBLEET S. 1984: *Microwave and Optical Ray Geometry*. John Wiley & Sons Ltd.
- DE VRIES D. and BERKHOUT A. J. 1984: Influence of velocity errors on the focusing aspects of migration. *Geophysical Prospecting* **32**, 4, pp. 629–648
- GAZDAG J. 1978: Wave equation migration with the phase-shift method. *Geophysics* **43**, 7, pp. 1342–1351
- LOEWENTHAL D., LU L., ROBERSON R. and SHERWOOD J. 1976: The wave equation applied to migration. *Geophysical Prospecting* **24**, 2, pp. 380–399
- SNEDDON I.N. 1957: *Elements of partial differential equations*. McGraw-Hill Book Company, Inc.

A $t(0)$ IDŐSZELVÉNY MIGRÁCIÓJÁNAK FÓKUSZÁLÓ HATÁSAI

Einar MAELAND

A hibás sebességű migráció íves (mosoly) alakú görbét eredményez, amely mentén az energia szétszóródik. A mosoly alakú görbéhez egy másik görbe társul, a kausztika, amely a sugárelmélet alkalmazhatóságának határát jelöli ki. Ez utóbbit kiszámítva látható, hogy csúcsos. A $t_0(x)$ szelvény migrációja rossz sebességgel csak abban az esetben fókuszálhat egy pontra, ha a kausztika csúcs helyzetének megfelelően módosítjuk a leképzés elvét. Ha a hullámegyenlet paraxiális közelítését alkalmazzuk, a fókusz egybeesik a kausztika csúcsával, függetlenül attól, hogy helyes sebességértéket vettünk-e fel vagy sem.

ФОКУСИРУЮЩИЕ ЭФФЕКТЫ МИГРАЦИИ ВРЕМЕННОГО ПРОФИЛЯ $t(0)$.

Эйнер МЕЙЛАНД

Миграцию, имеющую ошибочную скорость, характеризует дугообразная кривая, вдоль которой распределяется энергия. Взаимосвязанная с ней кривая, каустика, определяет границу использования теории струй. Расчетами определяется ее пиковый характер. Миграция профиля $t_0(x)$ в случае неправильной скорости только тогда фокусируется в одной точке, если принцип отражения видоизменяется согласно положению пика каустики. При использовании параксимального приближения волнового уравнения фокус совмещается с пиком каустики независимо оттого, что взятые значения скоростей правильны или нет.

ELECTROMAGNETIC PARAMETERS AT THE SURFACE OF A CONDUCTIVE HALFSPACE IN TERMS OF THE SUBSURFACE CURRENT DISTRIBUTION

László SZARKA* and Gaston FISCHER**

Electric and magnetic fields at the horizontal surface of a conductor (e.g. the earth) were derived in terms of the currents flowing in its interior. The formulae obtained are valid for any magnetotelluric or controlled-source electromagnetic problem. In the simple limits of one- and two-dimensional magnetotelluric situations they provide a clear physical meaning for impedance, apparent resistivity and phase. For example, the imaginary part of the surface impedance gives the depth to the centre of gravity of the currents which are in phase with the surface magnetic field, and the real part of the impedance yields the mean depth of the out-of-phase currents. The apparent resistivity – depending on its definition – always reflects the period-dependence of some function of the real and/or imaginary part of the complex mean depth of the subsurface current system, while the phase tangent is the ratio of the mean depths of inphase and out-of-phase currents. In *E*-polarization, when the currents flowing horizontally in the earth are modified by the dip-variation of the vertical magnetic field, all formulae may be written in a form analogous to the one-dimensional situation. The *H*-polarization impedance on the other hand, breaks up into the sum of two terms: the first is simply the one-dimensional formula and the second reflects the dip-variation of the vertical electric component in the medium (normalized to the total current at depth) that is due to charges appearing at resistivity interfaces. To compute the fields at a point inside the conductor it suffices to modify the corresponding integration limit.

Keywords: electromagnetic induction, magnetotelluric methods, controlled-source electromagnetic methods, impedance, apparent resistivity, electromagnetic phase

1. Introduction

All electromagnetic sounding methods relying on natural or artificially-generated fields, try to determine the subsurface conductivity structures by means of some interpretational parameters (e.g. impedance, apparent resistivity, phase), which are derived from the distribution and/or period-dependence of the field components at the surface.

Even after the basic geo-electromagnetic induction studies in the frequency domain [e.g. CAGNIARD 1953, WEIDELT 1972, PRICE 1973] and results on different interpretational parameters (e.g. FISCHER [1985] on the 2-D magnetotelluric phase, SPIES and EGGERS [1986] on the apparent resistivity, etc.) the physical meaning of the geophysical interpretational parameters in the fre-

* Geodetic and Geophysical Research Institute of the Hungarian Academy of Sciences, H-9401 Sopron, P.O.B. 5, Hungary

** Observatoire Cantonal, CH-2000 Neuchâtel, Switzerland

Manuscript received: 14 June, 1989

quency domain has not always become clear. Recently LEVY et al. [1988] attempted a physical interpretation in terms of a reflectivity section, a sort of analogue of the reflection seismic section.

In this paper the surface impedance and some corresponding parameters will be interpreted in a novel way, based on the distribution of the subsurface currents. Some elements of this approach can already be found in the papers by SCHMUCKER [1970], WEIDELT [1972] and HAAK [1978], and in some works on the skin-effect of solids [e.g. PIPPARD 1954].

We shall begin with the derivation of the surface electromagnetic field components, expressed in terms of currents flowing in the earth. The physical meanings of surface impedance, apparent resistivity and phase will then be discussed for the traditional, simple magnetotelluric situations.

2. Maxwell's equations adapted to surface electromagnetic methods

Assuming a harmonic time-dependence of the form $\exp(+i\omega t)$, the integral form of Maxwell's equations, when neglecting displacement currents, is as follows:

$$\oint \mathbf{H} \, ds = \iint_S \mathbf{j} \, dS, \quad (1)$$

$$\oint \mathbf{E} \, ds = -i\omega\mu \iint_S \mathbf{H} \, dS, \quad (2)$$

$$\oint \mathbf{H} \, dS = 0, \quad (3)$$

$$\oint \mathbf{E} \, dS = Q, \quad (4)$$

(all fields are functions of x , y and z , and in what follows ε and μ will be assumed constant, independent of time and position).

Starting from equations (1) – (4) the electric and magnetic field components at the surface will be derived as functions of the subsurface currents. The integration domains are shown in *Fig. 1* where z_m tends to infinity, at which limit we can assume all field components to vanish. The distance intervals $\Delta x = x_2 - x_1$ and $\Delta y = y_2 - y_1$ are assumed small.

At any depth the current density is the following vector:

$$\mathbf{j}(x, y, z) = \{j_x(x, y, z); j_y(x, y, z); j_z(x, y, z)\}.$$

2.1. Ampere's law

Equation (1) for the surface element normal to the x -axis of *Fig. 1* can be written in the form:

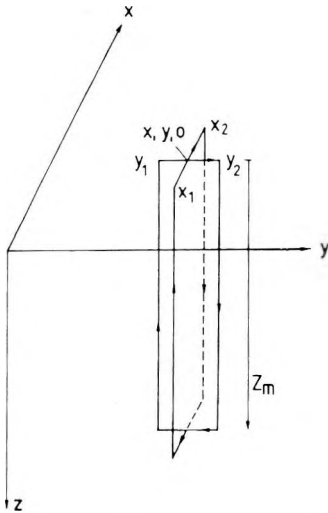


Fig. 1. Integration domains used in the derivation of electric and magnetic components at the surface in terms of subsurface currents

1. ábra. A felszíni elektromos és mágneses térkomponensek mélybeli áramrendszer segítségével történő leszámításához használt integrálási tartományok

Рис. 1. Интегральные области, в пределах которых с помощью глубинной системы тока происходит возникновение поверхностных электрических и магнитных компонентов.

$$\int_{y_1}^{y_2} H_y(x, y, 0) dy + \int_0^{z_m} H_z(x, y_2, z) dz + \int_{y_2}^{y_1} H_y(x, y, z_m) dy + \int_{z_m}^0 H_z(x, y_1, z) dz =$$

$$= \int_{y_1}^{y_2} \int_0^{z_m} j_x(x, y, z) dz dy.$$

If $\Delta y \rightarrow 0$,

$$H_z(x, y_2, z) - H_z(x, y_1, z) \approx \frac{\partial H_z(x, y, z)}{\partial y} \Delta y,$$

and if $z_m \rightarrow \infty$,

$$H_y(x, y, 0) = \int_0^{\infty} \left(j_x - \frac{\partial H_z}{\partial y} \right) dz. \quad (5)$$

Similarly, for the surface element normal to the y -axis the following equation can be derived:

$$H_x(x, y, 0) = - \int_0^{\infty} \left(j_y + \frac{\partial H_z}{\partial x} \right) dz. \quad (6)$$

2.2. Faraday's law

Equation (2) for the same closed loops of Fig. 1 can be written as follows:

$$\int_{x_1}^{x_2} E_x(x, y, 0) dx + \int_0^{z_m} E_z(x_2, y, z) dz + \int_{x_2}^{x_1} E_x(x, y, z_m) dx + \int_{z_m}^0 E_z(x_1, y, z) dz =$$

$$= i\omega\mu \int_{x_1}^{x_2} \int_0^{\infty} H_y(x, y, z) dz dx.$$

If $\Delta x \rightarrow 0$, then

$$E_z(x_2, y, z) - E_z(x_1, y, z) \approx \frac{\partial E_z(x, y, z)}{\partial x} \Delta x,$$

and with $z_m \rightarrow \infty$,

$$E_x(x, y, 0) = i\omega\mu \int_0^\infty \left[H_y(x, y, z) dz + \frac{i}{\omega\mu} \frac{\partial E_z(x, y, z)}{\partial x} \right] dz.$$

According to the rules of partial integration:

$$\int_0^\infty H_y(x, y, z) dz = [z H_y]_0^\infty - \int_0^\infty \frac{\partial H_y(x, y, z)}{\partial z} z dz = - \int_0^\infty z \frac{\partial H_y(x, y, z)}{\partial z} dz.$$

The x component of the differential form of eq. (1) is

$$\frac{\partial H_z(x, y, z)}{\partial y} - \frac{\partial H_y(x, y, z)}{\partial z} = j_x(x, y, z),$$

and therefore,

$$E_x(x, y, 0) = i\omega\mu \int_0^\infty z \left(j_x - \frac{\partial H_z}{\partial y} \right) dz - \int_0^\infty \frac{\partial E_z}{\partial x} dz. \quad (7)$$

For E_y along the other closed line shown in Fig. 1 the following equation can be given:

$$E_y(x, y, 0) = i\omega\mu \int_0^\infty z \left(j_y + \frac{\partial H_z}{\partial x} \right) dz - \int_0^\infty \frac{\partial E_z}{\partial y} dz. \quad (8)$$

Equations (5) – (8) hold on condition that the electromagnetic fields vanish at infinite depth, at least to second order, and the vertical field components E_z and H_z vary continuously in lateral directions. Both conditions are generally fulfilled for media with finite resistivity and conductivity.

2.3 Conservation of magnetic and electric field lines

With equation (3) the vertical magnetic field at the surface can be expressed by the sum of lateral variations of the horizontal components:

$$H_z(x, y, 0) = - \int_0^\infty \left[\frac{\partial H_x(x, y, z)}{\partial x} + \frac{\partial H_y(x, y, z)}{\partial y} \right] dz. \quad (9)$$

Equation (4) can similarly be written as follows (since we are neglecting displacement currents we have no vertical electric fields at the surface):

$$\int_0^{\infty} \left[\frac{\partial E_x(x, y, z)}{\partial x} + \frac{\partial E_y(x, y, z)}{\partial y} \right] dz = \frac{Q}{\epsilon} \tag{10}$$

In equations (9) and (10) the role of the subsurface currents is not immediately apparent, but in some special situations equation (10) can be expressed in terms of such currents. As an example we consider an *H*-polarization magnetotelluric situation: a vertical resistivity interface at $y=0$. The differential form of equation (4) relates the surface charge density $\tau(y=0, z)$ appearing at the interface to the discontinuity of the displacement vector [PRICE 1973, KAUFMANN and KELLER 1985]:

$$\Delta D_y = \tau,$$

where the x -axis is the strike direction. When neglecting displacement currents, the current density, which we denote by $j_y(y=0, z)$, will be the same on both sides of the interfaces. Therefore

$$\tau(y=0, z) = \epsilon(\rho_2 - \rho_1) j_y(y=0, z) \tag{11}$$

The anomalous electric field at the surface caused by the charge density $\tau(y=0, z)$ can be expressed by Coulomb's law:

$$\begin{aligned} E_{y\tau}(y, z=0) &= \frac{1}{4\pi\epsilon} \int_0^{+\infty} \int_{-\infty}^{+\infty} \tau(y=0, z) \frac{y}{r^3} dx dz = \\ &= \frac{\rho_2 - \rho_1}{4\pi} \int_0^{+\infty} \int_{-\infty}^{+\infty} \frac{y}{[x^2 + y^2 + z^2]^{3/2}} j_y(y=0, z) dx dz = \frac{\rho_2 - \rho_1}{2\pi} y \int_0^{\infty} \frac{j_y(y=0, z)}{y^2 + z^2} dz \end{aligned} \tag{12}$$

For vertical contact the electric field due to charges can readily be expressed in terms of the currents j_y flowing through the resistivity interface.

3. Significance of the foregoing results

As was expected, the horizontal magnetic field at the surface is determined by the entire current distribution inside the earth: the first term on the right of equations (5) and (6) is an integral of the currents over a penetrating path ($z_m \rightarrow \infty$); the second is a direct consequence of the lateral current variations since it depends on the lateral gradient of the field component along the integration path. It is worth noting, at this point, that the integration loops of Fig. 1 could have been chosen quite differently, though with the same horizontal portions at the surface; the two terms in the resulting integrals would retain the same significance, but refer to penetrating paths ($z_m \rightarrow \infty$) with other orientations. This clearly demonstrates the obvious fact that although in equations (5)

and (6) integration was chosen along a vertical path, it is the entire current distribution inside the conductor that determines the fields at the surface.

The horizontal electric field is also a sum of two terms: the first term on the right of equations (7) and (8) is the 'first moment' of the currents which determine the horizontal magnetic component, whereas the second again describes the effect of the lateral variations of the magnetic flux in terms of the lateral gradient of the vertical electric field. Note that the gradient of a magnetic field has the dimensions of a current density, whereas $\partial E_z/\partial x$ and $\partial E_z/\partial y$ are moment-like quantities, or rates of change of magnetic flux.

Equations (5) – (10), which are valid for any surface electromagnetic method, have simple physical meanings. These immediately become apparent in the common magnetotelluric 1-D and 2-D configurations. Equations (5) – (10), and several of their important consequences, are summarized briefly in *Table I* for these two magnetotelluric geometries: in the upper part of the table Maxwell's equations adapted to magnetotellurics are shown; in the lower part relations which emphasize the physical meaning of impedance, apparent resistivity, and magnetotelluric phase in terms of the current distribution at depth are given.

4. One-dimensional relationship between the surface field parameters and the subsurface current system

The horizontal magnetic field is simply given as the integral of the subsurface current distribution $j_y(z, \omega)$ whereas the electric field is the 'first moment' of this distribution.

4.1. Surface impedance in the one-dimensional situation

Surface impedance (i.e. the ratio of the corresponding electric and magnetic field components), based on Table 1, is given by:

$$Z_{1-D}^0 = -i\omega\mu \frac{\int_0^{\infty} z j_y(z, \omega) dz}{\int_0^{\infty} j_y(z, \omega) dz} = -i\omega\mu z^* \quad (13)$$

Disregarding the coefficient $-i\omega\mu$, the remaining factor z^* on the extreme right-hand side of equation (13) is a complex depth. If the magnetic field at the surface is assumed to be real (which in the 1-D configuration is not a restriction) the denominator in equation (13) will be real, too, and $\text{Re } z^*$ and $\text{Im } z^*$ can be expressed as follows:

		1-D	E-POLARIZATION	H-POLARIZATION
		$[E_x(z, \omega), H_y(z, \omega)]$	$[E_x(y, z, \omega), H_y(y, z, \omega), H_x(y, z, \omega)]$	$[E_x(y, z, \omega), E_z(y, z, \omega), H_x(y, z, \omega)]$
Maxwell's equations	Ampère's law	$H_y^0 = \int_0^{\infty} j_x dz = \text{const}(\omega)$	$H_y^0 = \int_0^{\infty} j_E dz$, where $j_E = j_x - \frac{\partial H_z}{\partial y}$	$H_z^0 = - \int_0^{\infty} j_y dz = \text{const}(\omega)$
	Faraday's law	$E_x^0 = i\omega\mu \int_0^{\infty} z j_x dz$	$E_x^0 = i\omega\mu \int_0^{\infty} z j_E dz$	$E_y^0 = i\omega\mu \int_0^{\infty} \left(z j_y + \frac{i}{\omega\mu} \frac{\partial E_z}{\partial y} \right) dz$
	Conservation of electric magnetic field lines	no free charges no extra currents	no free charges $H_z^0 = - \int_0^{\infty} \frac{\partial H_x}{\partial y} dz$	eg. for vertical interfaces at $y=0$: $E_{y\tau}^0 = \frac{\Delta\theta}{2\pi} y \int_0^{\infty} \frac{j_x}{y^2 + z^2} dz$ no extra currents
Interpretation	Surface impedance	$Z_{1,0}^0 = \frac{E_x^0}{H_y^0} = -i\omega\mu \frac{\int_0^{\infty} z j_x dz}{\int_0^{\infty} j_x dz}$	$Z_E^0 = - \frac{E_x^0}{H_y^0} = i\omega\mu \frac{\int_0^{\infty} z j_E dz}{\int_0^{\infty} j_E dz}$	$Z_H^0 = E_y^0/H_z^0 = -i\omega\mu \frac{\int_0^{\infty} z j_y dz + \int_0^{\infty} \frac{\partial E_z}{\partial y} dz}{\int_0^{\infty} j_y dz}$
	Complex depth of subsurface currents	$z_{1,0}^* = - \frac{1}{i\omega\mu} \frac{E_x^0}{H_y^0}$ $\text{Re } z_{1,0}^* = - \text{Im } Z_{1,0}^0/\omega\mu$ $\text{Im } z_{1,0}^* = \text{Re } Z_{1,0}^0/\omega\mu$	$z_E^* = - \frac{1}{i\omega\mu} \frac{E_x^0}{H_y^0}$ $\text{Re } z_E^* = - \text{Im } Z_E^0/\omega\mu$ $\text{Im } z_E^* = \text{Re } Z_E^0/\omega\mu$	$z_H^* = \frac{1}{i\omega\mu} \left[- \frac{E_z^0}{H_z^0} + f(E_z) \right]$ where $f(E_z) = \int_0^{\infty} \frac{\partial E_z}{\partial y} dz / \int_0^{\infty} i j_y dz$ $\text{Re } z_H^* = - [\text{Im } Z_H - \text{Im } f(E_z)]/\omega\mu$ $\text{Im } z_H^* = [- \text{Re } Z_H + \text{Re } f(E_z)]/\omega\mu$
	Magnetotelluric phase	$\varphi_{1,0}^0 = - \text{atan} \frac{\text{Re } z_{1,0}^*}{\text{Im } z_{1,0}^*}$	$\varphi_E^0 = - \text{atan} \frac{\text{Re } z_E^*}{\text{Im } z_E^*}$	$\varphi_H^0 = - \text{atan} \frac{\text{Re } z_H^* - \frac{1}{\omega\mu} \text{Im } f(E_z)}{\text{Im } z_H^* + \frac{1}{\omega\mu} \text{Re } f(E_z)}$

Table 1. Maxwell's equations for the magnetotelluric one-dimensional case and for the E- and H-polarization field components (upper part) and their magnetotelluric interpretation based on subsurface currents (lower part). The surface values are denoted by upper indices 0. Other designations are explained in the text

I. táblázat. Maxwell egyenletek a magnetotellurikus egydimenziós esetre és az E- és H-polarizációs térkomponensekre (felső rész), valamint az egyenletek magnetotellurikus értelmezése a felszín alatti áramok alapján (alsó rész). A felszíni értékeket 0 felső indexek jelölik. A további jelölések magyarázata a szövegben található

Таблица 1. Уравнения Максвелла для магнитотеллурического одномерного случая и для компонентов в поляризациях E и H (верхняя часть), а также магнитотеллурическое интерпретирование уравнений на основании подземных токов (нижняя часть).

Поверхностные значения обозначаются верхими индексами 0. Объяснение дальнейших условных обозначений находится в тексте

$$\operatorname{Re} z^* = \frac{\int_0^{\infty} z \operatorname{Re} j_y(z, \omega) dz}{\int_0^{\infty} \operatorname{Re} j_y(z, \omega) dz} \quad \text{and} \quad \operatorname{Im} z^* = \frac{\int_0^{\infty} z \operatorname{Im} j_y(z, \omega) dz}{\int_0^{\infty} \operatorname{Re} j_y(z, \omega) dz} \quad (14)$$

$\operatorname{Re} z^*$ gives the depth to the centre of gravity of the currents flowing in phase with the surface magnetic field. The imaginary part of z^* cannot be defined as a depth to the centre of gravity of out-of-phase currents since $\int_0^{\infty} \operatorname{Im} j_y(z, \omega) dz = 0$,

but $\operatorname{Im} z^*$ corresponds to the moment of the out-of phase currents normalized to the total current, and it gives the 'mean depth' of the out-of-phase currents. (SCHMUCKER 1970 used the concept of $\operatorname{Im} z^*$ to calculate apparent resistivity).

The formulae in Table I thus establish a meaningful relationship between surface impedance and the complex mean depth of the subsurface currents; the complex depth z^* and the impedance Z_{1-D} are strictly proportional to each other: the real part of the impedance corresponds to the mean depth of currents flowing out-of-phase to the surface magnetic field, while the imaginary part of the impedance (divided by $-i\omega\mu$) can be interpreted as the depth to the centre of the in-phase currents.

4.2 Apparent resistivities in one-dimensional structures

As was pointed out by SPIES and EGGERS [1986] for the one-dimensional situation, the magnetotelluric apparent resistivity can be defined in several arbitrary ways. Cagniard's definition is based on the absolute value of the impedance. In the Schmucker inversion an apparent resistivity, calculated from $\operatorname{Re} Z$, is used (according to the morphological study by SPIES and EGGERS [1986], this definition has proved to be the best one). But an apparent resistivity can be defined by a variety of functions of the surface impedance. With our relationship between the subsurface current system and surface impedance all of these different apparent resistivities are also connected directly with the subsurface current system: the apparent resistivity curve calculated from $\operatorname{Re} Z$ reveals how the mean depth of out-of-phase currents increases with the period; the apparent resistivity based on $\operatorname{Im} Z$, on the other hand, describes the period-dependence of the depth to the centre of gravity of in-phase currents; in the commonly-used Cagniard resistivity it is the mean square of these two depths related to the two current systems which is taken into account. Further apparent resistivity definitions can also be given; all of them will somehow reflect the period-dependence of $\operatorname{Re} z^*$ and/or $\operatorname{Im} z^*$.

4.3 The one-dimensional phase and its relationship to the apparent resistivity

The phase difference between the horizontal electric and magnetic components at the surface is given by the ratio of the imaginary and the real parts of the surface impedance, which is the same as the ratio of the real and imaginary parts of the complex current centre depth z^* :

$$\Phi_{1-D}^0 = \text{atan} \frac{\text{Im } Z_{1-D}(\omega)}{\text{Re } Z_{1-D}(\omega)} = -\text{atan} \frac{\text{Re } z^*(\omega)}{\text{Im } z^*(\omega)} \quad (15)$$

(With the assumption of $+45^\circ$ for the asymptotic value of the magnetotelluric phase, $\text{Im } z^*$ happens to have negative sign. In the interpretation it does not matter whether $\text{Im } z^*$ is positive or negative, since out-of-phase currents may arbitrarily be defined as being 90° behind or ahead, with appropriate positive or negative signs.)

According to equation (15) the behaviour of the phase curve against the period gives information on the ratio of the depth to the centre of gravity of 'in-phase' and the mean depth of the 'out-of-phase' currents (e.g. a phase value of 60° informs us that the centre of gravity of the in-phase currents is $\sqrt{3}$ times deeper than the mean depth of the out-of-phase currents).

The period-dependence of the current depths for the typical two-layered half spaces with $\rho_2/\rho_1 = 100$ and $\rho_2/\rho_1 = 0.01$ is shown in Fig. 2a and b. When the period, or λ_1/h (λ_1 is the wavelength in the upper layer defined as $\lambda_1 = \sqrt{10^7 \rho_1 T}$, h is the layer thickness) almost vanishes, the two depth values are equal. As the period increases the currents extend progressively to greater depths. When they approach the high-resistivity interface ($\rho_2/\rho_1 = 100$ case), the out-of-phase current centre (after small initial oscillations) goes to greater depths than the in-phase current centre. But towards $(\lambda_1/h) \rightarrow \infty$ the two depths again coincide. In the opposite configuration of a high-conductivity basement ($\rho_2/\rho_1 = 0.01$) the situation is reversed: here Fig. 2b shows that (except for the initial small oscillations) the out-of-phase depth will lag behind the in-phase depth, though towards $(\lambda_1/h) \rightarrow \infty$ the two depths will again coincide.

'Overshooting' in the frequency domain of the apparent resistivity and phase curves is a direct consequence of the small oscillations shown in Fig. 2a and b. Oscillation-free apparent resistivity and phase curves cannot be obtained in the frequency domain.

As was mentioned earlier, the most reliable apparent resistivity definition is related to the real part of the surface impedance. When $\rho_2/\rho_1 = 0.01$, SPIES and EGGERS [1986] observed that the apparent resistivity curve was more strongly featured, and they therefore concluded that this allowed a higher resolution for magnetotelluric soundings than in the opposite situation ($\rho_2/\rho_1 = 100$). According to Fig. 2a and b the mean depth of the out-of-phase currents is modified by a high-conductivity basement over a very narrow λ_1/h interval,

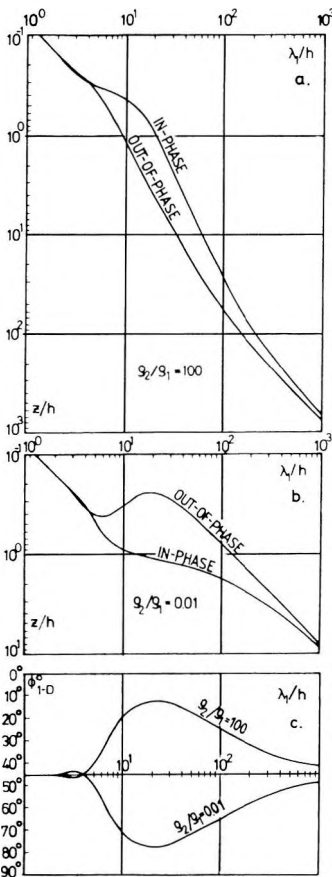


Fig. 2. Relationship between the mean depth of in-phase and out of phase currents and the magnetotelluric problem

- Mean depths of in-phase and out-of-phase currents as functions of λ_1/h for a high resistivity basement ($\rho_2/\rho_1 = 100$)
- Mean depths of in-phase and out-of-phase currents as functions of λ_1/h for a high-conductivity basement ($\rho_2/\rho_1 = 0.01$)
- Magnetotelluric phase curves for $\rho_2/\rho_1 = 100$ and $\rho_2/\rho_1 = 0.01$, calculated from relation:

$$\Phi_{1-D}^* = \tan^{-1}(\operatorname{Re} z_{1-D}^*/\operatorname{Im} z_{1-D}^*)$$

2. ábra. Összefüggés a fázisban levő és a 90° fázistolású áramok átlagmélységei és a magnetotellurikus fázis között egydimenziós magnetotellurikus probléma esetén

- A fázisban levő és a 90° fázistolású áramok átlagmélységei a λ_1/h függvényeként, nagyellenállású aljzat ($\rho_2/\rho_1 = 100$) esetén
- A fázisban levő és a 90° fázistolású áramok átlagmélységei a λ_1/h függvényeként, nagy vezetőképességű aljzat ($\rho_2/\rho_1 = 0,01$) esetén
- Magnetotellurikus fázisgörbék a $\rho_2/\rho_1 = 100$ és a $\rho_2/\rho_1 = 0.01$ esetre, a $\Phi_{1-D}^* = \operatorname{arctg}(\operatorname{Re} z_{1-D}^*/\operatorname{Im} z_{1-D}^*)$ összefüggéssel számítva

Рис. 2. Зависимость между средними глубинами токов, находящихся в одной фазе и смещенных по фазе на 90° , и магнитотеллурической фазой для одномерного магнитотеллурического случая

- Средние глубины токов, находящихся в одной фазе и смещенных по фазе на 90° , как зависимость λ_1/h , в случае фундамента с высоким сопротивлением ($\rho_2/\rho_1 = 100$)
- Средние глубины токов, находящихся в одной фазе и смещенных по фазе на 90° , как зависимость λ_1/h , в случае фундамента с высокой проводимостью ($\rho_2/\rho_1 = 0,01$)
- Магнитотеллурические фазовые кривые для случая $\rho_2/\rho_1 = 100$ и $\rho_2/\rho_1 = 0,01$, рассчитанные при $\Phi_{1-D}^* = \operatorname{arctg}(\operatorname{Re} z_{1-D}^*/\operatorname{Im} z_{1-D}^*)$.

while in the case of a high-resistivity basement the depth modification extends over a wide λ_1/h range. With a high-conductivity basement the depth increase of the current centres is strongly reduced as soon as the current system reaches the good conductor. Consequently, the apparent resistivity calculated from $\operatorname{Re} Z$ is seen to adjust to the basement resistivity over a much shorter period range.

On the other hand, and as is well known, the phase curves for $\rho_2/\rho_1 = 100$ and $\rho_2/\rho_1 = 0.01$ are symmetrical. The surface phase — in contrast with the apparent resistivity calculated from $\operatorname{Re} Z$ — is equally responsive to high-resistivity and high-conductivity units, in analogy with the apparent resistivity calculated from $|Z|$. This means that the corresponding statement of SPIES and EGGERS [1986] requires a slight modification: different resolving powers for

high-conductivity or high-resistivity structures are not strictly attributes of the magnetotelluric method itself, but are largely a problem of the parameters used for the interpretation. However, it is also true that the impedance is a ratio, which in theory can be computed to any desired accuracy. In practice, because of noise sources, it is often more difficult to measure the small field amplitudes one has over conductive structures; on the other hand, conductive structures are also a good shield against distant perturbations.

5. Remarks on the two-dimensional impedance, apparent resistivity, and phase formulae

According to the corresponding equations in Table I, the special two-dimensional distortion effects are as follows:

— in E -polarization the appearance of H_z and $\partial H_z/\partial y$ is due to extra currents. As can be seen in Table I, any change in the total current immediately leads to a modification of its moment;

— in H -polarization the magnetic field is a constant across the entire surface profile, but the electric field is modified by a depth-integral of $\partial E_z/\partial y$. E_z and $\partial E_z/\partial y$ in the medium originate from charges appearing at resistivity interfaces, or simply from variations in the current conducting cross-section. As we have seen in Sec. 3, $\partial E_z/\partial y$ can also be viewed as describing lateral variations of the magnetic flux. For example, in Table I, and for the special case of a vertical fault, the anomalous horizontal electric field due to free charges can also be expressed in terms of the currents flowing through the resistivity interface.

5.1 Two-dimensional surface impedance

Just as for the one-dimensional situation, the surface impedance in E -polarization also gives the complex depth of the current distribution, but instead of j_x the modified current density j_E should be used to compute the impedance, as shown in the upper part of Table I. In H -polarization the impedance formula is strongly modified by the appearance of $\partial E_z/\partial y$ in the medium, leading to the superposition of two terms: the first is equivalent to a perfect one-dimensional relation, but the second embodies the effects of $\partial E_z/\partial y$ ($\partial E_z/\partial y$ has a relative phase shift of 90° , which strongly suggests that it is indeed caused by surface charges).

5.2 On the two-dimensional apparent resistivities

In Table I the resolving powers one may expect with E - and H -polarization anomalies are also indicated: in E -polarization any of the apparent resistivities discussed will determine the complex depth z_E^* of the modified currents j_E ; in

H-polarization all that will be determined is a combination of the depths $\text{Re } z_H^*$ and $\text{Im } z_H^*$ with effects caused by surface changes.

Two-dimensional magnetotelluric variations of the Cagniard resistivities are well known, and their link with the subsurface currents is certainly more abstract than that of the apparent resistivities calculated from $\text{Re } Z$. But in spite of some advantageous properties of $\rho_{\text{Re } Z}$, it is not yet clear whether it is worth using it instead of $\rho_{|Z|}$.

5.3 The two-dimensional magnetotelluric phase

In *E*-polarization the magnetotelluric phase tangent can be interpreted as in the one-dimensional situation, since it is again the ratio of the real and the imaginary part of the complex depth z_E^* of the subsurface currents, but instead of currents flowing horizontally in the earth, the modified currents j_E should be used.

In *H*-polarization the depth to the centre of in-phase currents is combined with the out-of-phase part of $\partial E_z/\partial y$, while the mean depth of the out-of-phase currents is influenced by the in-phase part of $\partial E_z/\partial y$; this leads to complex magnetotelluric phase behaviour. Table I gives an example of the evaluation of $\partial E_z/\partial y$, in the case of a vertical resistivity interface, where the charge effects can also be expressed in terms of currents flowing through the resistivity interface.

Thus all geophysical parameters which are usually determined at the surface can directly be related to the distribution of the currents flowing in the earth.

A similar physical interpretation for the magnetotelluric phase has been given by FISCHER [1985]. His interpretation, which was derived at first for a two-dimensional *E*-polarization configuration and then 'extended' to the one-dimensional situation, is based on the occurrence of near-surface current concentrations or reductions: a near surface concentration of ohmic currents results in a phase decrease, whereas a current reduction there leads to a phase increase. Thus, with a simple intuitive rule about the distribution of the currents flowing in the earth, the resulting magnetotelluric phase anomalies can be predicted.

The apparent success of Fischer's phase rule results from several favourable circumstances:

- The distribution with depth of in-phase and out-of-phase currents always evolves differently with period near resistivity contrasts (see, e.g., Fig. 2a and b, where in-phase currents are pulled towards or into the medium of higher conductivity, while out-of-phase currents are attracted towards or into the medium of higher resistivity);
- the ohmic currents are closely related — at least at longer periods — to the in-phase current;
- apart from the anomalous currents occurring in *E*-polarization there are no further perturbing effects caused by surface charges;

— in *H*-polarization, difficulties arise because the effects due to the redistribution of the currents combine with effects produced by surface charges at resistivity discontinuities. These effects are going to be studied in detail by FISCHER, SZARKA and ÁDÁM in a paper now in preparation.

6. Remarks on three-dimensional magnetotelluric and controlled-source problems

Simplified formulae derived from equations (5)–(10), which are summarized in Table I, yield a clear physical meaning for the surface electromagnetic parameters usually used in magnetotelluric interpretation.

For the three-dimensional magnetotelluric problem, or for any controlled-source problem, equations (5)–(10) cannot be simplified (except for special controlled-source situations where some elements in the general relationships may vanish, yielding equations similar to those in Table I). In most cases both anomalous currents and charges are present, and from electromagnetic measurements carried out at the surface only very complex conclusions can be drawn. Equations (5)–(10) clearly illustrate the true complexity of the problem faced in three-dimensional magnetotellurics or in controlled-source methods.

7. Electromagnetic parameters at arbitrary depth

If we integrate Ampere's and Faraday's laws not from the surface, but from an arbitrary depth *z* to infinity, it can be shown that the basic formulae derived in this paper remain valid and express the fields at any arbitrary depth inside the conductor.

It is easy to show that the only difference appears in the derivation of eq. (7), where the product *z* · *H_y* cannot be neglected when *z* ≠ 0. A detailed derivation for this situation is given by SZARKA and FISCHER [1989] whose results for the three-dimensional configuration can be expressed as follows:

$$Z_{xy}(x, y, z) = -i\omega\mu(z_{3-D_x}^* - z) + f_{3-D_x}(E_z) \tag{16}$$

where

$$z_{3-D_x}^* = \frac{\int_z^\infty z' \left[j_x(x, y, z') - \frac{\partial H_z(x, y, z')}{\partial y} \right] dz'}{\int_z^\infty \left[j_x(x, y, z') - \frac{\partial H_z(x, y, z')}{\partial y} \right] dz'}$$

and

$$f_{3-D_x}(E_z) = \frac{\int_z^\infty \frac{\partial E_z(x, y, z')}{\partial x} dz'}{\int_z^\infty \left[j_x(x, y, z') - \frac{\partial H_z(x, y, z')}{\partial y} \right] dz'}$$

According to eq. (16) the impedance at any interior point of a conductor is entirely given by the complex mean depth of the currents flowing below the observation point. Although the amplitude and configuration of this current distribution are also determined by currents flowing above the measuring point, this does not appear explicitly in eq. (16). SZARKA and FISCHER [1989] also demonstrate that formulae like eq. (16) are of very general validity: they remain true even when the surface exhibits a complicated topography and when the primary inducing field is not uniform.

8. Conclusions

The electromagnetic field components at the surface of the earth have been derived in terms of the distribution of the currents flowing underground. From the derived relationships, some of which are listed in Table I, physical meanings closely related to subsurface currents have been given for the surface impedance, the apparent resistivity and the magnetotelluric phase.

Based on the relations summarized in Table I the magnetic fields H_y or H_x are determined mainly by the total current; the electric fields, E_x or E_y , on the other hand, are closely related to the first moment of these currents. The surface impedance (i.e., the ratio of the current moment to the total current, multiplied by $-\omega\mu$) represents a complex depth which can be interpreted as a combination of the depth to the centre of gravity of in-phase and the mean depth of out-of-phase subsurface currents. This definition is somewhat different from that of SCHMUCKER [1970] and WEIDELT [1972]. The surface impedance is closely related to this complex depth:

- in the one-dimensional configuration the real part of the impedance is proportional to the mean depth of the out-of-phase currents, while the imaginary part is proportional to the depth of the centre of gravity of the in-phase currents;
- in E -polarization the one-dimensional proportionality between the surface impedance and the complex depth of the subsurface current centre can be extended if one substitutes $j_E = j_x - \partial H_z / \partial y$ for j_x (or $j_E = j_y + \partial H_z / \partial x$ for j_y);
- in H -polarization the one-dimensional complex current depth must be corrected with terms which describe the dip-variation of the vertical electric component; the origin of these is essentially related to the appearance of surface charges at resistivity discontinuities.

The apparent resistivity curves reflect the period-dependence of certain functions of the mean depths of out-of-phase and/or in-phase currents. The phase curve (the phase difference between horizontal electric and magnetic components at the surface) is closely related to the ratio of these two depths.

The only assumptions made in this paper were (1) that displacement currents could be neglected, (2) that the electromagnetic fields as well as their first moments vanish at infinite depth, and (3) that electric permittivity and magnetic permeability are constant, independent of time and position. The

formulae derived for the surface can easily be extended to any measuring point inside the conductor. All subsurface electromagnetic parameters can be explicitly described in terms of the currents flowing below the observation point only.

The direct connection revealed in this paper between the commonly-used parameters in surface electromagnetic sounding methods and the subsurface current distribution makes it possible to propose a new and different physical interpretation of the governing electromagnetic phenomena based on the distribution of the subsurface currents.

Acknowledgments

The authors wish to express their gratitude toward their institutions, to the Hungarian and Swiss National Academic Research Foundations, as well as to the Geophysical Commission of the Swiss Academy of Natural Sciences for their support of this research project. The authors are indebted to A. Ádám, J. Verő and J. Weaver for valuable discussions on magnetotelluric phase behaviour.

REFERENCES

- CAGNIARD L. 1953: Basic theory of the magneto-telluric method of geophysical prospecting. *Geophysics* **18**, 3, pp. 605–635
- FISCHER G. 1985: Some remarks on the behaviour of the magnetotelluric phase. *Geophysical Prospecting* **33**, 5, pp. 716–722
- FISCHER G., SZARKA L., ADÁM A. 1989: Physics of the magnetotelluric phase in *H*-polarization. Manuscript in preparation
- HAAK V. 1978: Interpretations-Verfahren für die Magnetotellurik unter besonderer Berücksichtigung lateral variierender elektrischer Leitfähigkeit im Erdinnern und eines räumlich inhomogenen induzierenden Magnetfelds. Bayerische Akademie der Wissenschaften, Mathematisch-Naturwissenschaftliche Klasse. Abhandlungen: Neue Folge, Heft 158
- KAUFMAN A. and KELLER G.V. 1985: Inductive Mining Prospecting. Part I. Theory. Elsevier Science Publ. Co., Inc.
- LEVY S., OLDENBURG D. and WANG J. 1988: Subsurface imaging using magnetotelluric data. *Geophysics* **53**, 1, pp. 104–117
- PIPPARD A.B. 1954: Metallic conduction at high frequencies and low temperatures. *Adv. in Electronics and Electron Phys.*, Vol. VI, pp. 1–45
- PRICE A.T. 1973: The theory of geomagnetic induction. *Physics of the Earth and Planetary Interiors* **7**, 2, pp. 227–233
- SCHMUCKER U. 1970: Anomalies of geomagnetic variations in the Southwestern United States. *Bulletin of the Scripps Institution of Oceanography*. University of California, San Diego, Vol. 13, p. 69
- SPIES B.R. and EGGERS D.E. 1986: The use and misuse of apparent resistivity in electromagnetic methods. *Geophysics* **51**, 7, pp. 1462–1471
- SZARKA L., FISCHER G.: Subsurface electromagnetic parameters in terms of the distribution of current. Manuscript submitted to *Geophysical Transactions*
- WEIDELT P. 1972: The Inverse Problem of Geomagnetic Induction. *Zeitschrift für Geophysik* **38**, pp. 257–289

ELEKTROMÁGNESES PARAMÉTEREK VEZETŐ FÉLTÉR FELSZÍNÉN, A VEZETŐN BELÜLI ÁRAMELOSZTLÁS FÜGGVÉNYÉBEN

SZARKA László és Gaston FISCHER

Az elektromos és mágneses teret egy vezető vízszintes felszínén (pl. a föld felszínén) a mélyben folyó áramok segítségével irtuk le. Az összefüggések bármely természetes vagy mesterséges elektromágneses gerjesztés esetén érvényesek. A magnetotellurika alapeseteiben — azaz az egy- és kétdimenziós problémákban — a látszólagos fajlagos ellenállás és a fázis az összefüggésekből világos fizikai jelentést kapnak. A felszíni impedancia képzetes része például megadja a felszíni mágneses térrel azonos fázisú áramok súlypontjának mélységét; a valós rész pedig a 90° -kal eltolt fázisú áramok átlagmélységével van szoros kapcsolatban. A látszólagos fajlagos ellenállás — a definíciótól függő módon — mindig a felszín alatti áramrendszer komplex mélysége valós és/vagy képzetes részének periódusfüggését tükrözi, miközben a fázisszög tangense a fázisban levő és a 90° fáziseltolódású áramok átlagmélységének hányadosát adja meg. E -polarizációban, amikor a vízszintesen folyó áramok a vertikális mágneses komponens dőlésirányú változása miatt módosulnak, minden formulát ki lehet fejezni az egydimenziós esethez hasonló módon. A H -polarizációs impedancia azonban két tag összegeként írható fel: az első egy egyszerű egydimenziós kifejezés, a második pedig a függőleges elektromos tér dőlésirányú változását tükrözi (a mélybeli áramok teljes összegére normalálva), s a második hatás a határfelületi töltések következménye. Az elektromágneses térnek a vezető belsejében történő számításához elegendő a megfelelő integrálási határokat megváltoztatni.

ЭЛЕКТРОМАГНИТНЫЕ ПАРАМЕТРЫ НА ПОВЕРХНОСТИ ПРОВОДЯЩЕЙ ПОЛУПРОСТРАНСТВА В ЗАВИСИМОСТИ ОТ РАСПРЕДЕЛЕНИЯ ТОКА ПО ПРОВОДНИКУ.

Ласло САРКА и Гастон ФИШЕР

Электрическое и магнитное поле на горизонтальной поверхности проводника, например, на поверхности Земли, описывается с помощью глубинных токов. Установленные зависимости действительны в случае любого естественного или искусственного электромагнитного возмущения. По этим зависимостям для основных случаев магнитотеллурики — для одно- и двухмерных случаев — кажущееся удельное сопротивление и фаза получают ясное физическое толкование. Мнимая часть поверхностного импеданса определяет глубину центра тяжести токов, имеющих фазы, совпадающие с фазами поверхностного магнитного поля; а действительная часть находится в тесной связи со средней глубиной токов, фазы которых смещены на 90° . Кажущееся удельное сопротивление — в зависимости от метода определения — отображает зависимость действительной и/или мнимой части глубины подземной системы тока от периода поля, в то время, как тангенс фазового угла дает соотношение глубины однофазовых и смещенных по фазе на 90° токов. В поляризации E — когда горизонтальные токи изменяются вследствие изменения падения вертикальной магнитной компоненты — все формулы можно выразить как для одномерного случая. А импеданс H записывается как сумма двух членов: первый — простое одномерное выражение, а второй — отражает изменение падения вертикального электрического поля (нормализованы на сумму тока) и является следствием зарядов, находящихся на граничных поверхностях. Для расчета электромагнитного поля, находящегося внутри проводника, достаточно выбрать соответствующие интегральные границы.

DIRECT INTERPRETATION OF MAGNETIC ANOMALIES DUE TO SPHERICAL SOURCES — A HILBERT TRANSFORM METHOD

N. SUNDARARAJAN*, B. UMASHANKAR*, N. L. MOHAN*
and S. V. SESHAGIRI RAO*

A direct interpretation of magnetic anomalies due to spherical sources is devised from the first horizontal and vertical derivatives of the vertical component of the field. The vertical derivative of the field is computed from the horizontal derivative by means of the Hilbert transform. The parameters of the sphere are obtained as a function of the abscissae of the points of intersection of the derivatives, as illustrated in the text. Two theoretical examples demonstrate the utility of the method. Moderately good results are obtained on field data pertaining to the vertical magnetic anomalies over spherical sources in the Bankura area of West Bengal, India, and the Louga anomaly, in the USA. This interpretation is applicable to horizontal and total magnetic anomalies too. Gravity and self potential anomalies can also be interpreted by similar methods. This procedure can easily be programmed.

Keywords: magnetic anomalies, spherical models, direct problem, Hilbert transform

1. Introduction

Point poles, magnetic doublets and spheres are some of the most important three-dimensional models in mining geophysics. Many methods are available in geophysical literature to interpret magnetic anomalies of ground and air-borne magnetic data. [HENDERSON and ZIETZ 1948 and 1967, SMELLIE 1956, GAY 1965, RADHAKRISHNA MURTHY 1974, RAO et al. 1973]. These methods are subject to certain assumptions and are relatively cumbersome in their approach.

A more recent paper of MOHAN et al. [1982] proposes a novel interpretation of spherical sources by means of spectral analysis, although it again involves tedious mathematical operations. In this paper, we present an elegantly simple mathematical procedure to extract the parameters of the sphere, namely the depth to the centre, the polarization angle and the radius. This process involves the computation of the first horizontal derivative of the vertical magnetic anomaly, and hence the vertical derivative by means of the Hilbert transform. Making use of these two derivatives, the parameters are obtained by means of simple mathematical expressions.

The application of the Hilbert transform in the interpretation of ground-magnetic anomalies has been gaining greater importance of late. [NABIGHIAN 1972, MOHAN et al. 1982, SUNDARARAJAN 1982 and SUNDARARAJAN et al. 1983,

* Centre of Exploration Geophysics, Osmania University, Hyderabad—500 007, India
Manuscript received (revised version): 14 April, 1989

1985]. In all these papers the concept of amplitude of the analytic signal is used in precisely locating the origin. However, a mention can be made that this amplitude curve can also be used to delineate the sources from regional magnetic or gravity surveys. For all practical purposes, this method can also be realised by simple programming.

2. Vertical magnetic effect of a sphere

The geometry of the model is shown in *Figure 1*, with Z as the depth to the centre, R as the radius and Q as the magnetic polarization angle. The vertical magnetic effect of such a model is given by

$$V(x) = \frac{4}{3} \pi R^3 I \frac{(2Z^2 - x^2) \sin Q - 3xZ \cos Q}{(x^2 + Z^2)^{5/2}} \quad (1)$$

where I is the intensity of magnetisation [RAO et al. 1973].

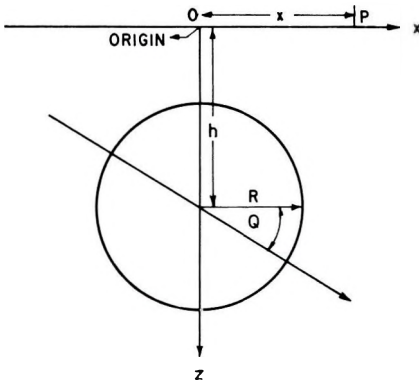


Fig. 1. Geometry of the spherical model

1. ábra. A modell geometriája

Рис. 1. Геометрия модели.

Differentiating equation (1) separately with respect to x and Z we obtain the first horizontal and vertical derivatives:

$$V_x(x) = \frac{4/3\pi R^3 I}{(x^2 + Z^2)^{7/2}} \cdot [(x^2 + Z^2) (2x \sin Q + 3Z \cos Q) + 5x(2Z^2 - x^2) \sin Q - 3xZ \cos Q] \quad (2)$$

$$V_z(x) = \frac{4/3\pi R^3 I}{(x^2 + Z^2)^{7/2}} \cdot [(x^2 + Z^2) (4Z \sin Q - 3x \cos Q) - 5Z(2Z^2 - x^2) \sin Q - 3xZ \cos Q] \quad (3)$$

DIRECT INTERPRETATION OF MAGNETIC ANOMALIES DUE TO SPHERICAL SOURCES — A HILBERT TRANSFORM METHOD

N. SUNDARARAJAN*, B. UMASHANKAR*, N. L. MOHAN*
and S. V. SESHAGIRI RAO*

A direct interpretation of magnetic anomalies due to spherical sources is devised from the first horizontal and vertical derivatives of the vertical component of the field. The vertical derivative of the field is computed from the horizontal derivative by means of the Hilbert transform. The parameters of the sphere are obtained as a function of the abscissae of the points of intersection of the derivatives, as illustrated in the text. Two theoretical examples demonstrate the utility of the method. Moderately good results are obtained on field data pertaining to the vertical magnetic anomalies over spherical sources in the Bankura area of West Bengal, India, and the Louga anomaly, in the USA. This interpretation is applicable to horizontal and total magnetic anomalies too. Gravity and self potential anomalies can also be interpreted by similar methods. This procedure can easily be programmed.

Keywords: magnetic anomalies, spherical models, direct problem, Hilbert transform

1. Introduction

Point poles, magnetic doublets and spheres are some of the most important three-dimensional models in mining geophysics. Many methods are available in geophysical literature to interpret magnetic anomalies of ground and airborne magnetic data. [HENDERSON and ZIETZ 1948 and 1967, SMELLIE 1956, GAY 1965, RADHAKRISHNA MURTHY 1974, RAO et al. 1973]. These methods are subject to certain assumptions and are relatively cumbersome in their approach.

A more recent paper of MOHAN et al. [1982] proposes a novel interpretation of spherical sources by means of spectral analysis, although it again involves tedious mathematical operations. In this paper, we present an elegantly simple mathematical procedure to extract the parameters of the sphere, namely the depth to the centre, the polarization angle and the radius. This process involves the computation of the first horizontal derivative of the vertical magnetic anomaly, and hence the vertical derivative by means of the Hilbert transform. Making use of these two derivatives, the parameters are obtained by means of simple mathematical expressions.

The application of the Hilbert transform in the interpretation of ground-magnetic anomalies has been gaining greater importance of late. [NABIGHIAN 1972, MOHAN et al. 1982, SUNDARARAJAN 1982 and SUNDARARAJAN et al. 1983,

* Centre of Exploration Geophysics, Osmania University, Hyderabad—500 007, India
Manuscript received (revised version): 14 April, 1989

1985]. In all these papers the concept of amplitude of the analytic signal is used in precisely locating the origin. However, a mention can be made that this amplitude curve can also be used to delineate the sources from regional magnetic or gravity surveys. For all practical purposes, this method can also be realised by simple programming.

2. Vertical magnetic effect of a sphere

The geometry of the model is shown in *Figure 1*, with Z as the depth to the centre, R as the radius and Q as the magnetic polarization angle. The vertical magnetic effect of such a model is given by

$$V(x) = \frac{4}{3} \pi R^3 I \frac{(2Z^2 - x^2) \sin Q - 3xZ \cos Q}{(x^2 + Z^2)^{5/2}} \quad (1)$$

where I is the intensity of magnetisation [RAO et al. 1973].

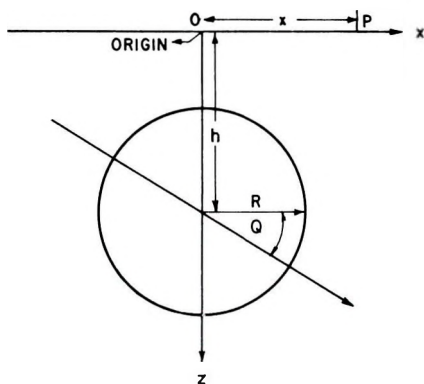


Fig. 1. Geometry of the spherical model

1. ábra. A modell geometriája

Рис. 1. Геометрия модели.

Differentiating equation (1) separately with respect to x and Z we obtain the first horizontal and vertical derivatives:

$$V_x(x) = \frac{4/3\pi R^3 I}{(x^2 + Z^2)^{7/2}} \cdot [(x^2 + Z^2) (2x \sin Q + 3Z \cos Q) + 5x(2Z^2 - x^2) \sin Q - 3xZ \cos Q] \quad (2)$$

$$V_z(x) = \frac{4/3\pi R^3 I}{(x^2 + Z^2)^{7/2}} \cdot [(x^2 + Z^2) (4Z \sin Q - 3x \cos Q) - 5Z(2Z^2 - x^2) \sin Q - 3xZ \cos Q] \quad (3)$$

DIRECT INTERPRETATION OF MAGNETIC ANOMALIES DUE TO SPHERICAL SOURCES — A HILBERT TRANSFORM METHOD

N. SUNDARARAJAN*, B. UMASHANKAR*, N. L. MOHAN*
and S. V. SESHAGIRI RAO*

A direct interpretation of magnetic anomalies due to spherical sources is devised from the first horizontal and vertical derivatives of the vertical component of the field. The vertical derivative of the field is computed from the horizontal derivative by means of the Hilbert transform. The parameters of the sphere are obtained as a function of the abscissae of the points of intersection of the derivatives, as illustrated in the text. Two theoretical examples demonstrate the utility of the method. Moderately good results are obtained on field data pertaining to the vertical magnetic anomalies over spherical sources in the Bankura area of West Bengal, India, and the Louga anomaly, in the USA. This interpretation is applicable to horizontal and total magnetic anomalies too. Gravity and self potential anomalies can also be interpreted by similar methods. This procedure can easily be programmed.

Keywords: magnetic anomalies, spherical models, direct problem, Hilbert transform

1. Introduction

Point poles, magnetic doublets and spheres are some of the most important three-dimensional models in mining geophysics. Many methods are available in geophysical literature to interpret magnetic anomalies of ground and airborne magnetic data. [HENDERSON and ZIETZ 1948 and 1967, SMELLIE 1956, GAY 1965, RADHAKRISHNA MURTHY 1974, RAO et al. 1973]. These methods are subject to certain assumptions and are relatively cumbersome in their approach.

A more recent paper of MOHAN et al. [1982] proposes a novel interpretation of spherical sources by means of spectral analysis, although it again involves tedious mathematical operations. In this paper, we present an elegantly simple mathematical procedure to extract the parameters of the sphere, namely the depth to the centre, the polarization angle and the radius. This process involves the computation of the first horizontal derivative of the vertical magnetic anomaly, and hence the vertical derivative by means of the Hilbert transform. Making use of these two derivatives, the parameters are obtained by means of simple mathematical expressions.

The application of the Hilbert transform in the interpretation of ground-magnetic anomalies has been gaining greater importance of late. [NABIGHIAN 1972, MOHAN et al. 1982, SUNDARARAJAN 1982 and SUNDARARAJAN et al. 1983,

* Centre of Exploration Geophysics, Osmania University, Hyderabad—500 007, India
Manuscript received (revised version): 14 April, 1989

1985]. In all these papers the concept of amplitude of the analytic signal is used in precisely locating the origin. However, a mention can be made that this amplitude curve can also be used to delineate the sources from regional magnetic or gravity surveys. For all practical purposes, this method can also be realised by simple programming.

2. Vertical magnetic effect of a sphere

The geometry of the model is shown in *Figure 1*, with Z as the depth to the centre, R as the radius and Q as the magnetic polarization angle. The vertical magnetic effect of such a model is given by

$$V(x) = \frac{4}{3} \pi R^3 I \frac{(2Z^2 - x^2) \sin Q - 3xZ \cos Q}{(x^2 + Z^2)^{5/2}} \quad (1)$$

where I is the intensity of magnetisation [RAO et al. 1973].

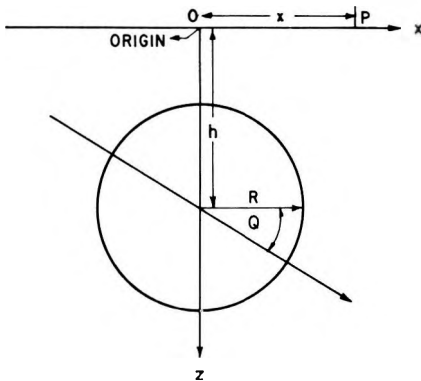


Fig. 1. Geometry of the spherical model

1. ábra. A modell geometriája

Рис. 1. Геометрия модели.

Differentiating equation (1) separately with respect to x and Z we obtain the first horizontal and vertical derivatives:

$$V_x(x) = \frac{4/3\pi R^3 I}{(x^2 + Z^2)^{7/2}} \cdot [(x^2 + Z^2) (2x \sin Q + 3Z \cos Q) + 5x((2Z^2 - x^2) \sin Q - 3xZ \cos Q)] \quad (2)$$

$$V_z(x) = \frac{4/3\pi R^3 I}{(x^2 + Z^2)^{7/2}} \cdot [(x^2 + Z^2) (4Z \sin Q - 3x \cos Q) - 5Z((2Z^2 - x^2) \sin Q - 3xZ \cos Q)] \quad (3)$$

According to NABIGHIAN [1972], the horizontal and vertical derivatives of a potential field forms a Hilbert transform pair. It can be represented here symbolically as:

$$V_x(x) \xleftarrow{H} V_z(x)$$

For mathematical convenience [SUNDARARAJAN 1982], either the positive or negative of the vertical derivative can be taken as the Hilbert transform of the horizontal derivative, since in both cases the magnitude of the field is the same, with a 180° phase difference to each other.

The relationship between the vertical and horizontal derivatives can be given in the form of Hilbert Transform equation as

$$V_z(x) = V_x(y) = \frac{1}{\pi} \cdot P \int_{-\infty}^{+\infty} \frac{V_x(x)}{x-y} dx \quad (4)$$

where P is Cauchy's principal value of the integral [THOMAS 1969].

This can be expressed in the form of convolution as:

$$V_z(x) = V_x(x) * \frac{1}{\pi} x \quad (5)$$

where $*$ denotes the convolution.

3. Interpretation

The location of the source—indispensable in geophysical interpretation—can be determined by solving a simple equation of the horizontal and vertical derivatives of the form

$$A(x) = [V_x(x)^2 + V_z(x)^2]^{1/2} \quad (6)$$

The function $A(x)$ is termed the amplitude curve of the analytic signal in geophysical literature [NABIGHIAN 1972 and SUNDARARAJAN 1982]. The graph of $A(x)$ attains its maximum value over the causative body. This is true for 2-D and 3-D structures.

At $x=0$, equations (2) and (3) reduce to,

$$V_x(0) = 3K \frac{\cos Q}{Z^4} \quad (7)$$

$$V_z(0) = 6K \frac{\sin Q}{Z^4} \quad (8)$$

where $K = \frac{4}{3} \pi R^3 I$.

Dividing equation (8) by equation (7) we obtain the angle of polarization as:

$$Q = \tan^{-1} \left(\frac{V_z(0)}{2V_x(0)} \right) \quad (9)$$

From Figs. 2 and 3 we see that the horizontal and vertical derivatives intersect at three distinct points. Therefore we can consider,

$$V_x(x) = V_z(x) \quad \text{at} \quad x = x_1, x_2 \text{ and } x_3$$

where x_1 , x_2 and x_3 are the abscissae of the points of the intersection of the derivatives, as cited above. Then, using equations (2) and (3) the polynomial equation will be

$$F(x) = 3x^3(\sin Q + \cos Q) + 3x^2Z(4 \cos Q - 3 \sin Q) - 12xZ^2(\sin Q + \cos Q) - 3Z^3(\cos Q - 2 \sin Q) \quad (10)$$

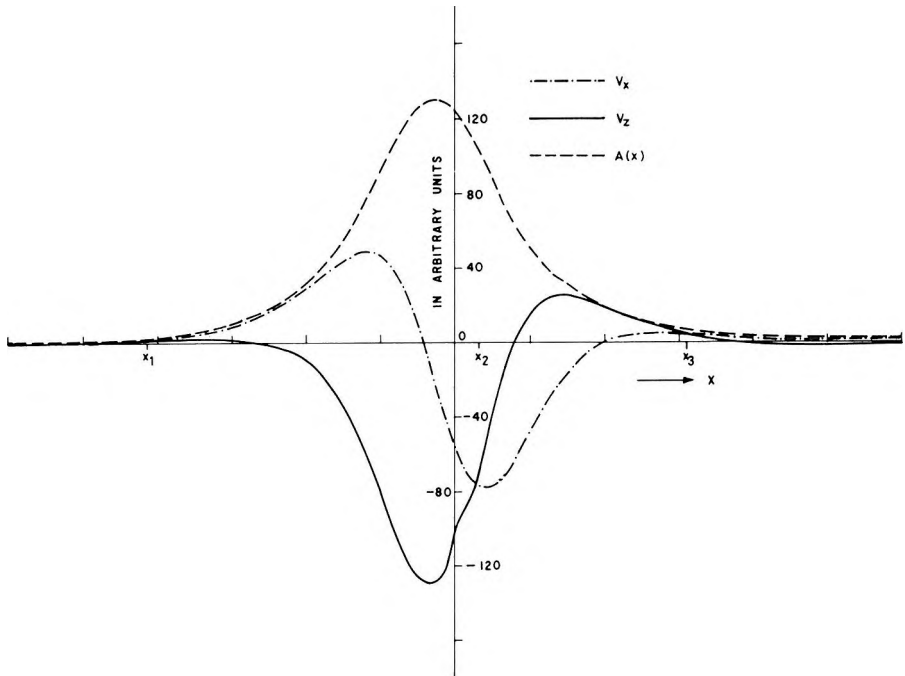


Fig. 2. The first horizontal (V_x) and vertical derivatives (V_z) of the vertical magnetic anomaly and their amplitude curve ($A(x)$) due to a sphere (Model I., for model parameters see Table I)

2. ábra. Egy gömbi ható (I. modell, paramétereit lásd az I. táblázatban) ΔZ anomáliájának első horizontális (V_x) és vertikális (V_z) deriváltja, valamint az ezekből képzett amplitudó görbe ($A(x)$)

Рис. 2. Первая горизонтальная (V_x) и вертикальная (V_z) производная аномалии ΔZ , обусловленной сферической возмущающей силой (модель I, параметры ее см. в табл. I), а также полученная по ним амплитудная кривая ($A(x)$).

According to NABIGHIAN [1972], the horizontal and vertical derivatives of a potential field forms a Hilbert transform pair. It can be represented here symbolically as:

$$V_x(x) \xleftrightarrow{H} V_z(x)$$

For mathematical convenience [SUNDARARAJAN 1982], either the positive or negative of the vertical derivative can be taken as the Hilbert transform of the horizontal derivative, since in both cases the magnitude of the field is the same, with a 180° phase difference to each other.

The relationship between the vertical and horizontal derivatives can be given in the form of Hilbert Transform equation as

$$V_z(x) = V_x(y) = \frac{1}{\pi} \cdot P \int_{-\infty}^{+\infty} \frac{V_x(x)}{x-y} dx \quad (4)$$

where P is Cauchy's principal value of the integral [THOMAS 1969].

This can be expressed in the form of convolution as:

$$V_z(x) = V_x(x) * \frac{1}{\pi} x \quad (5)$$

where $*$ denotes the convolution.

3. Interpretation

The location of the source—indispensable in geophysical interpretation—can be determined by solving a simple equation of the horizontal and vertical derivatives of the form

$$A(x) = [V_x(x)^2 + V_z(x)^2]^{1/2} \quad (6)$$

The function $A(x)$ is termed the amplitude curve of the analytic signal in geophysical literature [NABIGHIAN 1972 and SUNDARARAJAN 1982]. The graph of $A(x)$ attains its maximum value over the causative body. This is true for 2-D and 3-D structures.

At $x=0$, equations (2) and (3) reduce to,

$$V_x(0) = 3K \frac{\cos Q}{Z^4} \quad (7)$$

$$V_z(0) = 6K \frac{\sin Q}{Z^4} \quad (8)$$

where $K = \frac{4}{3} \pi R^3 I$.

Dividing equation (8) by equation (7) we obtain the angle of polarization as:

$$Q = \tan^{-1} \left(\frac{V_z(0)}{2V_x(0)} \right) \quad (9)$$

From *Figs. 2* and *3* we see that the horizontal and vertical derivatives intersect at three distinct points. Therefore we can consider,

$$V_x(x) = V_z(x) \quad \text{at} \quad x = x_1, x_2 \text{ and } x_3$$

where x_1 , x_2 and x_3 are the abscissae of the points of the intersection of the derivatives, as cited above. Then, using equations (2) and (3) the polynomial equation will be

$$F(x) = 3x^3(\sin Q + \cos Q) + 3x^2Z(4 \cos Q - 3 \sin Q) - 12xZ^2(\sin Q + \cos Q) - 3Z^3(\cos Q - 2 \sin Q) \quad (10)$$

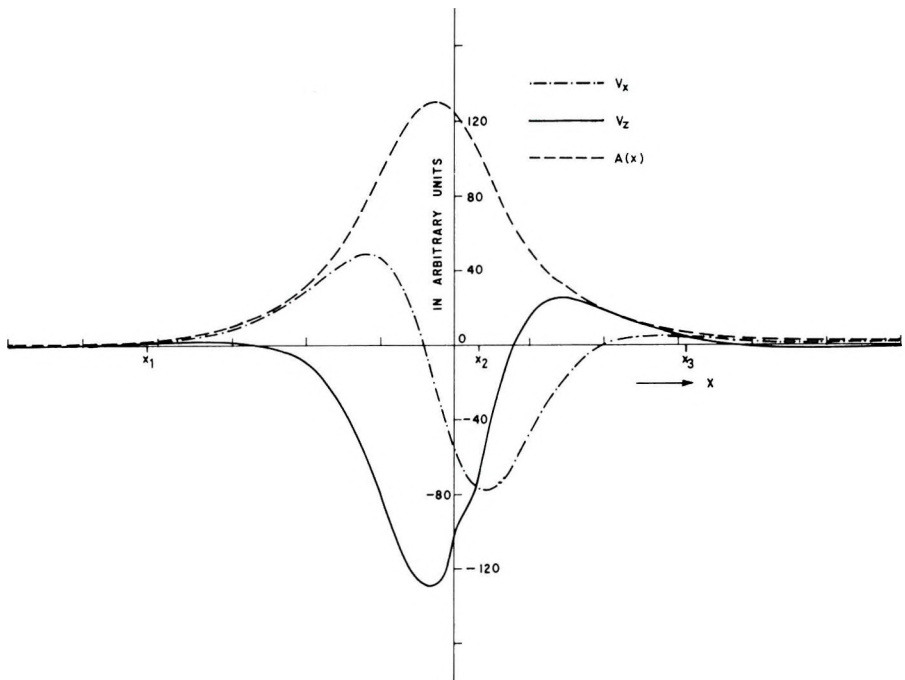


Fig. 2. The first horizontal (V_x) and vertical derivatives (V_z) of the vertical magnetic anomaly and their amplitude curve ($A(x)$) due to a sphere (Model I., for model parameters see Table I)

2. ábra. Egy gömbi ható (I. modell, paramétereit lásd az I. táblázatban) ΔZ anomáliájának első horizontális (V_x) és vertikális (V_z) deriváltja, valamint az ezekből képzett amplitudó görbe ($A(x)$)

Рис. 2. Первая горизонтальная (V_x) и вертикальная (V_z) производная аномалии ΔZ , обусловленной сферической возмущающей силой (модель I, параметры ее см. в табл. I), а также полученная по ним амплитудная кривая ($A(x)$).

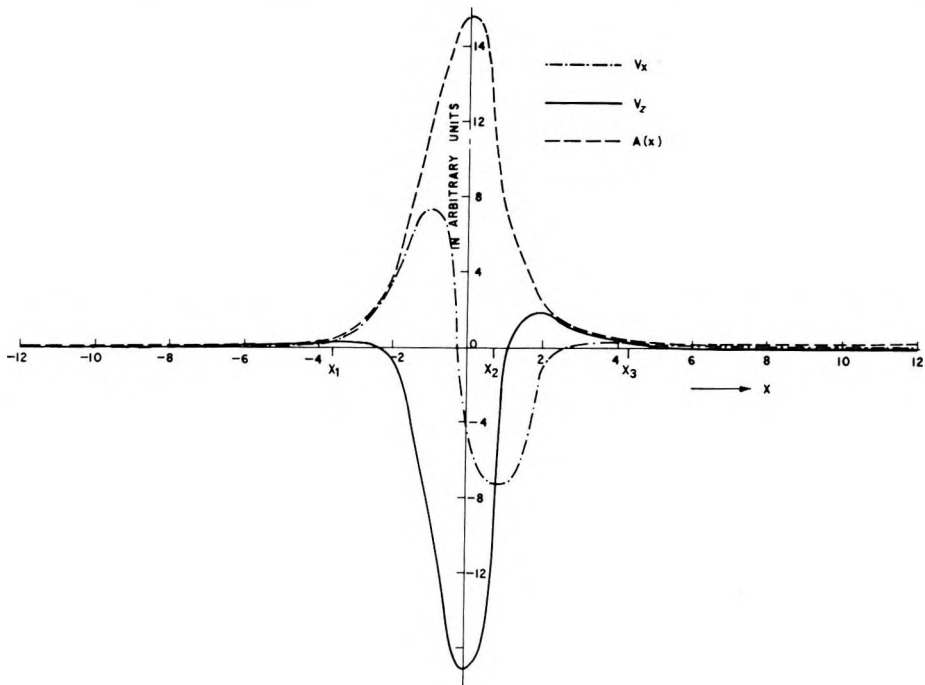


Fig. 3. The first horizontal (V_x) and vertical derivatives (V_z) of the vertical magnetic anomaly and their amplitude curve ($A(x)$) due to a sphere (Model II., for model parameters see Table I.)

3. ábra. Egy gömbi ható (II. modell, paramétereit lásd az I. táblázatban) ΔZ anomáliájának első horizontális (V_x) és vertikális (V_z) deriváltja, valamint az ezekből képzett amplitudó görbe ($A(x)$)

Рис. 3. Первая горизонтальная (V_x) и вертикальная (V_z) производная аномалии ΔZ , сферической возмущающей силы (модель II, параметры ее см. в табл. I), а также полученная по ним амплитудная кривая ($A(x)$).

This cubic equation in x could easily be solved for Z , i.e., the depth to the centre of the sphere is obtained as:

$$Z^3 = (A/B) x_1 \cdot x_2 \cdot x_3 \quad (11)$$

Where x_1 , x_2 and x_3 are the three real roots of equation (10), which also implies that equations (2) and (3) possess these roots. The constants A and B are given as:

$$A = \sin Q + \cos Q$$

$$B = \cos Q - 2 \sin Q$$

Since Q is already known, the depth Z to the centre of the sphere could easily be obtained from equation (11).

Squaring and adding equations (7) and (8) we get K as:

$$K = \frac{Z^4}{3} \left(\frac{V_x(0)^2 + V_z(0)^2}{4 - 3 \cos^2 Q} \right)^{1/2} \quad (12)$$

Thus, K yields either the radius (R) of the sphere or the intensity of magnetization (I) given as:

$$R = \left(\frac{3K}{4\pi I} \right)^{1/3} \quad (13)$$

$$I = \frac{3K}{4\pi R^3} \quad (14)$$

4. Theoretical examples

The procedure outlined above is demonstrated with two theoretical examples (*Table I*). Using equations (2) and (3), the first horizontal and vertical derivatives of the magnetic field are computed and shown in Figures 2 and 3. These figures include the amplitude curve of the derivatives. It is observed that there are three distinct abscissae at the points of intersection of the horizontal and vertical derivatives.

The parameters, namely the magnetic polarization angle (Q), the depth to the centre of the sphere (Z) and the radius (R), are evaluated using equations (9), (11) and (13). The results are presented in *Table I* and it can be observed that the assumed and interpreted values agree very closely, thereby supporting the validity of the method.

	Parameters	Q^*	Z^*	R^*
MODEL I	Assumed values	45	2.00	1.00
	Evaluated values	45	1.96	1.00
MODEL II	Assumed values	60	2.50	0.75
	Evaluated values	60.14	2.49	0.75

(* in arbitrary units and + in degrees)

Table I. Theoretical examples

I. táblázat. Elméleti példák

Таблица I. Теоретические примеры.

5. Field examples

The technique under discussion is tested on two field examples, the first pertaining to the vertical component of the magnetic field in the Bankura area of West Bengal, India (Fig. 4), and the second to the Louga anomaly in the USA (Fig. 6, after NETTLETON 1976). Both anomalies can be approximated by spherical models.

(a) The Bankura Anomaly, West Bengal, India

The total length of the Bankura anomaly is around 9.28 km and it is digitized into 100 equal parts at an interval of 92.8 meters. The first horizontal derivative is computed manually and then it is convolved with $(1/x)$ to obtain the discrete Hilbert transform. Also the amplitude curve is computed, using equation (6). The horizontal derivative, the discrete Hilbert transform and the amplitude curve are shown in Fig. 5. Using equations (9), (11) and (13) the parameters, namely the polarization angle (Q), the depth to the centre of the sphere (Z) and the radius of the sphere are evaluated. Thus, the results obtained (Table II) are compared with that of RAO et al. [1977], and with those obtained by the method of MOHAN et al. [1982].

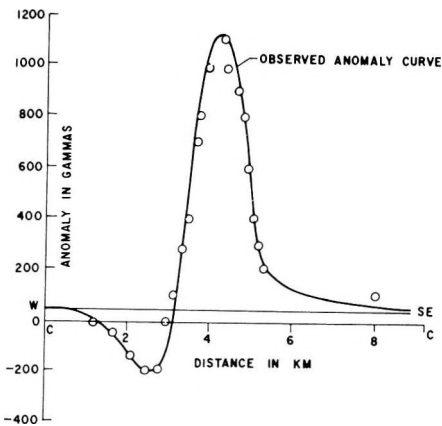


Fig. 4. The vertical component of the magnetic anomaly in the Bankura area of West Bengal, India

4. ábra. Nyugat Bengáliában Bankura területen (India) mért ΔZ anomália

Рис. 4. Аномалия ΔZ , замеренная в территории Банкура в Западной Бенгалии (Индия).

THE BANKURA ANOMALY, WEST BENGAL, INDIA

Parameters	Z (km)	R (km)	Q
Hilbert Transform method	1.252	1.099	41.52°
Spectral Analysis method [MOHAN et al. 1982]	1.312	0.993	41.50°
RAO et al. [1977]	1.32		

Table IIa. Field examples IIa. táblázat. Terepi példák Таблица IIa. Полевые примеры.

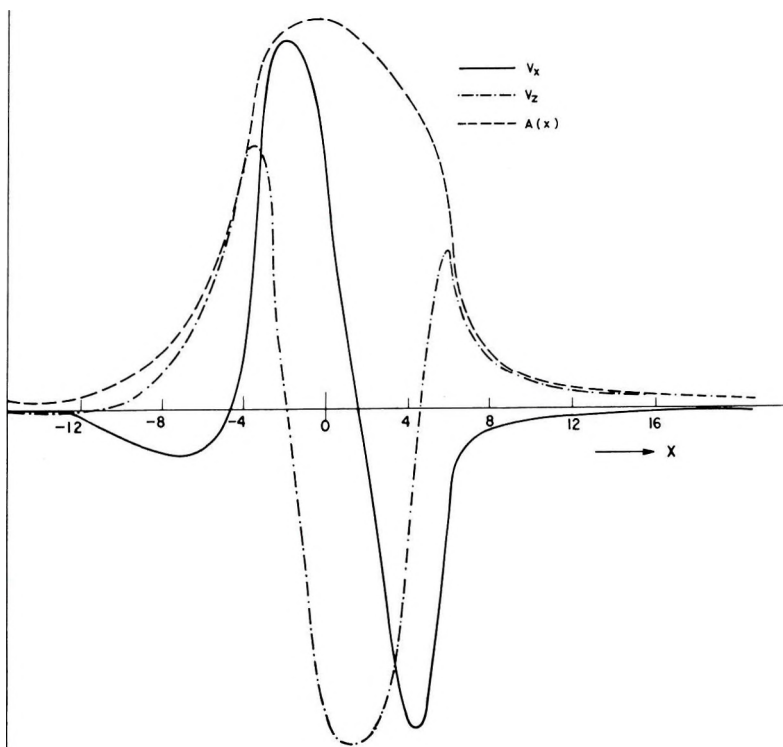


Fig. 5. The first horizontal derivative (V_x), the Hilbert transform (V_z) and their amplitude curve ($A(x)$) of the vertical component of the magnetic anomaly in the Bankura area of West Bengal, India

5. ábra. A Bankura ΔZ -anomália első horizontális deriváltja (V_x), ennek Hilbert transzformáltja (V_z) és az ezekből képzett amplitúdó görbe ($A(x)$)

Рис. 5. Первая горизонтальная производная (V_x) аномалии ΔZ в Банкура, ее вид (V_z) по трансформации Гильберта и полученная по ним аномальная кривая ($A(x)$).

(b) *The Louga Anomaly, USA*

Figure 6 shows the profile of the vertical magnetic anomaly on a north–south line and a cross section of the probable source, a heavily magnetised spherical body, after NETTLETON [1976]. The entire length of the profile of around 65 km is digitised into 101 equal parts, and then the horizontal derivative is computed. As in the previous case the vertical derivative and the amplitude curve have been calculated and shown in Figure 7. The parameters are evaluated based on the procedure detailed in the text. The results obtained agree very well with that of NETTLETON [1976], presented in Table II. In addition, these results are also compared with those of MOHAN et al. [1986], who used the Mellin transform method for the integration of the gravity anomaly.

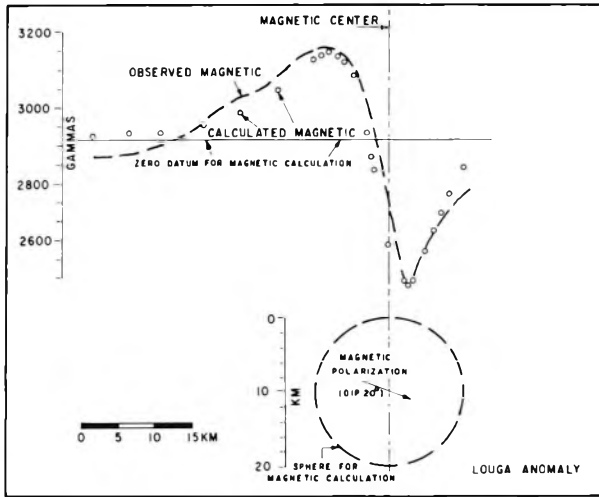


Fig. 6. The vertical component of the magnetic anomaly of Louga, USA, and the probable source [after NETTLETON 1976]

6. ábra. A Louga (USA) ΔZ -anomália és a valószínű ható [NETTLETON 1976 nyomán]

Рис. 6. Аномалия ΔZ в Луга (США) и вероятная возмущающая сила [по Неттлетону, 1976].

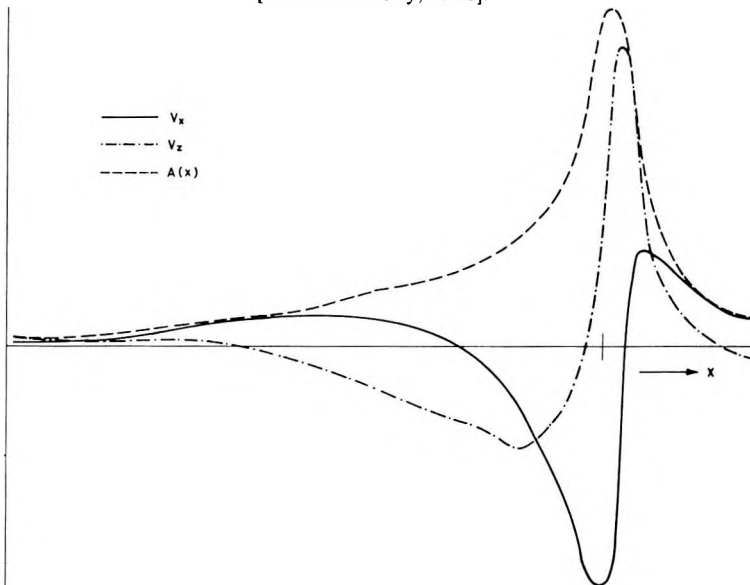


Fig. 7. The first horizontal derivative (V_x), the Hilbert transform (V_z) and the amplitude curve ($A(x)$) of the vertical component of the magnetic anomaly of Louga, USA

7. ábra. A Louga (USA) mágneses ΔZ -anomália első horizontális deriváltja (V_x), ennek Hilbert transzformáltja (V_z) és az ezekből képzett amplitudó görbe ($A(x)$)

Рис. 7. Первая горизонтальная производная (V_x), ее вид по трансформации Гильберта (V_z) и полученная по ним амплитудная кривая ($A(x)$).

THE LOUGA ANOMALY, USA

Parameters	Z (km)	Q
Hilbert Transform method of the authors	9.78	19.40°
The method of NETTLETON [1976]	9.88	20.00°
Mellin transform method [MOHAN et al. 1986]	9.31	

Table IIb. Field examples IIb. táblázat. Terepi példák Таблица IIb. Полевые примеры.

6. Conclusions

The method of interpretation of magnetic anomalies over 3-D sources by the Hilbert transform is very accurate, reliable, simple and effective in its approach. The amplitude curve of the analytic signal is extremely valuable for the interpretation of sources of arbitrary shape as well.

REFERENCES

- GAY S. P. 1963: Standard curves for interpretation of magnetic anomalies over long tabular bodies. *Geophysics* **28**, 2, pp. 161–200
- HENDERSON R. G. and ZIETZ I. 1948: Analysis of total magnetic-intensity anomalies produced by point and line sources. *Geophysics* **13**, 3, pp. 428–436
- HENDERSON R. G. and ZIETZ I. 1967: Magnetic-doublet theory in the analysis of total intensity anomalies, in *Mining Geophysics*. Vol. II. 490. SEG
- MOHAN N. L., SUNDARARAJAN N. and SESHAGIRI RAO S. V. 1982: Interpretation of some two-dimensional magnetic bodies using Hilbert transforms. *Geophysics* **47**, 3, pp. 376–387
- MOHAN N. L., ANANDABABU L. and SESHAGIRI RAO S. V. 1986: Gravity interpretation using the Mellin transform. *Geophysics* **51**, 1, pp. 114–122
- NABIGHIAN M. N. 1972: The analytic signal of two-dimensional magnetic bodies with polygonal cross-section; its properties and use for automated anomaly interpretation. *Geophysics* **37**, 3, pp. 507–517
- NETTLETON L. L. 1976: *Gravity and magnetics in oil prospecting*. McGraw-Hill, New York
- RADHAKRISHNA MURTHY I. V. 1974: Analysis of total field anomalies of magnetised spherical ore deposits. *Geoprospection* **12**, 1, pp. 41–50
- RAO B. S. R., RADHAKRISHNA MURTHY I. V. and VISWESWARA RAO C. 1973: A computer program for interpreting vertical magnetic anomalies of spheres and horizontal cylinders. *Pure and Applied Geophysics* **110**, pp. 2056–2065
- RAO B. S. R., PRAKASA RAO T. K. S. and KRISHNA MURTHY A. S. 1977: A note on magnetized spheres. *Geophysical Prospecting* **25**, 4, pp. 746–757
- SMELLIE D. W. 1956: Elementary approximations in aeromagnetic interpretation. *Geophysics* **21**, 4, pp. 1021–1040
- SUNDARARAJAN N. 1982: *Interpretation techniques in Geophysical Exploration using the Hilbert transform*. Ph. D. Thesis submitted to Osmania University, Hyderabad, India
- SUNDARARAJAN N., MOHAN N. L. and SESHAGIRI RAO S. V. 1983: Gravity interpretation of two-dimensional fault structures using Hilbert transforms. *Journal of Geophysics* **53**, 1, pp. 34–41
- SUNDARARAJAN N., MOHAN N. L., VIJAYA RAGHAVA M. S. and SESHAGIRI RAO S. V. 1985: Hilbert transform in the interpretation of magnetic anomalies of various components due to a thin infinite dike. *Pure and Applied Geophysics* **123**, 4, pp. 557–566
- THOMAS J. B. 1969: *An introduction to statistical communication theory*. John Wiley, New York

**GÖMB ALAKÚ HATÓK OKOZTA MÁGNESES ANOMÁLIÁK ÉRTELMEZÉSE
– EGY HILBERT TRANSZFORMÁCIÓS MÓDSZER**

N. SUNDARARAJAN, B. UMASHANKAR, N. L. MOHAN és S. V. SESHAGIRI RAO

Gömb alakú hatók okozta mágneses anomáliák közvetlen értelmezésére dolgoztunk ki egy módszert a mágneses tér első horizontális és vertikális deriváltjai felhasználásával. A tér vertikális deriváltját Hilbert transzformációval számítottuk ki a horizontális deriváltból. A gömb paramétereit a deriváltak metszéspontjai abszcisszái függvényeként határoztuk meg. Két elméleti példán bizonyítjuk a módszer használhatóságát. Mérsékeltlen jó eredményeket nyertünk a Nyugat-Bengáliai Bankura és az egyesült államokbeli Louga területen, a gömb alakú ható okozta ΔZ -anomáliák értelmezése során. Ez az értelmezés alkalmazható ΔH - és ΔT -anomáliákra is. Gravitációs és természetes potenciál anomáliákat is értelmezhetünk hasonló módszerekkel. A módszer előnye, hogy könnyen programozható.

**ИНТЕРПРЕТАЦИЯ МАГНИТНЫХ АНОМАЛИЙ, ВЫЗВАННЫХ СФЕРИЧЕСКИМИ
ВОЗМУЩАЮЩИМИ СИЛАМИ, МЕТОДОМ ТРАНСФОРМАЦИИ ГИЛЬБЕРТА**

X. СУНДАРАРАДЖАН, Б. УМАШХАНКАР, Н. Л. МОХАН и С. В. СЕСХАГИРИ РАО

Для непосредственной интерпретации аномалий выработан метод, основанный на использовании первых вертикальных и горизонтальных производных магнитного поля. Вертикальная производная рассчитывается из горизонтальной производной трансформацией Гильберта. Параметры сферы определяются как зависимости абсцисс точек пересечения производных. Возможность применения метода доказывается на двух теоретических примерах. Относительно хорошие результаты были получены для Банкура (Западная Бенгалия) и для Луга (США) при интерпретации аномалий ΔZ . Метод используем и для интерпретации аномалий ΔH и ΔT . Подобными методами возможна также интерпретация гравитационных аномалий и аномалий естественного потенциала. Преимущество метода – легкая возможность компьютеризации.

MAGNETIC SUSCEPTIBILITY ANISOTROPY MEASUREMENTS ON MIOCENE IGIMBRITES FROM BÜKKALJA, HUNGARY

Róbert BORDÁS*

The results of susceptibility anisotropy measurements of Miocene ignimbrite samples from 4 localities in Bükkalja, Northeastern Hungary, are presented. It is concluded that the magnetic fabric of the rocks was affected by Miocene or younger stress fields. Using the intermediate susceptibility axes two compression directions can be identified: 11° – 191° for Bogács (upper ignimbrite level) and 135° – 315° for Sály (lower ignimbrite level) and these are in good agreement with compression directions derived from microtectonic measurements.

Keywords: magnetic susceptibility, anisotropy, Miocene, ignimbrite, Hungary, Bükk Mountains

1. Introduction

The anisotropy of low-field magnetic susceptibility can provide information about the magnetic fabric of rocks. The principal susceptibility directions are related to the geological structural elements and the stress field, e.g. the schistosity plane and bedding plane, respectively, the compression axes, etc. Several authors have used anisotropy data in geological structural analysis [e.g. HROUDA, 1979, 1982; RATHORE 1985; HIRT et al. 1988; ROCHETTE 1988].

In the Bükk Mountains the existing fault zones as well as the distribution of the Miocene volcanism indicate a rather complicated stress pattern. The ignimbrites of the Bükkalja that we measured also show clear magnetic anisotropy which we attempt to interpret here in structural geological terms.

2. Geology and sampling

There was a large-scale and recurring volcanic activity in NE Hungary during the Miocene age. Rhyolitic and dacitic tuffs were forced up during eruptions which covered the whole Bükkalja area and even the Bükk Mountains. Ignimbrites formed two levels in the rhyolite tuff:

- a) the lower level resembles rhyolitic lavas and contains many dark grey perlitic or pitchstone inclusions of fluidal texture;
- b) the upper level is of dacitic composition. The rock is hard, dark grey, brown or red, vitrophyric-porphyrific, contains pitchstone and often has a fluidal texture [BALOGH and RÓNAI 1965].

* Eötvös Loránd Geophysical Institute of Hungary, Budapest P.O.B 35, H-1440, Hungary
Manuscript received (revised version): 22 March, 1989

Stratigraphical dating of the Bükkalja ignimbrites is problematic. BALOGH and RÓNAI [1965] claim that the two types of ignimbrites are of different age: a) is considered as lower Helvetian (Ottangian) and b) as Tortonian (Badenian).

Radiometric dates range from about 60 to 12 Ma [HÁMOR et al. 1979].

78 independently oriented samples were drilled from 4 localities (Bogács: upper ignimbrite level; Kács, Sály and Kisgyőr: lower ignimbrite level) both for palaeomagnetic and anisotropy measurements (Fig. 1). The samples were collected from several sampling points at Bogács (4 points), Sály (2), Kisgyőr (4) and from one point at Kács. Either the visible fabric and colour of the rocks at these points was different, or the sampling points represent different blocks of rock. One to four standard size specimens were cut from each sample.

The macroscopic texture of the ignimbrites showed well developed foliation at all localities. This foliation plane is subhorizontal, the dip ranges from 0 to 20 degrees.

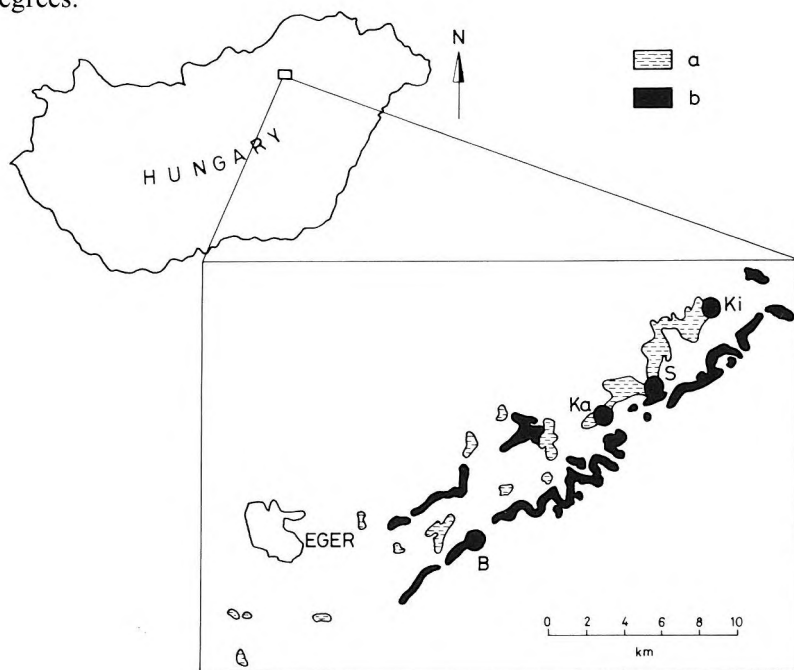


Fig. 1. Ignimbrite outcrops in the Bükkalja region, from BALOGH and RÓNAI [1965]. a: lower ignimbrite level; b: upper ignimbrite level. Dots—sampling localities: B — Bogács, Ka — Kács, S — Sály, Ki — Kisgyőr

1. ábra. Ignimbrit feltárások a Bükkalján BALOGH és RÓNAI [1965] után. a: alsó ignimbrit szint; b: felső ignimbrit szint. Pontok — mintavételi helyek: B — Bogács, Ka — Kács, S — Sály, Ki — Kisgyőr

Рис. 1. Игнимбритовые обнажения в Бюккалья по Балогу и Ронаи [1965]. а: нижний игнимбритовый горизонт; б: верхний игнимбритовый горизонт. Точки — места взятия проб: В — Богач, Ка — Кач, С — Шай, Ки — Кишдьер.

3. Susceptibility anisotropy and data evaluation

The magnetic susceptibility is a general property of rocks. In a weak magnetic field, H , there is a linear relationship between H and the induced magnetization, J , as follows:

$$J = \mu_0 \mathbf{k}H$$

where $\mu_0 = 4 \times 10^{-7}$ A/m and \mathbf{k} is a symmetric tensor of second rank, called the 'susceptibility tensor' [HROUDA 1982]. Tensor \mathbf{k} can be represented by a triaxial ellipsoid (susceptibility ellipsoid) of which the directions and length of the principal axes define the directions and the magnitudes of the so called principal susceptibilities (κ_{\max} , κ_{inter} , κ_{\min}), respectively.

The following anisotropy parameters have been found useful [HROUDA 1982]:

anisotropy degree:

$$P = \frac{\kappa_{\max}}{\kappa_{\min}},$$

magnetic lineation:

$$L = \frac{\kappa_{\max}}{\kappa_{\text{inter}}},$$

magnetic foliation:

$$F = \frac{\kappa_{\text{inter}}}{\kappa_{\min}},$$

ellipsoid form:

$$E = \frac{F}{L} = \frac{\kappa_{\text{inter}}^2}{\kappa_{\max} \kappa_{\min}},$$

and

mean susceptibility:

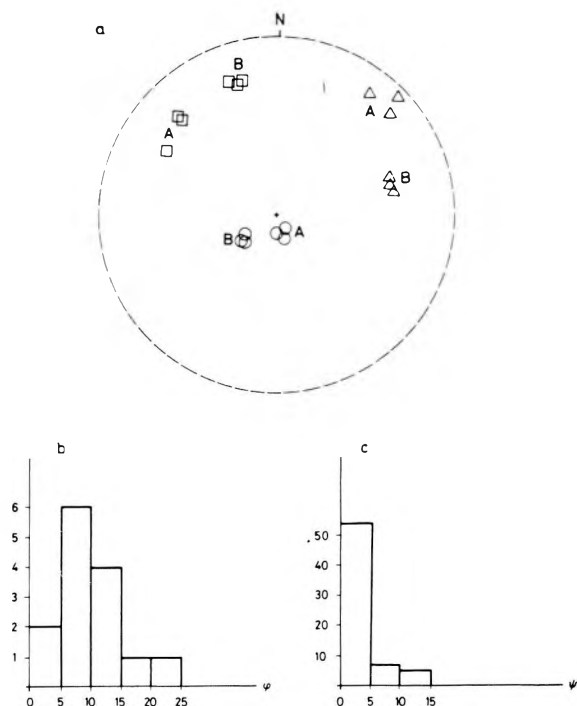
$$\bar{\kappa} = \frac{\kappa_{\max} + \kappa_{\text{inter}} + \kappa_{\min}}{3}.$$

It is these parameters through which the magnetic anisotropy data can be related to the geological structure.

The directional susceptibility of the specimens was measured on a low-field susceptibility bridge (Kappabridge KLY-2) which is capable of measuring susceptibilities up to 2×10^{-1} SI with a precision of 5×10^{-8} (or 0.1%).

15 directional susceptibilities are measured [JELÍNEK 1977] and the elements of matrix \mathbf{k} , its eigenvalues and eigenvectors determined by a computer program written for on-line measurements with an IBM PC/XT. A least square approach is used for estimating the standard error of the measurement, the error angles of the principal directions, etc. An F-test is performed to decide whether the anisotropy of the specimen is significant. The principal directions are plotted on a stereographic projection for each site or locality to monitor the grouping of the principal directions in the geographic and/or tectonic system.

In the course of the measurements it turned out that the principal directions and the respective anisotropy parameters of the sister specimens differ considerably. To determine the origin of these differences the measurements were repeated three times and it was found that the three measurements of the *A* sister differ significantly from those of the *B* sister, i.e. the principal directions within the sister are closer than the ones between sisters (*Fig. 2*). The same is apparent in the variability of the anisotropy parameters (*Table I*). It can be concluded that these features are caused by the different magnetic fabric of the sisters (e.g. inhomogeneous distribution of ferromagnetic minerals) and not by measuring errors. To eliminate the effect of heterogeneity, the anisotropy tensors of the sisters were averaged for each sample and the averaged tensors served as input for a statistics program. The latter was written for the evaluation of the anisotropy data on a group of specimens representing a geological body making use of Jelínek's statistical approach [JELÍNEK 1978]. The mean anisotropy tensor and its parameters were determined for each sampling point and locality. A T^2 -statistics was used for characterizing the significance of the anisotropy at the 0.05 probability level.



Measurements Sister	Mean susc. (10^{-6} SI)			P			L			F		
	1	2	3	1	2	3	1	2	3	1	2	3
A	171	169	170	1.030	1.030	1.029	1.006	1.007	1.006	1.024	1.022	1.022
B	156	155	155	1.055	1.052	1.055	1.021	1.020	1.020	1.033	1.032	1.034

Table I. Mean susceptibility and anisotropy parameters of three repeated measurements of two sister specimens (*A* and *B*, see Fig. 2 for corresponding principal directions). $\bar{\kappa}$: mean susceptibility; P : anisotropy degree; L : magnetic lineation, F : magnetic foliation

I. táblázat. Egy minta két példányán végzett háromszori mérés átlag szuszceptibilitásai és anizotrópia paraméterei (*A* és *B* mintapéldányok, a megfelelő főirányokat lásd a 2. ábrán). $\bar{\kappa}$: átlag szuszceptibilitás; P : anizotrópia fok; L : mágneses lineáció, F : mágneses foliáció

Таблица I. Параметры анизотропии и средние чувствительности трехкратного измерения, выполненного на двух образцах пробы. (*A* и *B* – образцы, соответствующие главные направления см. на рис. 2). $\bar{\kappa}$: средняя восприимчивость; P : степень анизотропии; L : магнитная линейность; F : магнитная фолиация.

Fig. 2. Repeatability of anisotropy measurements (cf. Table I)

- a) Principal directions from three repeated measurements of sisters *A* and *B* of sample No. 4938. Stereographic projection, lower hemisphere. Squares: maximum, triangles: intermediate, circles: minimum susceptibility directions
- b) Frequency distribution of angular distance (φ) between the minimum directions of sisters
- c) Frequency distribution of angular distance (ψ) between the minimum directions of repeated measurements of one specimen

2. ábra. Anizotrópia mérések ismételtősége (ld. I. táblázat)

- a) A 4938 sz. minta *A* és *B* példányain végzett háromszori mérés főirányai. Sztereografikus vetület, alsó félgömb. Négyzetek: maximum, háromszögek: közepes, körök: minimum szuszceptibilitás irányok
- b) Mintapéldányok minimum irányai közötti szögtávolság (φ) gyakorisági eloszlása
- c) Egy mintapéldány ismételt méréseinek minimum irányai közötti szögtávolság (ψ) gyakorisági eloszlása

Рис. 2. Повторяемость измерений анизотропии (см. таблицу I).

- a) Главные направления трехкратного измерения, проведенного на образцах *A* и *B* пробы N 4938. Стереграфическая проекция, нижняя полусфера. Направления максимальной (квадраты), средней (треугольники), минимальной (круги) восприимчивости.
- b) Частотное распределения углового расстояния (φ) между минимальными направлениями.
- c) Частотное распределение углового расстояния (ψ) между минимальными направлениями повторных измерений на одном образце пробы.

4. Results

The mean susceptibilities have lower values for the lower ignimbrite level (Kács, Sály, Kisgyőr: $1.5 - 4 \times 10^{-4}$ SI) than for the upper level (Bogács: $2 - 6 \times 10^{-3}$ SI). The anisotropy degree is rather low: 1.02 – 1.07 for the lower level and 1.01 – 1.03 for the upper level. The natural remanent magnetization (NRM) intensities vary between 2×10^{-2} and 3×10^{-1} A/m for the lower level while the upper level shows a variation in intensity between 10^{-1} and 10^0 A/m.

Fig. 3 shows the variation of the anisotropy degree with the mean susceptibility (a), respectively the NRM intensity (b) for each sampling point. At Bogács a weak correlation is suggested while for the other three localities there is no correlation either between the anisotropy degree and the mean susceptibility or between the anisotropy degree and the NRM intensity.

Fig. 4 shows the NRM intensity versus mean susceptibility for each specimen of the lower ignimbrite level. As the mean susceptibility is below 10^{-3} SI units, it can be assumed that the susceptibility anisotropy is dominated by the paramagnetic minerals present [ROCHETTE 1988]. The trend of the NRM intensity versus mean susceptibility leads to an estimation of the paramagnetic susceptibility to be about 10^{-4} SI units.

Despite the low anisotropy degrees found, the principal directions, especially the minimum directions, form well defined groups. The latter are near vertical and the magnetic foliation plane (defined by the maximum and intermediate directions) is subhorizontal, i.e. very close to the macroscopic foliation observed in the field.

Fig. 5 shows two typical patterns of the distribution of the principal directions. At Bogács (*Fig. 5a*) all the three directions cluster while at Kács (*Fig. 5b*) only the minimum directions group and the maximum and intermediate directions show no preferred orientation in the foliation plane. From the other two localities, the principal directions resemble the first pattern at Sály and the second one at Kisgyőr.

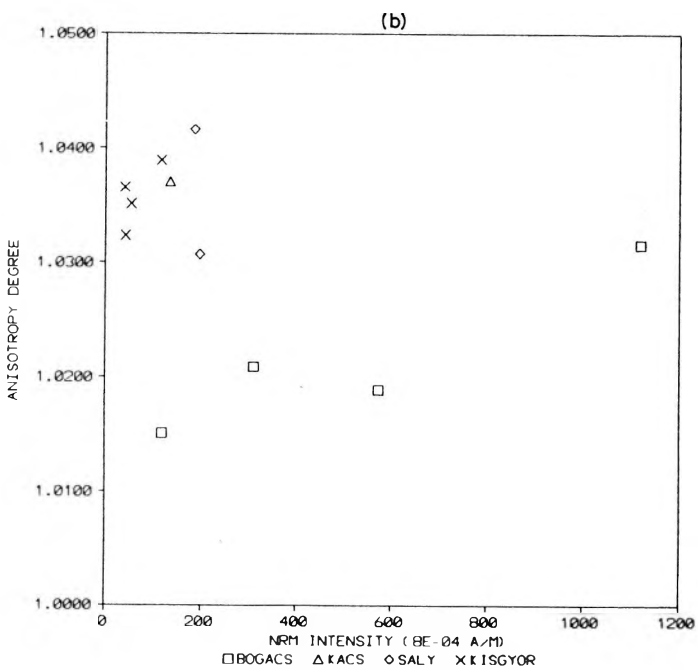
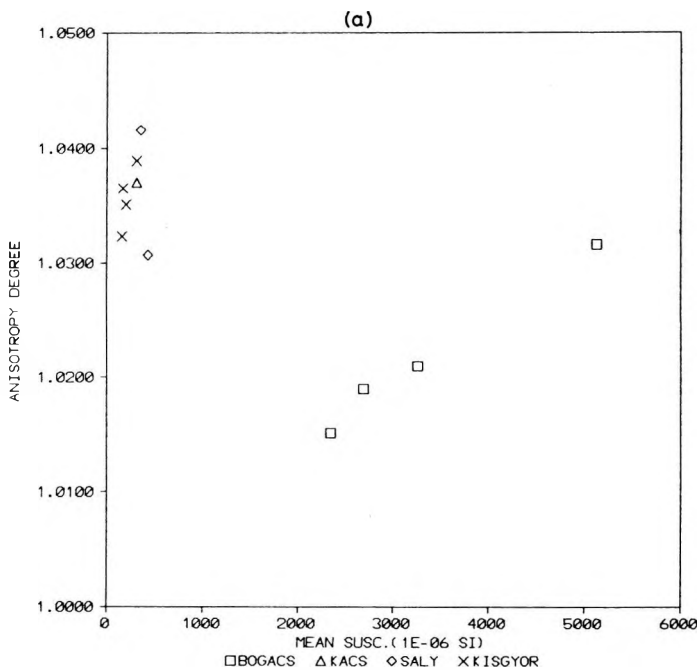
Fig. 6 is an $L - F$ (lineation vs foliation) diagram for the studied localities from which it is clear that the foliation is dominant over lineation for all localities. However, the foliation/lineation ratio (ellipsoid shape) is lower for Bogács and Sály than for the other two localities.

Fig. 3. Anisotropy distribution of sampling point means
a) versus mean susceptibility
b) versus NRM intensity

3. ábra. Mintavételi pontok átlagértékeinek anizotrópia fok eloszlása
a) az átlag szuszceptibilitás függvényében
b) a természetes remanens mágnesezettség (NRM) függvényében

Рис. 3. Распределение степени анизотропии средних значений по точкам отбора проб.
а) в зависимости от средней восприимчивости
б) в зависимости от естественной остаточной намагниченности (NRM).





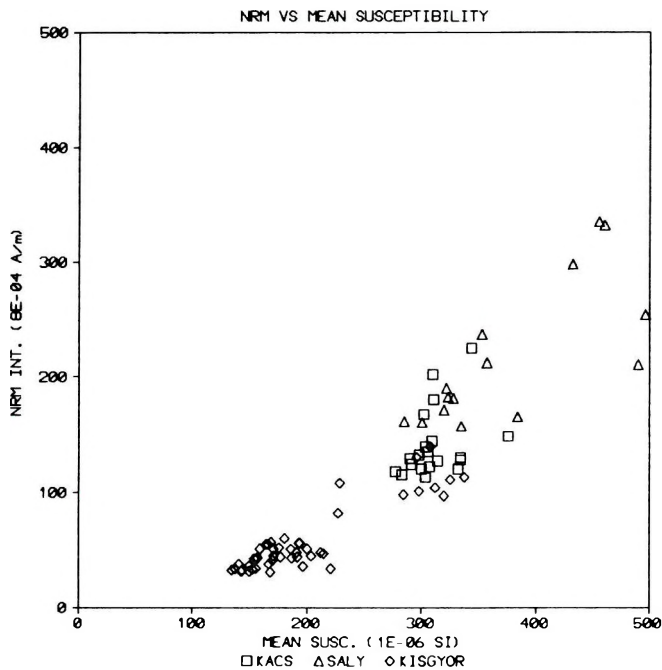


Fig. 4. NRM intensity vs mean susceptibility for the susceptibility range $< 10^{-3}$ SI units (specimen values)

4. ábra. NRM intenzitás az átlag szuszceptibilitás függvényében a $< 10^{-3}$ SI egység szuszceptibilitás tartományra (mintapéldányok értékei)

Рис. 4. Интенсивность естественной остаточной намагниченности (NRM) в зависимости от средней восприимчивости для области $< 10^{-3}$ SI (значения по образцам).

Table II summarizes the anisotropy results of the studied localities giving the anisotropy parameters and the principal directions, in polar coordinates (azimuth/inclination), of the mean anisotropy tensor for each locality with the confidence angles between the pairs of the principal directions. The lower E12 confidence angles for Bogács and Sály show that the clustering of the intermediate and maximum principal directions (Fig. 5a) is statistically significant.

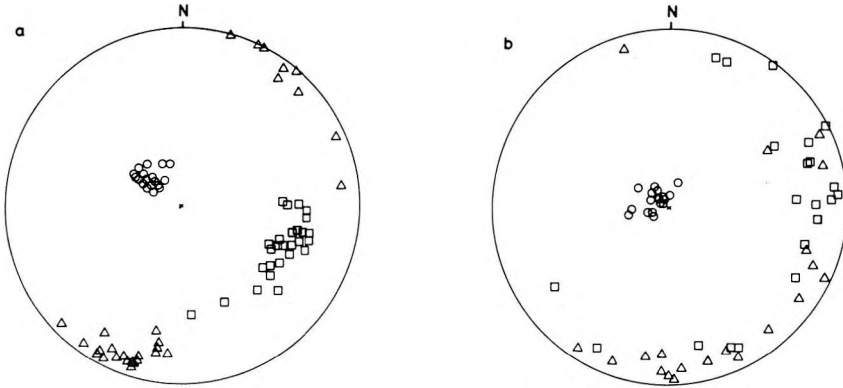


Fig. 5. Principal directions of specimens from a sampling point of Bogács (a) and Kács (b). Stereographic projection, lower hemisphere. Squares: maximum, triangles: intermediate, circles: minimum susceptibility directions

5. ábra. Bogács (a) és Kács (b) egy mintavételi pontjáról származó mintapéldányok főirányai. Sztereografikus vetület, alsó félgömb. Négyzetek: maximum, háromszögek: közepes, körök: minimum szuszceptibilitás irányok

Рис. 5. Главные направления образцов, взятых с участков Богач (а) и Кач (b). Стратиграфическая проекция, нижняя полусфера. Направления максимальной (квадраты), средней (треугольники), минимальной (круги) восприимчивости.

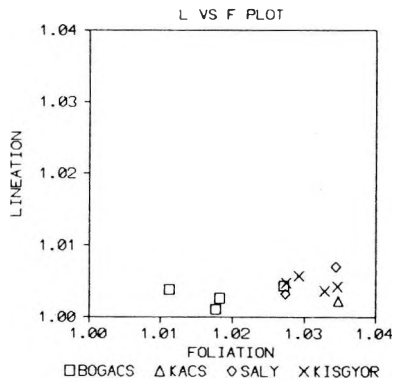


Fig. 6. Lineation vs foliation plot for sampling point means

6. ábra. Lineáció–foliáció diagram mintavételi pontok átlagértékeire

Рис. 6. Диаграмма линейность–фолиация средних значений по точкам отбора проб.

Locality	Spec./ Sample	Mean susc. (10 ⁻⁶ SI)	P	L	F	E	Principal directions (D/I)			Confidence angles		
							MAX	INTER	MIN	E12	E23	E31
Bogács	63/30	3637	1.0225	1.0022	1.0202	1.0180	98.9/19.0	191.0/5.8	297.3/70.1	30.7	2.6	4.6
Kács	21/15	310	1.0371	1.0023	1.0348	1.0324	75.4/8.3	166.1/4.2	282.6/80.7	47.9	1.1	4.4
Sály	15/8	389	1.0359	1.0050	1.0308	1.0257	45.2/0.1	135.2/1.7	312.5/88.3	26.0	1.3	7.3
Kisgyőr	46/25	201	1.0336	1.0023	1.0313	1.0289	311.5/12.0	42.0/2.2	142.3/77.8	46.3	2.4	3.2

Table II. Anisotropy results for the localities studied. N/N_0 : number of specimens/samples; $\bar{\kappa}$: mean susceptibility; P : anisotropy degree; L : magnetic lineation; F : magnetic foliation; E : ellipsoid shape. κ_{\max} , κ_{inter} , κ_{\min} : principal directions in polar coordinates (azimuth/inclination).

E12, E23 and E31 are confidence angles between two principal directions (1—maximum, 2—intermediate, 3—minimum)

II. táblázat. Anizotrópia eredmények a vizsgált mintavételi helyekre. N/N_0 : példányok/minták száma; $\bar{\kappa}$: átlag szuszceptibilitás; P : anizotrópia fok; L : mágneses lineáció; F : mágneses foliáció; E : ellipszoid alak. κ_{\max} , κ_{inter} , κ_{\min} : főirányok polárkoordinátákban (azimut/inclináció). E12, E23, és E31 két főirány közti konfidenciaszögek (1—maximum, 2—közepes, 3—minimum)

Таблица II. Результаты анизотропии по участкам отбора проб. N/N_0 : количество образцов/проб; $\bar{\kappa}$: средняя восприимчивость; P : степень анизотропии; L : магнитная линейность; F : магнитная фолиация; E : эллипсоидальная форма; κ_{\max} , κ_{inter} , κ_{\min} : главные направления в полярных координатах (азимут/склонение). E12, E23, и E31 – доверительные углы по двум главным направлениям (1—максимум, 2—среднее значение, 3—минимум).

5. Discussion and conclusion

Palaeomagnetic and rock magnetic experiments of the samples, which will be reported elsewhere, show that the main carriers of the remanence are minerals of the magnetite type. In this case the susceptibility anisotropy is controlled by the shape anisotropy and the preferred orientation of the longer axes of the grains [HROUDA 1982].

The high mean susceptibility values as well as the existing correlation between the anisotropy degree and the mean susceptibility and between the anisotropy degree and the NRM intensity for the upper ignimbrite level, show that the susceptibility anisotropy at Bogács must be caused predominantly by ferromagnetic minerals. However, for the localities of the lower level there is no significant correlation between these parameters, but the NRM intensity increases with the mean susceptibility. This supports the hypothesis that the paramagnetic contribution plays a dominant role in the anisotropy of the lower level.

Both the magnetic and the macroscopic foliation is subhorizontal, with the minimum susceptibility axes being very close to the normal of the visible foliation plane as with sediments deposited in a low energy environment. However, the clustering of the maximum and intermediate axes in the foliation plane shows that the anisotropy of the ignimbrites was most probably affected by some additional orientation mechanism. The clustering has statistically significant confidence parameters for two localities, i.e. for Bogács from the

upper ignimbrite level and for Sály from the lower level. At the other two localities of the lower level, i.e. at Kács and Kisgyőr, the paramagnetic contribution is higher than at Sály, as can be seen from the lower values of the mean susceptibility (Table II). The planar orientation of the paramagnetic minerals overprints the linear orientation of the ferromagnetic grains: the mean susceptibility ellipsoids are more flattened.

The linear-planar anisotropy pattern of both ignimbrite levels is similar to that of the sediments affected by weak horizontal stress [GRAHAM 1966]. In such cases the compression directions can be related to the direction of the intermediate axes. Fig. 7 shows the minimum and intermediate directions of the

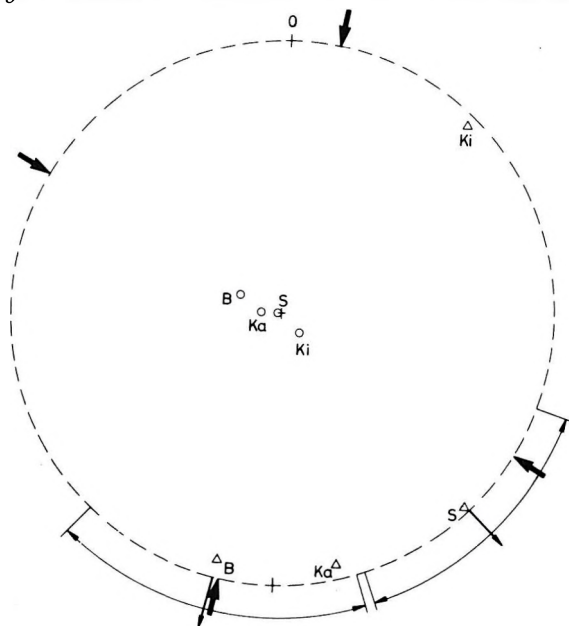


Fig. 7. Principal directions for the localities studied and their correlation with microtectonic results. Stereographic projection, lower hemisphere. Circles: minimum, triangles: intermediate directions; thin arrows: azimuthal direction of intermediate susceptibilities; arcs: confidence angles of respective intermediate directions; heavy arrows: compression directions from microtectonic measurements

7. ábra. A vizsgált mintavételi helyekre vonatkozó főirányok és korrelációjuk a mikrotektonikai eredményekkel. Sztereografikus vetület, alsó félgömb. Körök: minimum, háromszögek: közepes irányok; vékony nyilak: közepes szuszceptibilitások azimutális irányjai; ívek: a megfelelő közepes irányok konfidencia szögei; vastag nyilak: mikrotektonikai mérésekből származó nyomásirányok

Рис. 7. Главные направления по участкам отбора проб и их корреляция с результатами микротектоники. Стратиграфическая проекция, нижняя полусфера.

Минимальные (круги), средние (треугольники) направления; тонкие стрелки: азимутальные направления средних восприимчивостей; дуги: доверительные углы соответствующих средних направлений; утолщенные стрелки: направления сжатий, определенные микротектоническими измерениями.

mean anisotropy tensor for the studied localities. For Bogács and Sály the horizontal projections of the confidence angles of the intermediate directions (E12, arcs) are also indicated. As these do not overlap, two horizontal compression directions can be identified, i.e. 11° – 191° for Bogács (upper ignimbrite level) and 135° – 315° for Sály (lower ignimbrite level).

Microtectonic measurements in different Miocene rocks of the Bükkalja area [BERGERAT and CSONTOS 1988; TARI 1988] have indicated compression directions of 10° – 190° and 120° – 300° at Sály and Kisgyőr, and of 10° – 190° at Bogács (Fig. 7, heavy arrows), and it can be concluded that the anisotropy derived compression data are in good agreement with these.

Acknowledgements

This work was partially supported by the National Scientific Research Fund of Hungary in the framework of the „Investigation of the lithosphere and the asthenosphere“ project. The author is most grateful to E. Márton for encouragement and her advices and criticism of the manuscript. P. Márton and A. Nagymarosi are thanked for reviewing and critical comments.

REFERENCES

- BALOGH K. and RÓNAI GY. 1965: Commentary to the geological map series (at a scale of 1:200,000) of Hungary (in Hungarian). L-34-III. Eger. Magyar Állami Földtani Intézet, 173 p.
- BERGERAT F. and CSONTOS L. 1988: Neotectonic stress field measurements in northern Hungary. (in prep.)
- GRAHAM J. W. 1966: Significance of magnetic anisotropy in Appalachian sedimentary rocks. In Steinhart J. S. and Smith T. J. (eds): The Earth beneath the continents. Geophys. Monogr. 10, pp. 627–648
- HÁMOR G., RAVASZ-BARANYAI L., BALOGH K. and ÁRVA-SÓS E. 1979: K/Ar dating of Miocene piroclastic rocks in Hungary. Ann. Géol. Pays Hellén. (Hors sér.), 2, pp. 491–500
- HIRT A. M., LOWRIE W., CLENDENEN W. S. and KLIGFIELD R. 1988: The correlation of magnetic anisotropy with strain in the Chelmsford Formation of the Sudbury Basin, Ontario. Tectonophysics 145, pp. 177–189
- HROUDA F. 1979: The strain interpretation of magnetic anisotropy in rocks of the Nízky Jeseník Mountains (Czechoslovakia). Užitá geofyzika, Sborník geologických ved 16, pp. 27–62
- HROUDA F. 1982: Magnetic anisotropy of rocks and its application in geology and geophysics. Geophysical Surveys 5, pp. 37–82
- JELÍNEK V. 1977: The statistical theory of measuring anisotropy of magnetic susceptibility of rocks and its application. Geofyzika Brno. 88 p.
- JELÍNEK V. 1978: Statistical processing of magnetic susceptibility measured on group of specimens. Stud. Geophys. Geod., 22, pp. 50–62
- RATHORE J. S. 1985: Some magnetic fabric characteristics of sheared zones. J. Geodyn., 2, pp. 291–301
- ROCHETTE P. 1988: La susceptibilité anisotrope des roches faiblement magnétiques origines et applications. PhD Thesis, University of Grenoble. 211 p.
- TARI G. 1988: Strike-slip origin of the Vatta–Maklar trough, Northeastern Hungary. Acta Geologica Hungarica 31, 1–2, pp. 101–109

**MÁGNESES SZUSZCEPTIBILITÁS ANIZOTRÓPIA MÉRÉSEK BÜKKALJAI MIOCÉN
IGNIMBRITEKEN**

BORDÁS Róbert

A tanulmány a Bükkalja 4 mintavételi helyéről származó miocén ignimbrit mintákon végzett szuszceptibilitás anizotrópia mérések eredményeit mutatja be. Arra a következtetésre jut, hogy a kőzetek mágneses szövetére hatással volt a miocén vagy annál fiatalabb feszültségter. A közepes szuszceptibilitás tengelyek alapján két nyomásirány ismerhető fel: Bogácsra (felső ignimbrit szint) 11° – 191° , Sályra pedig (alsó ignimbrit szint) 135° – 315° . Ezek a meghatározások megegyeznek a mikrotektonikai mérésekkel felismert nyomásirányokkal.

**ИЗМЕРЕНИЯ АНИЗОТРОПИИ МАГНИТНОЙ ВОСПРИИМЧИВОСТИ
МИОЦЕНОВЫХ ИГНИМБРИТОВ В БЮККАЛЯ.**

Роберт БОРДАШ

Приводятся результаты измерений анизотропии восприимчивости, проведенные на образцах миоценовых игнимбритов, отобранных на 4-х участках Бюккаля. Делается вывод, что на магнитную структуру пород оказывало влияние поле напряжения миоценового или более молодого возраста. По осям средней восприимчивости определяется два направления давления: в Богач (верхний игнимбритовый горизонт) — 11° – 191° ; в Шай (нижний игнимбритовый горизонт) — 13° – 135° . Приведенные результаты совпадают с направлениями сжатия, установленными микротектоническими измерениями.

THE PROPAGATION OF CHANNEL WAVES IN A COAL SEAM WITH HORIZONTAL AND VERTICAL INHOMOGENEITIES

V. N. DANILOV*, M. DOBRÓKA** and V. SZ. YAMSHIKOV*

The complex dispersion relation and the amplitude functions were derived for Love seam waves propagating in an inhomogeneous waveguide. To describe the inelastic behaviour of the medium, the constant Q -model method is used. The density and the complex shear modulus of the coal are assumed to be weakly dependent on the vertical and horizontal coordinates, so the WKB method can be used. Numerical solutions for the absorption–dispersion equation are given to demonstrate the influence of horizontal and vertical inhomogeneities on the channel wave propagation properties.

Keywords: in-mine seismics, coal seams, Love waves, channel waves, wave dispersion, wave absorption, shear modulus, waveguide, WKB solution

1. Introduction

In the analysis of channel wave propagation properties the simple three-layered geological model is often used because the most important features of seam waves can easily be discussed by means of this model and the results can be extended to more complicated structures in a straightforward way. The absorption–dispersion characteristics of Love seam waves in a symmetric horizontally layered (layer-wise homogeneous) dissipative structure has been discussed by KREY et al. [1982]. DOBRÓKA and ORMOS [1983] analyzed the influence of the asymmetry of the three-layered structure on the propagation characteristics of Love-type seam waves. Using the finite difference method, synthetic seismograms for channel waves were given by BODOKY et al. [1982]. The displacement field of Love seam waves was analytically derived by BUCHANAN [1978] for a symmetric three-layered model. The results were extended to an asymmetrical model by YAMSHIKOV et al. [1986]. The effect of weak horizontal inhomogeneities on channel wave propagation was first discussed by DOBRÓKA [1987] while the problem of weak vertical inhomogeneities was first analyzed by DANILOV et al. [1987]. In this paper, assuming weak variations in the material characteristics of the coal seam along both horizontal and vertical directions, we give analytical solutions to the equation of motion, and derive the complex dispersion relation for Love seam waves that propagate in a three-layered weakly inhomogeneous waveguide.

* Moscow Mining Institute, Dept. Physical–Technical Control of Extraction, Moscow, Lenin prosp. 6

** Technical University for Heavy Industry, Dept. of Geophysics, Miskolc Egyetemváros, H–3515, Hungary

Symbols used in the paper

\vec{s}	displacement vector
u	displacement component
ϱ	density
μ	shear modulus
ω	angular frequency
$v = u\sqrt{\mu}$	transformed displacement variable
β	shear velocity
Q	quality factor
$\varepsilon = \frac{1}{Q}$	
N	body wave refractive index
n	channel wave refractive index
k_0	constant with the dimension of wavenumbers
$k = k_0 n$	channel wave wavenumber
$v_p = \frac{\omega}{\operatorname{Re}\{k\}}$	phase velocity
$v_g = \frac{\omega}{\partial(\operatorname{Re}\{k\})/\partial\omega}$	group velocity
$a = \operatorname{Im}\{k\}$	absorption coefficient
$H = 2d$	the seam thickness
b, c, A_0, B_0, A_1, B_1 X_0, X_2, Z_1, Z_2	} constants introduced for the calculations
α	

2. Analytical solutions

In weakly inhomogeneous media one can, to a good approximation, neglect coupling between transverse and longitudinal waves. This offers the possibility of discussing Love seam waves — as horizontally polarized shear waves — separately. If we restrict ourselves to the more simplified problem of the horizontal inhomogeneities occurring only along a specific direction (say x_1) and discuss wave propagation parallel with x_1 , then for Love seam waves the displacement vector can be taken as $\vec{s} = (0, u, 0)$. If we assume $e^{i\omega t}$ to be a separated time factor, the equation of motion takes the form

$$\rho\omega^2u + \mu\Delta u + \text{grad } \mu \text{ grad } u = 0$$

where $\rho(x_1, x_3)$ is the bulk density, $\mu(x_1, x_3)$ is the complex shear modulus. In the framework of the constant Q model $\mu = \mu^* (1 + i\varepsilon)$ and $\varepsilon(x_1, x_3) = 1/Q(x_1, x_3)$, $\mu^*(x_1, x_3)$ being the real shear modulus, Q being the frequency independent quality factor.

Introducing the $v = u\sqrt{\mu}$ variable the equation of motion gives

$$\Delta v + k_0^2 N^2 v + \left[\frac{1}{4} \left(\frac{1}{\mu} \text{grad } \mu \right)^2 - \frac{1}{2\mu} \Delta \mu \right] v = 0$$

where the notations $k_0 = \omega/\beta_0$ (β_0 is a constant phase velocity) and $N = \beta/\beta_0$ has been used with $\beta = \sqrt{\mu/\rho}$ (complex shear velocity). In weakly inhomogeneous media, as a good approximation, we can write

$$\left| \frac{1}{4} \frac{1}{\mu} (\text{grad } \mu)^2 - \frac{1}{2\mu} \Delta \mu \right| \ll k_0^2 |N|^2$$

so our equation for the $v = u\sqrt{\mu}$ variable takes the form

$$\Delta v + k_0^2 N^2 v = 0. \tag{1}$$

The quantity $N = N(x_1, x_3)$ can be considered as a complex-body-wave refractive index with different N_j values for the layers ($j=0, 1, 2$) (Fig. 1).

For Love channel waves the solution of Eq. (1) can be separated as

$$v(x_1, x_3) = \tilde{v}(x_3, N(x_1, x_3)) v^*(x_1) \tag{2}$$

where \tilde{v} is the x_3 dependent amplitude (with x_1 dependence only in $N(x_1, x_3)$) and v^* the function describing the wave propagation along the x_1 axis. Inserting the form (2) into Eq. (1) we get

$$\frac{1}{\tilde{v}} \left(\frac{\partial^2 \tilde{v}}{\partial x_3^2} + k_0^2 N \tilde{v} \right) + \frac{1}{v^*} \frac{\partial^2 v^*}{\partial x_1^2} = 0.$$

The last term of the equation doesn't contain quantities dependent on x_3 , so introducing the separation function (to be determined later) $-k_0 n^2$ ($k_0 H$, $N_0(x_1, x_3=0)$, $N_0(x_1, x_3=-H)$, N_1 , N_2) we can write the separated equations

$$\frac{\partial^2 v^*}{\partial x_1^2} + k_0^2 n^2 v^* = 0 \tag{3}$$

$$\frac{\partial^2 \tilde{v}}{\partial x_3^2} + k_0^2 (N^2 - n^2) \tilde{v} = 0. \tag{4}$$

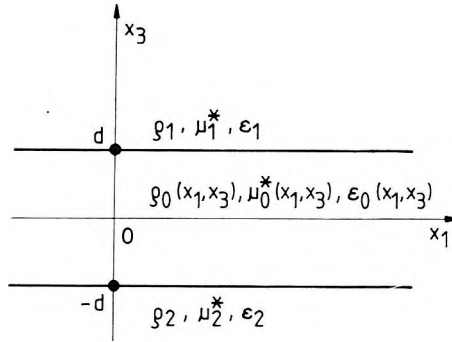


Fig. 1. The geometry of the three-layered inhomogeneous waveguide. ρ_j -s are the densities, μ_j^* -s are real shear moduli, $\epsilon_j = 1/Q_j$, where Q_j -s are quality factors ($j=0, 1, 2$ with $j=0$ for the coal seam)

1. ábra. A háromrétegű inhomogén hullámvezető geometriája. ρ_j a sűrűséget, μ_j^* a valódi nyírási modulust jelöli, $\epsilon_j = 1/Q_j$, ahol Q_j a minőségi faktor ($j=0, 1, 2, j=0$ a széntelepét jelöli)

Рис. 1. Геометрия трехслойного неоднородного волновода. Через ρ_j — обозначена плотность, через μ_j^* — истинный модуль скалывания; $\epsilon_j = 1/Q_j$, где Q_j — фактор качества ($j=0, 1, 2$; через $j=0$ обозначен угольный пласт).

In a second order WKB approximation the solution of Eq. (3) can be written as

$$v^* \sim \frac{1}{\sqrt{n}} e^{ik_0 \int_0^x n dx} \quad (5)$$

if the condition

$$\left| \frac{1}{k_0 n^2} \frac{\partial n}{\partial x_1} \right| \ll 1 \quad (6)$$

is valid [BUDDEN 1966]. Similarly, in the same approximation the solution of Eq. (4) takes the form

$$\tilde{v} \sim \frac{1}{4\sqrt{N^2 - n^2}} \left(A e^{ik_0 \int_0^z \sqrt{N^2 - n^2} dz} + B e^{-ik_0 \int_0^z \sqrt{N^2 - n^2} dz} \right) \quad (7)$$

if the condition

$$\left| \frac{1}{k_0(N^2 - n^2)} \frac{\partial \sqrt{N^2 - n^2}}{\partial x_3} \right| \ll 1 \quad (8)$$

is met. As vertical inhomogeneities were assumed only in the coal seam, the solution of the wave equation in the upper and lower half spaces is the same

as those derived for horizontally inhomogeneous wave guides [DOBROKA 1987]. So the displacement functions (regular at $x_3 \rightarrow \pm \infty$) can be written as

$$\begin{aligned}
 u_1 &= \frac{1}{\sqrt{\mu_1 n}} A_1 e^{ik_0 m_1 x_3} e^{ik_0 \int_0^{x_3} n dx} & x_3 > 0 \\
 u_0 &= \frac{1}{\sqrt{\mu_0 n m_0}} \left(A_0 e^{ik_0 \int_0^{x_3} m_0 dz} + B_0 e^{-ik_0 \int_0^{x_3} m_0 dz} \right) e^{ik_0 \int_0^{x_3} n dx} & -H < x_3 < 0 \\
 u_2 &= \frac{1}{\sqrt{\mu_2 n}} B_2 e^{-ik_0 m_2 x_3} e^{ik_0 \int_0^{x_3} n dx}
 \end{aligned}$$

where $m_j = \sqrt{N_j^2 - n^2}$ and the quantities, A_1, A_0, B_0, B_2 can be determined by means of the boundary conditions.

At the rock-coal interfaces ($x_3 = 0$ and $x_3 = -H$), the displacements as well as the σ_{32} stresses must be continuous. This gives the set of homogeneous linear equations

$$\begin{aligned}
 cA_1 &= A_0 + B_0 \\
 bB_2 \frac{1}{X_2} &= A_0 X_0 + B_0 \frac{1}{X_0} \\
 cZ_1 A_1 &= A_0 - B_0 \\
 -bZ_2 B_2 \frac{1}{X_2} &= A_0 X_0 - B_0 \frac{1}{X_0}
 \end{aligned} \tag{9}$$

where the notation

$$\begin{aligned}
 X_0 &= e^{ik_0 \int_0^H m_0 dz}, & X_2 &= e^{ik_0 H \sqrt{N_2^2 - n^2}} \\
 Z_1 &= \frac{\mu_1}{\mu_0(x_3=0)} \sqrt{\frac{N_1^2 - n^2}{N_0^2(x_3=0) - n^2}}, & Z_2 &= \frac{\mu_2}{\mu_0(x_3=-H)} \sqrt{\frac{N_2^2 - n^2}{N_0^2(x_3=-H) - n^2}} \\
 c &= \sqrt{\frac{\mu_0(x_3=0) m_0(x_3=0)}{\mu_1}}, & b &= \sqrt{\frac{\mu_0(x_3=-H) m_0(x_3=-H)}{\mu_2}}
 \end{aligned}$$

has been used. In order to have non-trivial solutions, the determinant of the set of equations (9) must vanish. This gives the complex dispersion relation for Love seam waves propagating in our three-layered inhomogeneous model

$$e^{2ik_0 \int_0^H \sqrt{N_0^2 - n^2} dz} = \frac{1 - Z_1}{1 + Z_1} \frac{1 - Z_2}{1 + Z_2} \tag{10}$$

Using this result, the amplitude functions take the form

$$u(x_1, x_3) = 2A_0 e^{ik_0 \int_0^{x_1} n dx} \begin{cases} \frac{1}{c(1+Z_1)} e^{ik_0 x_3 \sqrt{N_1^2 - n^2}} & \text{if } x_3 > 0 \\ \frac{1}{2} \left(e^{ik_0 \int_0^{x_3} \sqrt{N_0^2 - n^2} dz} + \frac{1-Z_1}{1+Z_1} e^{-ik_0 \int_0^{x_3} \sqrt{N_0^2 - n^2} dz} \right) & \text{if } -H \leq x_3 \leq 0 \\ \frac{X_0 X_2}{b(1-Z_2)} e^{-ik_0(x_3+H) \sqrt{N_2^2 - n^2}} & \text{if } x_3 < -H \end{cases}$$

3. Numerical results

In order to analyze the absorption–dispersion properties of the Love seam wave propagating in a vertically inhomogeneous channel, Eq. (10) should be solved numerically. Let us define a parabolic inhomogeneity as

$$\begin{aligned} \rho_0 &= 1300 [1 + \alpha x_3^2] \text{ (kg/m}^3\text{)}, \\ \beta_0 &= 1000 [1 + \alpha x_3^2] \text{ (m/s)}, \\ \varepsilon_0 &= 0.03/[1 + \alpha x_3^2] \end{aligned} \tag{11}$$

with $\alpha = 0.01$ and use the parameters in our numerical solution $\rho_1 = \rho_2 = 2000 \text{ kg/m}^3$, $\beta_1 = \beta_2 = 2000 \text{ m/s}$, $\varepsilon_1 = \varepsilon_2 = 0$ for the roof and floor. Function (10) results in a change of the waveguide parameters of the order of 4%. By means of Eq. (10), the complex dispersion relation, the phase and group velocities and the absorption coefficient, a (Fig. 2), can be determined. For comparison, the results computed for homogeneous models defined by the above functions at $x_3 = 0$ (model 1) and $x_3 = H$ (model 3) are also shown. It can be seen that the phase and group velocities as well as the absorption coefficient for the Love seam wave that propagates in a vertically inhomogeneous channel, are between those computed for models 1 and 2. It is shown by the figure that the inhomogeneity of the seam dominates at high (above the Airy-) frequencies. This is proved also by Fig. 3, where the derivative $d \log v / d \log \alpha$ is plotted as a function of the frequency.

In order to demonstrate the effect of the horizontal inhomogeneities on the wave propagation properties, we define the α quantity as

$$\alpha = 0.01 e^{-\left(\frac{x_1}{10H}\right)^2} \tag{12}$$

Using Eqs. (11) with Eq. (12) we can solve the complex dispersion equation numerically. The result found at $f \cdot d = 300 \text{ Hzm}$ is shown in Fig. 4. For the sake of comparability, the change in the phase and group velocities as well as that in the absorption coefficient (relative to the ones at $x_1 = 0$) are plotted as a function of the relative coordinate x_1/H .

4. Conclusions

Results proved that the WKBJ method can be employed to determine the amplitude functions and the absorption–dispersion relationship for Love seam waves propagating in a weakly (both vertically and horizontally) inhomogeneous waveguide. The numerical analysis of the dispersion equation shows that the inhomogeneity of the seam is dominant near to or above the Airy-frequency.

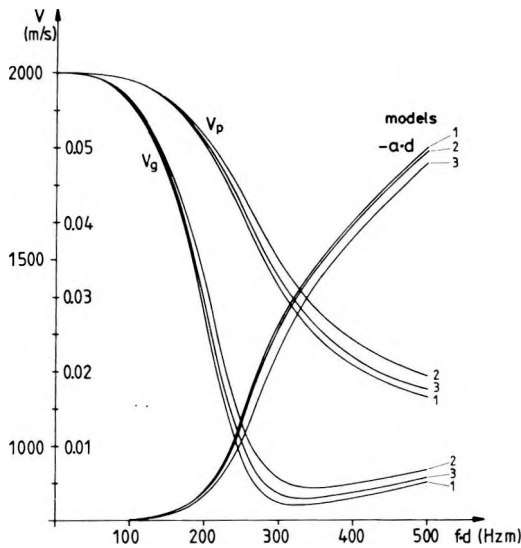


Fig. 2. Phase- and group velocities as well as dimensionless absorption coefficient ($a \cdot d$) of Love seam waves versus frequency times half thickness ($f \cdot d$). The parameters of the roof and floor layers are $\rho_1 = \rho_2 = 2000 \text{ kg/m}^3$, $\beta_1 = \beta_2 = 2000 \text{ m/s}$, $\epsilon_1 = \epsilon_2 = 0$ while for the coal seam they are computed by means of Eq. (11) with $x_3 = 0$ for model 1, $0 < x_3 < H$ for model 2 and $x_3 = H$ for model 3

2. ábra. A fázis (V_p) és csoportsebességek (V_g), valamint a Love típusú csatornahullámok dimenzió nélküli abszorpciós koefficiense ($a \cdot d$) a frekvencia és fél vastagság szorzata ($f \cdot d$) függvényében. A feké és fedő paraméterei $\rho_1 = \rho_2 = 2000 \text{ kg/m}^3$, $\beta_1 = \beta_2 = 2000 \text{ m/s}$, $\epsilon_1 = \epsilon_2 = 0$; míg a széntelepre a 11. egyenlettel kapjuk meg a paramétereket $x_3 = 0$ -val az 1. modellre, $0 < x_3 < H$ -val a 2. modellre és $x_3 = H$ -val a 3. modellre

Рис. 2. Скорости фазовые (V_p) и групповые (V_g), а также безразмерный абсорбиционный коэффициент ($a \cdot d$), каналных волн типа Лава как функция произведения частоты на полумощность ($f \cdot d$). Параметры перекрывающих и подстилающих образований: $\rho_1 = \rho_2 = 2000 \text{ кг/м}^3$, $\beta_1 = \beta_2 = 2000 \text{ м/с}$, $\epsilon_1 = \epsilon_2 = 0$; в то же время параметры угольного пласта определяются по уравнению 11 при $x_3 = 0$ для модели 1, при $0 < x_3 < H$ для модели 2 и при $x_3 = H$ для модели 3.

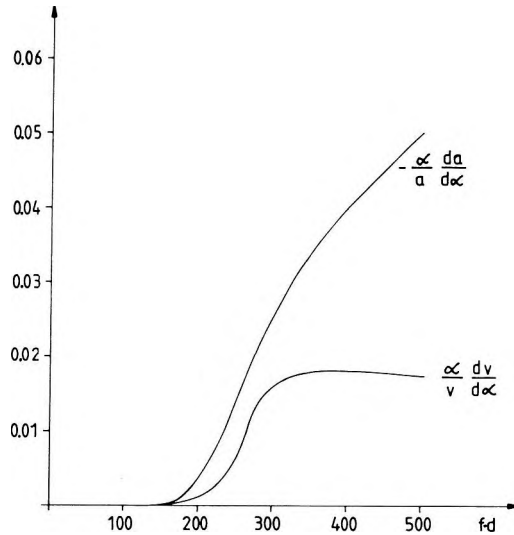
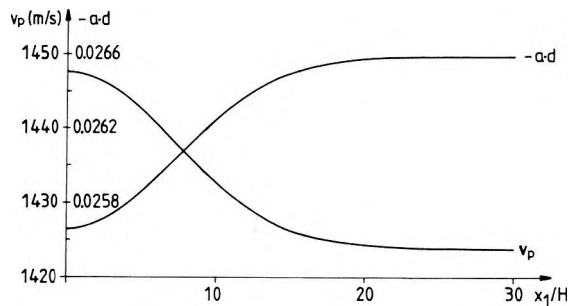


Fig. 3. The derivatives $d \log v / d \log \alpha$ and $d \log a / d \log \alpha$ — characterizing the sensitivity of the phase velocity and absorption coefficient with respect to weak vertical inhomogeneities — as a function of the frequency times half thickness

3. ábra. A $d \log v / d \log \alpha$ és $d \log a / d \log \alpha$ deriváltak a frekvencia és fél vastagság szorzatának függvényében. A deriváltak a fázissebesség és az abszorpciós koefficiens érzékenységét jellemzik a gyenge vertikális inhomogenitásokra

Рис. 3. Дифференциалы $d \log v / d \log \alpha$ и $d \log a / d \log \alpha$ функции произведений частот на полумощности. Дифференциалы характеризуют чувствительность фазовой скорости и абсорбционного коэффициента к слабым вертикальным неоднородностям.




REFERENCES


- BODOKY T., BODOKY A., 1982: Numerical modelling of seismic seam waves. Proc. 27th Int. Geophys. Symp. Bratislava, A(1), pp. 41–52
- BUCHANAN D. J. 1978: The propagation of attenuated SH channel waves. Geophysical Prospecting **26**, 1, pp. 16–28
- BUDDEN K. G. 1966: Radio waves in the ionosphere. Cambridge Univ. Press, pp. 130–136
- DANILOV V. N., VARTANOV A. Z. 1987: Some peculiarity of Love channel waves in a small, flaky coal seam. Izv. VUZ. Gornii Journal No. **7**, pp. 1–5
- DOBRÓKA M. and ORMOS T. 1983: Absorption–dispersion relations for Love channel waves. Geophysical Transactions **29**, 2, pp. 117–128
- DOBRÓKA M. 1987: Love seam waves in a horizontally inhomogeneous three-layered medium. Geophysical Prospecting **35**, 5, pp. 502–516
- KREY TH., ARNETZL H. and KNECHT M. 1982: Theoretical and practical aspects of absorption in the application of in-seam seismic coal exploration. Geophysics **47**, 12, pp. 1645–1656
- YAMSHIKOV V. S., DANILOV V. N., VARTANOV A. Z. 1986: Some properties of characteristics of the Love waves in multilayered structures. Izv. VUZ. Gornii Journal No. **4**, pp. 1–5


A CSATORNAHULLÁMOK TERJEDÉSE HORIZONTÁLISAN ÉS VERTIKÁLISAN INHOMOGÉN KŐSZÉNTÉLEPBE

V. N. DANILOV, M. DOBRÓKA és V. SZ. JAMSHIKOV

Komplex diszperzió- és amplitúdó összefüggéseket vezetnek le inhomogén hullámvezetőben terjedő Love telephullámokra. A közeg anelasztikus sajátosságainak leírására a konstans Q -modellt használták. A szén sűrűségét és komplex nyírási modulusát a vertikális és horizontális koordinátáktól gyengén függőnek tételezik fel, úgyhogy a WKBJ módszert lehet használni. Az abszorpció–diszperzió egyenletre numerikus megoldásokat adnak, amelyekkel szemléltetik a horizontális és vertikális inhomogenitások hatását a telephullám terjedésére.

 *Fig. 4.* Phase velocity as well as dimensionless absorption coefficient in a vertically and horizontally weakly inhomogeneous waveguide. The inhomogeneities are defined by means of Eqs. (11) and (12)

 *4. ábra.* A fázissebesség és a dimenzió nélküli abszorpciós koefficiens vertikálisan és horizontálisan gyengén inhomogén hullámcsatornában. Az inhomogenitásokat a (11) és (12) egyenlettel definiáltuk

 *Рис. 4.* Фазовые скорости и безразмерные абсорбционные коэффициенты в слабо неоднородном по горизонтали и вертикали волновом канале. Неоднородности определялись уравнениями (11) и (12).

РАСПРОСТРАНЕНИЕ КАНАЛЬНЫХ ВОЛН В НЕОДНОРОДНОМ ПО ГОРИЗОНТАЛИ И ВЕРТИКАЛИ УГОЛЬНОМ ПЛАСТЕ**В. Н. ДАНИЛОВ, М. ДОБРОКА И В. С. ЯМЩИКОВ**

Выведены комплексные уравнения дисперсий и амплитуд для пластовых волн Лава, распространяющихся в неоднородном волноводе. Неупругость среды описывались способом постоянной Q -модели. Плотность и комплексный модуль скалывания углей предполагаются слабо зависимыми от вертикальных и горизонтальных координат, так что имеется возможность пользоваться методом WKBJ. Для уравнения абсорбция—дисперсия даются численные решения, которыми иллюстрируется воздействие горизонтальных и вертикальных неоднородностей на распространение пластовой волны.

PARAMETER SENSITIVITY OF UNDERGROUND DC MEASUREMENTS

Ákos GYULAI*

Parameter sensitivities are useful for comparing underground dc techniques and for planning surveys. After defining the thickness (depth) sensitivity and the resistivity sensitivity, the parameter sensitivity functions for different deposit models (coal, bauxite) are presented then, based on these, some characteristic features of underground measurements.

Keywords: electric methods, resistivity, in-mine geophysics, direct current methods, parameter sensitivity

1. Introduction

Various in-mine geophysical, among them dc, methods have been developed to determine the rock and deposit parameters and the disturbances of deposits. Usually, reliable geological interpretation required by the mining industry can be achieved by the combined application of several methods. The efficient use of these methods is possible if the resolution of the individual methods is known and utilized. Selection of the methods making up the optimum measurement set is harder and more complex than in surface geophysical surveys, because underground measurements are carried out in a whole space; in other words, the investigation can be directed downwards, upwards or laterally. A further drawback is that up till now we have far less empirical experience.

2. Determination of the layer parameters

Underground geoelectric measurements have several new possibilities. If one gets closer to the object to be investigated not only can geological deviations undetectable by the known surface methods be revealed but there are also novel possibilities for field generation and measurement. Using these possibilities the sensitivity of geoelectric surveys, thus their efficiency, can be increased by several orders of magnitude.

Underground measurements also offer the special possibility of measuring with vertical dipoles in drifts and boreholes. Soundings can be carried out at

* Technical University for Heavy Industry, Department of Geophysics, Miskolc–Egyetemváros, H-3515, Hungary

Manuscript received (revised version): 21 July, 1989

several levels below ground. A further underground method is the transillumination of the space between drifts, between a drift and a drillhole, and between drillholes.

One type of survey task is represented by investigating the seam itself by determining the seam thickness, seam disturbances and seam quality. Geoelectric seam-sounding and seam-transillumination methods can solve these tasks [CSÓKÁS 1974, CSÓKÁS et al. 1986, DOBRÓKA et al. 1987b, KIRÁLY-SZIGETI 1985].

Investigation of the layers over- and underlying the seam represents an other group of tasks. The geoelectrical methods used for these purposes can be summarized under drift-sounding and -profiling [GYULAI 1979, GYULAI 1985, SZABÓ-GÉRESI 1983].

To determine the layer parameters of a coal-bearing complex the above methods are combined [BREITZKE et al. 1987]. Several possibilities offer themselves for comparing different methods. One of the procedures is to compare the penetration depths [EGERSZEGI 1980]. Another way of comparison is to examine the sounding curves of various models. Let us choose this method first to compare seam-sounding, roof-sounding and floor-sounding. *Figure 1* shows sounding curves calculated for a five-layer model with different seam resistivities. (It is assumed that the thickness of the first layer, M_1 , can be considered infinite). It can be seen that for a vertical dipole (Fig. 1/c) the apparent resistivity values (ϱ_a) increase when the resistivity of the seam (ϱ_2) increases, and this effect is even more pronounced at larger separations. In roof- (Fig. 1/a) and floor-soundings (Fig. 1/b) a considerably smaller increase is experienced than in the previous case.

Changes caused by an increase in the seam resistivity can be better observed in *Fig. 2*, which shows the deviations from the quasi-four-layer model. Differences between the different electrode arrays can be seen as well. Seam-sounding (Fig. 2/c) is very sensitive to changes in seam resistivity. In the case of drift-soundings, that one is more sensitive to the changes in seam resistivity which is measured on the side of the host rock that has higher resistivity.

3. The parameter sensitivities

Different electrode arrays can most simply be compared if the measure of variations in apparent resistivity curves caused by the changes in layer parameters is examined. That array is considered to be the most favourable which exhibits the highest sensitivity.

The relation between apparent resistivity (ϱ_a) and parameter (M_i , ϱ_i) changes can be defined by the equations

$$\psi_i = \frac{\partial \varrho_a}{\partial M_i} \frac{M_i}{\varrho_a} = \frac{\partial(\ln \varrho_a)}{\partial(\ln M_i)} \quad (1)$$

and

$$\varphi_i = \frac{\partial \varrho_a}{\partial \varrho_i} \frac{\varrho_i}{\varrho_a} = \frac{\partial(\ln \varrho_a)}{\partial(\ln M_i)} \quad (2)$$

ψ_i and φ_i are the so-called thickness and resistivity sensitivities [DOBRÓKA et al. 1987a]. The sensitivities can be described by the following formulae as well:

$$\psi^* = \frac{\partial \varrho_a}{\partial M_i} \frac{1}{\varrho_a} = \frac{\partial(\ln \varrho_a)}{\partial M_i} \quad (3)$$

and

$$\varphi^* = \frac{\partial \varrho_a}{\partial \varrho_i} \frac{1}{\varrho_a} = \frac{\partial(\ln \varrho_a)}{\partial \varrho_i} \quad (4)$$

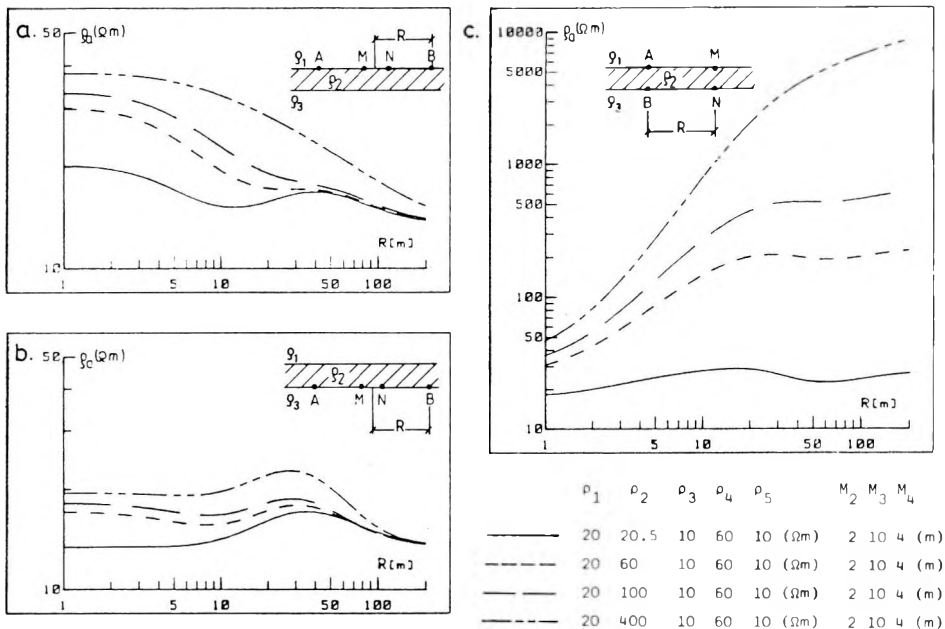


Fig. 1. Apparent resistivity (ϱ_a) curves for five-layer models. Basis for comparison: A quasi-four-layer ($\varrho_1 \sim \varrho_2$) model. Model parameters can be seen in the lower right corner, the electrode arrays are shown near the respective curve
 a) Roof-sounding; b) Floor-sounding; c) Seam-sounding

1. ábra. Látszólagos fajlagos ellenállás (ϱ_a) görbék ötréteges modellekre. Összehasonlítási alap: a négyrétegesnek tekinthető ($\varrho_1 \sim \varrho_2$) modell. A modell paraméterek a jobb alsó sarokban, az elektróda elrendezések a megfelelő szondázási görbék mellett láthatók
 a) Fedőszondázás; b) Feküszondázás; c) Telepszondázás

Рис. 1. Кривые кажущихся удельных сопротивлений (ϱ_a) для пятислойных моделей. Основа для сопоставлений: модель ($\varrho_1 \sim \varrho_2$), которая может рассматриваться в качестве четырехслойной. Параметры модели – в правом нижнем углу, при кривых зондирования, соответствующих установке.

a) Зондирование кровли; b) Зондирование почвы; c) Зондирование пласта

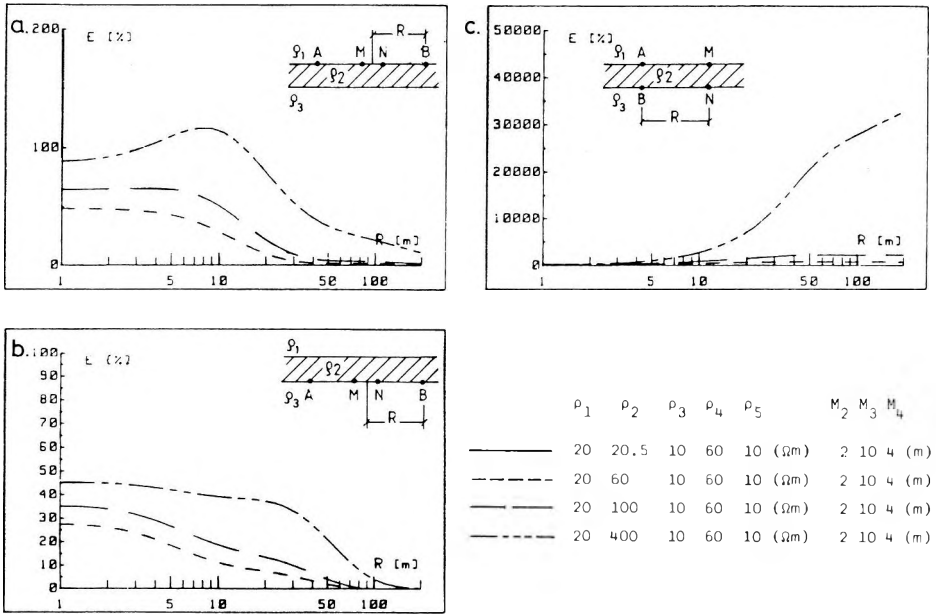


Fig. 2. Deviation (E) of the sounding curves shown in Fig. 1 from the quasi-four-layer curve which contains no coal seam

a) Roof-sounding; b) Floor-sounding; c) Seam-sounding

2. ábra. Az 1. ábrán látható szondázási görbék eltérése (E) a szénréteget nem tartalmazó, négyrétegesnek tekinthető görbétől

a) Fedőszondázás; b) Fekűszondázás; c) Telepszondázás

Рис. 2. Отклонение (E) кривой зондирования на рис. 1 от кривой разреза без угольного пласта, которая может рассматриваться в качестве четырехслойной.

a) Зондирование кровли; б) Зондирование почвы; в) Зондирование пласта

or by the quantities

$$m = \frac{\partial \lg Q_a}{\partial M_i} \tag{5}$$

$$n = \frac{\partial \lg Q_a}{\partial Q_i} \tag{6}$$

Figure 3 shows such curves. When sounding curves are interpreted they are compared in a $\lg Q_a - \lg AB/2$ system thus it is expedient to use the quantities defined by Eqs. (1)–(4) which contain logarithmic gradient. The use of formulae (1) and (2) is the most advantageous because these characterize the relation between the apparent resistivity function and the parameter changes in a dimensionless form. It should be noted that in inversion methods either relations (1) and (2) or (3) and (4) are used [KOEFOED 1979]. The information matrix which

is used to characterize the reliability of statistical interpretation [GOLC'MAN 1976, SALÁT et al. 1982] is derived from derivatives (1) and (2).

It can be seen in Fig. 3 that functions m , ψ^* and ψ change sign at small thickness. This is of interest to us for two reasons: on the one hand, there exists a critical thickness at every separation in the vicinity of which change in thickness does not manifest itself in apparent resistivities, on the other hand, at thicknesses smaller or larger than this a change in thickness may cause a change of opposite direction in apparent resistivity.

In addition it can be seen in the figure too that although the depth sensitivity changes, there exists a depth interval in which it can be considered constant. For example, for function ψ , $\bar{\psi}$ equals -0.46 between 12 and 33 m, where $\bar{\psi}$ and similarly $\bar{\psi}^*$ and \bar{m} , is the mean value of ψ in the given interval. It means that in this thickness (depth) interval a 0.46% decrease in apparent resistivity suggests a 1% increase in thickness.

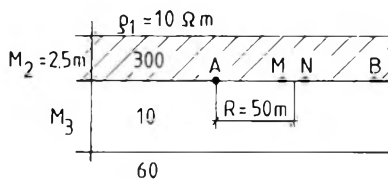
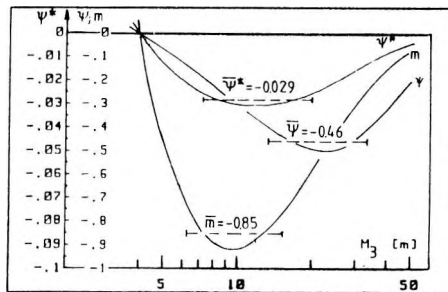


Fig. 3. Thickness sensitivity (ψ , ψ^* , m) curves of the model and electrode array shown in the figure as a function of the thickness of the layer underlying the coal seam (M_3)

3. ábra. Vastagság érzékenység (ψ , ψ^* , m) görbék az ábrán látható modellre és elektróda elrendezésre, a széntelep alatti fekvőréteg vastagságának (M_3) függvényében.

Рис. 3. Кривые чувствительности к мощности (ψ , ψ^* , m) для модели и установки, изображенных на рисунке, как функция мощности слоя (M_3), подстилающего угольный пласт.

Let us see, based on the sensitivities defined by (1) and (2), what kind of further statements can be made concerning the already mentioned model and soundings. In *Fig. 4* the sensitivity to the seam resistivity can be seen as a function of the seam resistivity (ρ_2) for different arrays. The low sensitivity of the floor-sounding can be observed: at a separation of 100 m and (ρ_2) = 300 Ωm ϕ_2 is less than 0.05. It means that a 10% increase in the seam resistivity causes a 0.5% increase in the apparent resistivity. The sensitivity of the roof-sounding is twice as high as the previous one. The ϕ_2 sensitivity of the seam-sounding is outstandingly high; in an optimum case ϕ_2 is 2. This feature of the measurement with vertical dipoles becomes apparent at large separations, but the sensitivity already reaches the favourable value of 1 at about $R=5$ m. It is important to note that the high resistivity sensitivity related to the layer situated between the vertical dipoles can be observed at low resistivity contrasts, too.

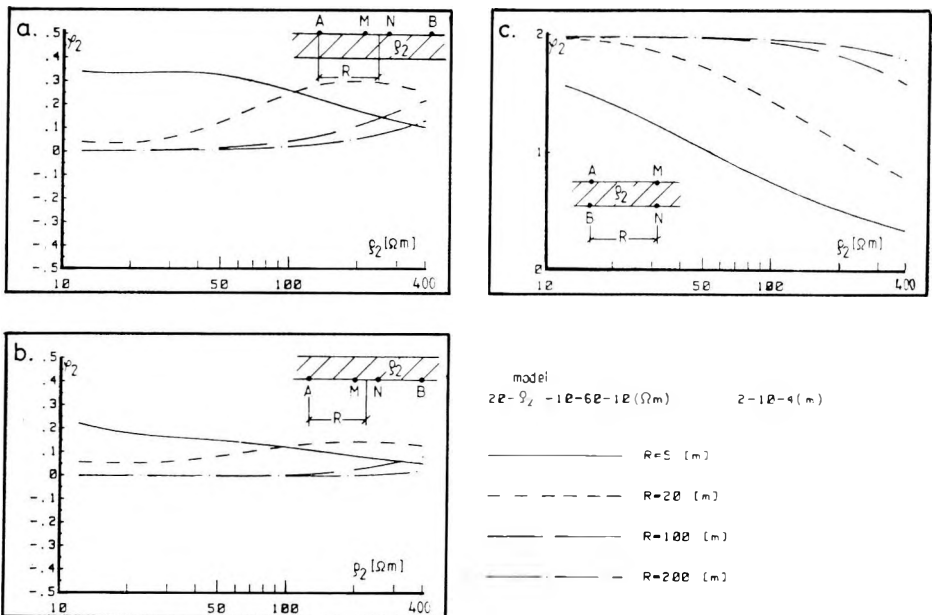


Fig. 4. Resistivity sensitivity (ϕ) curves at four separations as a function of coal seam resistivity (ρ_2)

a) Roof-sounding; b) Floor-sounding; c) Seam-sounding

4. ábra. Fajlagosellenállás érzékenység (ϕ) görbék négy különböző terítési távolságra, a széntelep ellenállásának (ρ_2) függvényében

a) Fedőszondázás; b) Feküszondázás; c) Telepszondázás

Рис. 4. Кривые чувствительности к сопротивлению (ϕ) для четырех различных разнесов, как функция мощности (M_2) угольного пласта.

а) Зондирование кровли; б) Зондирование почвы; в) Зондирование пласта

Figure 5 shows the seam thickness sensitivity (ψ_2). It is valid of the thickness sensitivity, too, that the sensitivity of the roof-sounding is twice as high as that of the floor-sounding. Thickness sensitivity can be calculated from the apparent resistivities of the vertical dipole measurement, too, but completely different results will be obtained. This kind of sensitivity is approximately the same as the resistivity. If the resistivity of the seam is high ($\rho_2 = 400 \Omega\text{m}$) the sensitivity approximates the value of 2 in thin seams and only at large separations. High thickness sensitivity means that the vertical dipole array can advantageously be applied to investigate the thickness variations of the seam between the electrodes.

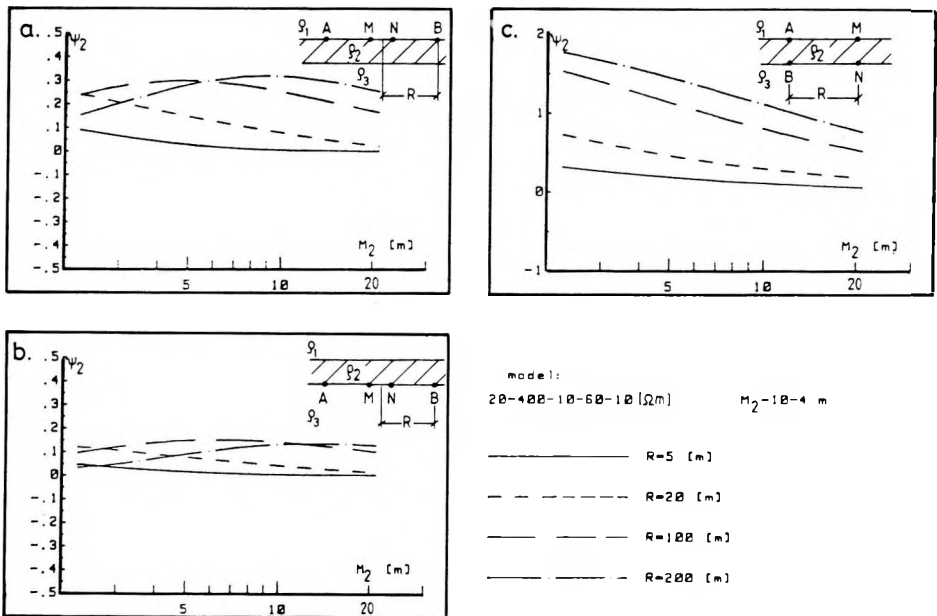


Fig. 5. Thickness sensitivity (ψ) curves at four separations as a function of coal seam thickness (M_2)

a) Roof-sounding; b) Floor-sounding; c) Seam-sounding

5. ábra. Vastagság érzékenység (ψ) görbék négy különböző terítési távolságra, a széntelep vastagságának (M_2) függvényében

a) Fedőszondázás; b) Fekűszondázás; c) Telepszondázás

Рис. 5. Кривые чувствительности к мощности (ψ) для четырех различных разносов, как функция мощности (M_2) угольного пласта.

a) Зондирование кровли; б) Зондирование почвы; в) Зондирование пласта

In Figs. 6. and 7. the resistivity sensitivities of the measurements performed in a bauxite deposit can be seen. The measurements are carried out somewhere within the deposit and the effect of the lower (floor side) and the upper part (roof side) of the deposit is examined. Fig. 6 shows the sensitivity to the floor side of the deposit, Fig. 7 that to the roof side. The sensitivity of the Schlumberger array at larger separations ($R = 50, 100$ m) hardly differs from zero in Fig. 6; this kind of measurement is insensitive to changes in the high resistivity floor side. In the case of deposit changes in the roof side φ_2 is greater than 0.5 at the same separations and it increases with the resistivity of this deposit part (contrary to the previous case). At shorter separations ($R = 10, 20$ m) the sensitivities are the same in both directions. It is noted that at larger separations the sensitivity of the vertical dipole array is ~ 1.5 , in addition, φ_3 is positive in the $R = 10 - 100$ m interval. Sensitivities related to the deposit part outside the vertical dipoles hardly differ from zero at shorter separations (10, 20 m) in Fig. 7; at larger separations (50, 100 m) the sensitivity increases though it is opposite in sign compared to the sensitivity related to the deposit part between the vertical dipoles.

It can be seen that the investigation can be directed downwards or upwards even if the complex is not cut in two parts by a high resistivity layer (e.g. coal seam). Further it can be stated, too, that the sensitivity related to the layer between the vertical dipoles is high in every case thus this array can favourably be applied not only to coal seam models (seam-sounding).

Figure 8. shows underlying layer thickness sensitivity functions for a coal seam model. This model corresponds to a case in which a water saturated sand layer ($\rho_4 = 60 \Omega\text{m}$) can be found in the underlying sequence and this is separated from the coal seam (ρ_2) by a low resistivity clay layer, the so-called protective layer.

Let us take a closer look at the behaviour of the sensitivity functions:

- for roof-sounding $\psi_3 \sim 0$, therefore this is unsuitable for investigating the protective layer,
- for floor-sounding at $R = 5$ m and $M_3 \sim 3$ m the sensitivity is favourable: $\psi_3 = -0.5$ but it rapidly decreases with increasing thickness of the protective layer; the optimum of the sensitivity function is at $M_3 = 8 - 10$ m for $R = 20$ m: $\psi_3 \sim 0.4$; the sensitivity has a critical point at $R = 50$ m, $M_3 = 10$ m ($\psi_3 \sim 0$) and the sensitivity changes sign; at $R = 100$ m, ψ_3 is positive for $M_3 = 2 - 20$ m, i.e. when the thickness of the low resistivity layer increases the apparent resistivity increases, too (contrary to our expectation),
- sensitivities of the seam-sounding fall between -0.2 and 0.2 , they are positive at $R = 50, 100$ m in the thickness interval under consideration.

The effect of variation in the deposit thickness for a bauxite model is shown in Figs. 9, 10 and 11. for different drift-sounding arrays. These curves were calculated for a dolomite basement having a resistivity of $2500 \Omega\text{m}$. It can already be seen in Fig. 9 that from the resistivity sounding curves of the model containing a 20 m or 30 m thick bauxite layer the largest deviation appears in the curves of the dipole-dipole array. The highest value of the deviation is 10%

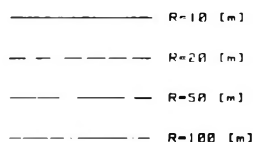
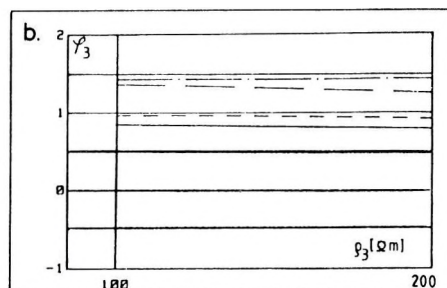
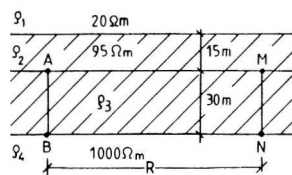
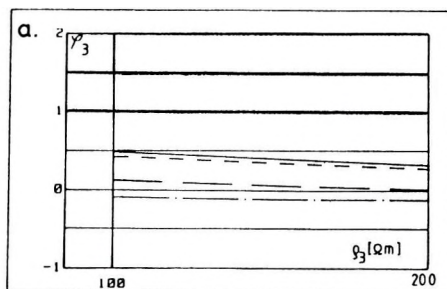
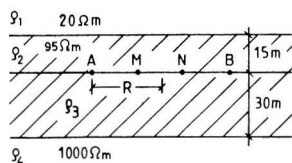
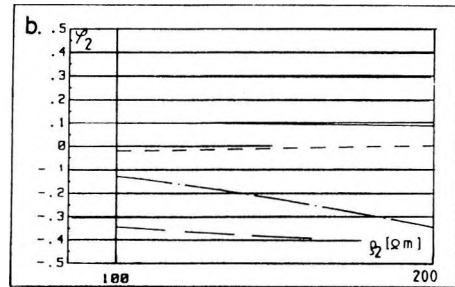
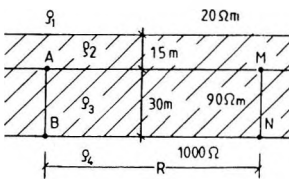
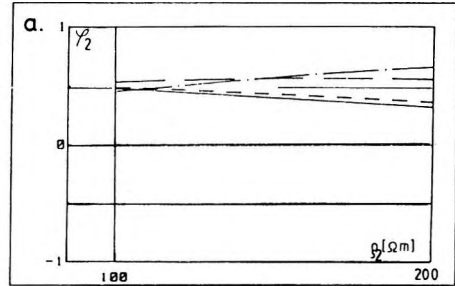
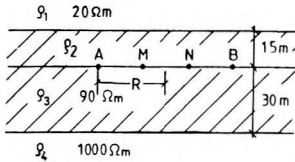


Fig. 6. Resistivity sensitivity (φ) curves of a bauxite deposit model, at four separations, as a function of the resistivity of the lower, floor-side 30 m thick part of the deposit
 a) Schlumberger sounding carried out in the roof-side part of the deposit, at the boundary between the constant and variable resistivity parts
 b) Sounding carried out with vertical dipoles spanning the 30 m thick, floor-side, variable resistivity part of the deposit

6. ábra. Fajlagosellenállás érzékenység (φ) görbék egy bauxittelep modellre, négy terítési távolságra, a telep alsó, fekü felőli, 30 m vastag része ellenállásának függvényében
 a) A telep fedő oldali részében, az állandó és változó ellenállású részt elválasztó felületen végzett Schlumberger-szondázás
 b) A telep fekü oldali, változó ellenállásúnak tekintett, 30 m vastag részét átfogó függőleges dipólokkal végzett szondázás

Рис. 6. Кривые чувствительности к сопротивлению (φ) для модели бокситовой залежи при четырех различных разносах, как функция сопротивления нижней, припочвенной части залежи мощностью 30 м.

- a) Зондирование установкой Шлюмберже, выполненное в прикровельной части залежи, на поверхности, разделяющей области постоянных и переменных сопротивлений.
 b) Зондирование вертикальными диполями, охватывающими припочвенную часть залежи мощностью 30 м, рассматриваемую как область переменных сопротивлений.



- R=10 (m)
- R=20 (m)
- · - · - R=50 (m)
- R=100 (m)

Fig. 7. Resistivity sensitivity (φ) curves of a bauxite deposit model, at four separations, as a function of the resistivity of the upper, roof-side, 15 m thick part of the deposit
 a) Schlumberger sounding carried out in the roof-side part of the deposit, at the boundary between the constant and variable resistivity parts
 b) Sounding carried out with vertical dipoles spanning the 30 m thick floor-side, 90 Ω m resistivity part of the deposit

7. ábra. Fajlagosellenállás érzékenység (φ) görbék egy bauxittelép modellre, négy terítési távolságra, a telep felső, fedő felőli, 15 m vastag része ellenállásának függvényében
 a) A telep fedő oldali részében, a változó és állandó ellenállású részt elválasztó felületen végzett Schlumberger-szondázás
 b) A telep fekü oldali, 90 Ω m fajlagosellenállásújának tekintett, 30 m vastag részét átfogó függőleges dipólokkal végzett szondázás

Рис. 7. Кривые чувствительности к сопротивлению (φ) для модели бокситовой залежи при четырех различных разносах, как функция сопротивления верхней, прикровельной части залежи мощностью 15 м.
 а) Зондирование установкой Шлюмберже, выполненное в прикровельной части залежи, на поверхности, разделяющей области постоянных и переменных сопротивлений.
 б) Зондирование вертикальными диполями, охватывающими припочвенную часть залежи мощностью 30 м, рассматриваемую как область с сопротивлением в 90 ом-м.

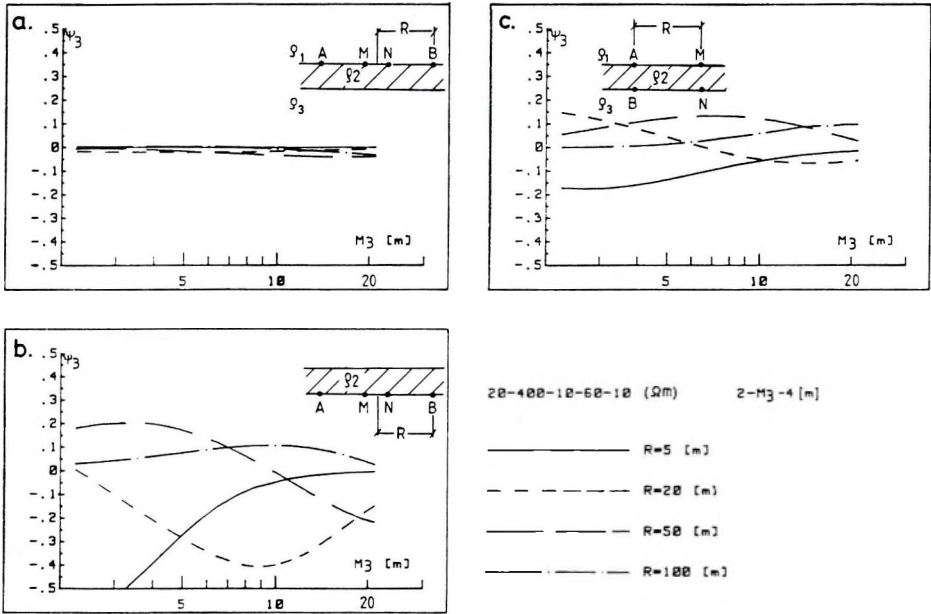


Fig. 8. Thickness sensitivity (ψ) curves of a model with a coal seam, at four separations, as a function of the thickness of the layer underlying the coal seam (M_3)
 a) Roof-sounding; b) Floor-sounding; c) Seam-sounding

8. ábra. Vastagság érzékenység (ψ) görbék egy széntelepessel, négy terítési távolságra, a széntelep alatti feküreg vastagságának (M_3) függvényében
 a) Fedőszondázás; b) Feküszondázás; c) Teleszondázás

Рис. 8. Кривые чувствительности к мощности (ψ) для модели угольного пласта при четырех различных разносах, как функция мощности (M_3) слоя, подстилающего угольный пласт.

a) Зондирование кровли; б) Зондирование почвы; в) Зондирование пласта

for the two-electrode array (AM), 15% for the Schlumberger array (AMNB) and 20% for the dipole-dipole array (ABNM) (Fig. 10). The various thickness sensitivities are shown in Fig. 11. The sensitivity is unfavourable for the Schlumberger array, at $R=100$ m in the depth interval of 15–25 m, $|\psi| \leq 0.05$ (Fig. 11/b). Such little values of sensitivity occur for other arrays as well (Figs. 11/a, 11/c).

Figure 12. shows sounding and sensitivity curves for different levels of measurement. Based on the apparent resistivity curves we would expect that the sensitivity conditions for detecting a high resistivity layer (basement) are most favourable if the level of measurement is as close to it as possible. (The effect of the high resistivity layer can unambiguously be seen in curve 4 only.) The sensitivity curves demonstrate that the sensitivity does not change observably by changing the level of measurement at $AB/2 = 5$ and 10 m. At $AB/2 = 20$ and 50 m, however, the sensitivities are different for each level.

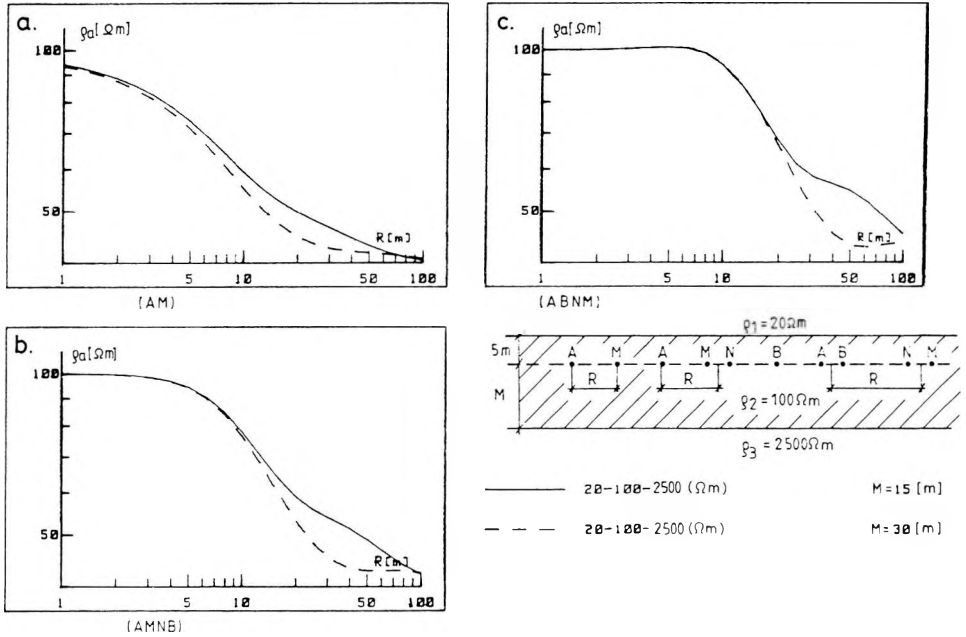


Fig. 9. Sounding curves for measurements carried out within a bauxite deposit, 5 m below the overlying layer. The high resistivity basement is 15 and 30 m below the level of measurements
a) Roof-sounding; b) Floor-sounding; c) Seam-sounding

9. ábra. Szondázási görbék a bauxitlepen belül, a fedőtől 5 m-re végzett mérésekre.

A nagyellenállású fekvő a mérés szintje alatt (M) 15, illetve 30 m-re van
a) Kételektrodás; b) Schlumberger; c) Dipól-dipól elrendezés

Рис. 9. Кривые зондирования для измерений, выполненных в пределах бокситовой залежи, на расстоянии 5 м от кровли. Высокоомная почва находится ниже уровня измерений (M) на 15 и 30 м.

a) Двухэлектродная установка; б) Установка Шлюмберже; в) Установка диполь-диполь

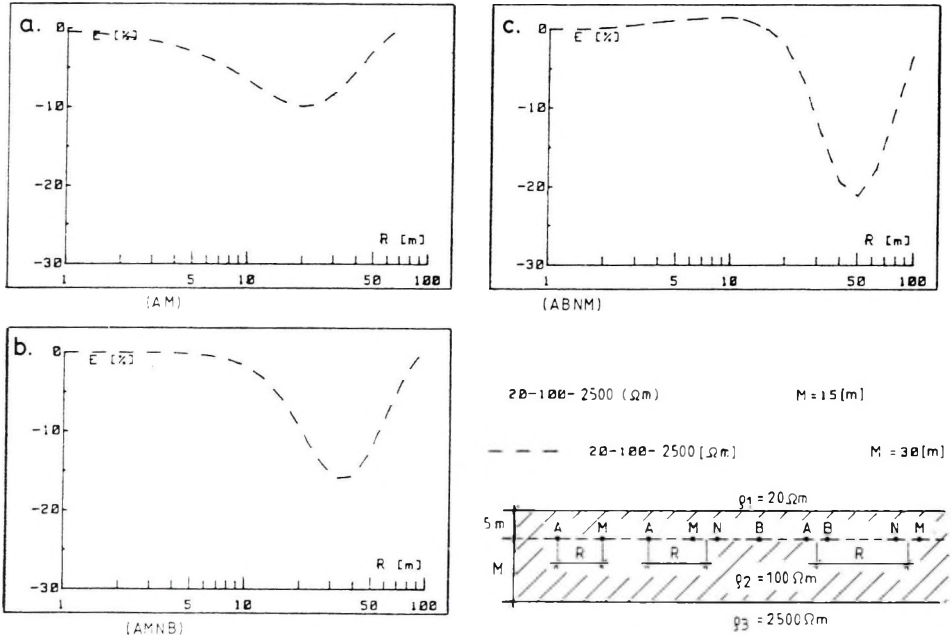


Fig. 10. Deviation (E) curves of the sounding curves shown in Fig. 9

a) Two-electrode; b) Schlumberger; c) Dipole-dipole array

10. ábra. A 9. ábrán látható szondázási görbék eltérés (E) görbéi

a) Kételektrodás-; b) Schlumberger-; c) Dipól-dipól elrendezés

Рис. 10. Кривые отклонений (E) кривых зондирования на рис. 9.

a) Двухэлектродная установка; б) Установка Шлюмберже; в) Установка диполь-диполь

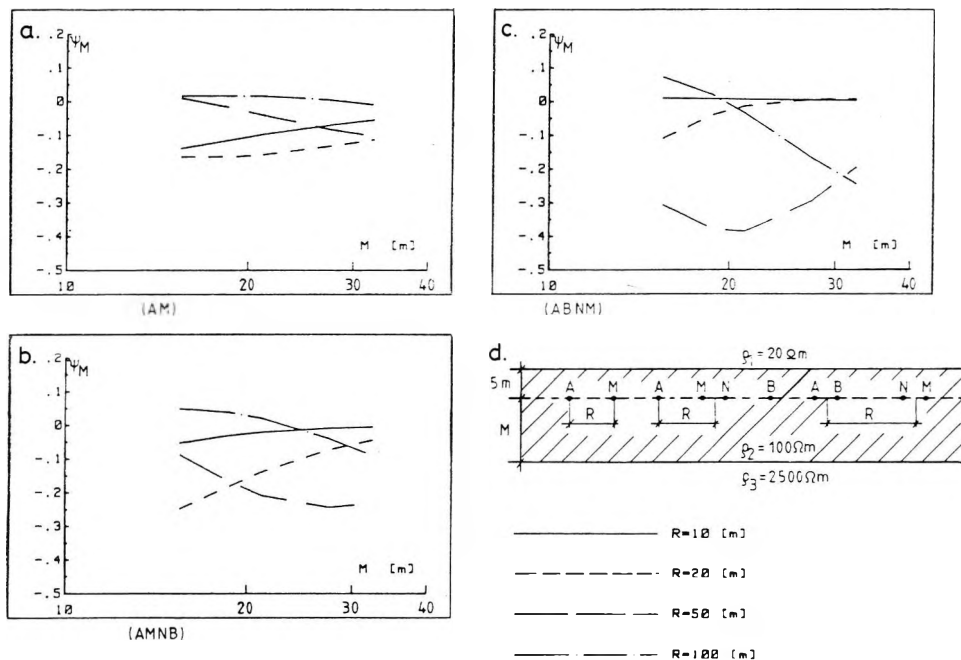


Fig. 11. Thickness sensitivity (ψ) curves obtained for the model shown in Fig. 9 as a function of separation between the measurement level and basement (M), for four electrode separations
 a) Two-electrode; b) Schlumberger; c) Dipole-dipole array

11. ábra. A 9. ábrán látható modell esetén kapott vastagság érzékenység (ψ) görbék a fektávolság (M) függvényében, négy terítési távolságra
 a) Kételektrodás; b) Schlumberger-; c) Dipól-dipól elrendezés

Рис. 11. Кривые чувствительности к мощности (ψ) для модели рис. 9 как функция расстояния до почвы (M) при четырех различных разносах.
 а) Двухэлектродная установка; б) Установка Шлюмберже; в) Установка диполь-диполь

In the sensitivity curves for $R=20$ m and 50 m we have marked those points which represent the thicknesses belonging to the respective levels. By connecting these points (dotted line) the curve showing the variation of sensitivities for different levels of measurement is obtained. It is mentioned that at $R=20$ m (and for a bauxite thickness of 15 m) the sensitivity is highest at the 2nd level and lowest at the 4th level.

4. Summary

In the planning of underground measurements the sensitivities are essential parameters. The basic concept of planning is that a measuring technique and separation should be utilized whose sensitivity is high in relation to the layer parameter to be studied and low in relation to the others. Based on the ex-

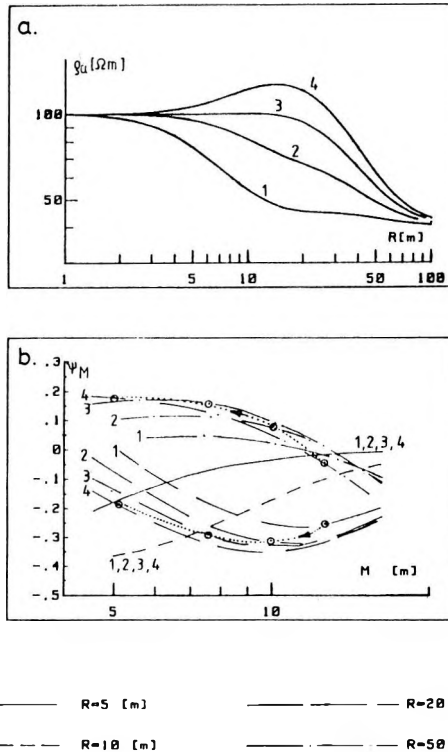


Fig. 12. Schlumberger soundings carried out at different levels above the high resistivity basement within a 15 m thick bauxite layer

a) Apparent resistivity (ρ_a) curves; b) Thickness sensitivity (ψ) curves at four separations; (numbers refer to levels of measurement, for other symbols see text)

12. ábra. 15 m vastag bauxitrétegben, a nagyellenállású aljzat felett különböző szinteken végzett Schlumberger-szondázások

a) Látszólagos fajlagos ellenállás (ρ_a) görbéi; b) Vastagság érzékenység (ψ) görbéi négy terítési távolságra (az ábrán a számok a szinteket jelölik, a többi jel magyarázatát lásd a szövegben)

Рис. 12. Зондирования установкой Шлюмберже в пределах бокситовой залежи на различных вертикальных расстояниях от высокоомной почвы.

a) Кривые кажущихся удельных сопротивлений (ρ_a).

b) Кривые чувствительности к мощности (ψ) для четырех различных разносов.

perience gained from the underground measurements carried out up to now it seems that measuring techniques with $\psi_i, \phi_i < 0.1$ are not worth applying.

In the interpretation of soundings, sensitivities belonging to several separations should be considered. Statistical interpretation methods [GOLC' MAN 1976, SALÁT et al. 1982] provide a possibility for that both in the period of planning and in the interpretation of field measurements. Such a study is currently being prepared.

REFERENCES

- BREITZKE M., DRESEN L., CSÓKÁS J., GYULAI Á., ORMOS T. 1987: Parameter estimation and fault detection by three-component seismic and geoelectrical surveys in a coal mine. *Geophysical Prospecting* **35**, 7, pp. 832–863
- CSÓKÁS J. 1974: Detection of tectonic disturbances associated with a coal bed by geoelectrical measurements in mine drifts. *Acta Geodaet., Geophys. et Montanist. Acad. Sci. Hung. Tomus* **9**, (1–2), pp. 111–119
- CSÓKÁS J., DOBRÓKA M., GYULAI Á. 1986: Geoelectric determination of quality changes and tectonic disturbances in coal deposits. *Geophysical Prospecting* **34**, 7, pp. 1067–1081
- DOBRÓKA M., GYULAI Á., TAKÁCS E. 1987a: Development of a mathematical physical model to determine the spatial position of coal seams (in Hungarian). Final research report, UHI, Department of Geophysics, Miskolc
- DOBRÓKA M., GYULAI Á., ORMOS T., TAKÁCS E. 1987b: Development of combined seismic-geoelectric in-mine geophysical methods (in Hungarian). Research report, UHI, Department of Geophysics, Miskolc
- EGERSZEGI P. 1980: Effect of the location of electrodes and of the use of two feeding circuits with geoelectric soundings (in Hungarian with English summary). *Magyar Geofizika* **XXI**, 5, pp. 185–192
- GOLC'MAN F. M. 1976: Komplexinterpretation bei der Lösung inverser geophysikalischer Aufgaben. *Gerlands Beitr. Geophysik, Leipzig*. **85**, 5, pp. 379–384
- GYULAI Á. 1979: Evaluation of mine roadway soundings in coal bed series (in Hungarian with English summary). *Magyar Geofizika* **XX**, 4, pp. 142–148
- GYULAI Á. 1985: Three dimensional geoelectric measurements in mines for the determination of the protective layer. *Annales, Universitates Scientiarum Budapestiensis de Rollando Eötvös Nominatae, Sectio Geophysica et Meteorologica, Tomus I–II*, pp. 167–181
- KIRÁLY E., SZIGETI G. 1985: New method for the exploration of solid mineral deposits of complex tectonics. *ELGI Annual Report 1985*, pp. 197–200
- KOEFOD O. 1979: Geosounding principles, I. Resistivity sounding measurements. Elsevier, Amsterdam–Oxford–New York, 276 p.
- SALÁT P., TARCSAI GY., CSEREPES L., VERMES M., DRAHOS D. 1982: Information statistical methods of geophysical interpretation (ed. P. Salát) Tankönyvkiadó, Budapest, 302 p.
- SZABÓ J., GÉRESI GY. 1983: Geoelectrical method for analysing rock mechanical events in mine-shafts. *Magyar Geofizika* **XXIV**, 4, pp. 141–147

FÖLDALATTI EGYENÁRAMÚ MÉRÉSEK PARAMÉTERÉRZÉKENYSÉGE

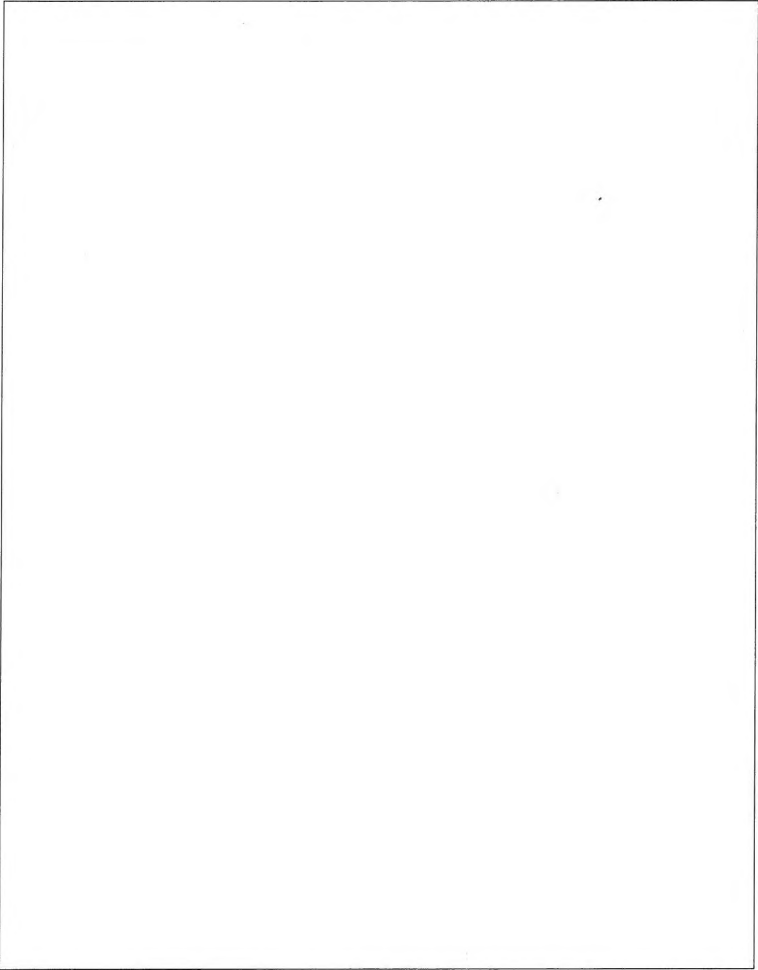
GYULAI Ákos

Földalatti egyenáramú mérési módszerek összehasonlításához, a kutatás megtervezéséhez célszerű az ún. paraméterérzékenységek bevezetése és alkalmazása. A mélység- (vastagság-) érzékenységek és a fajlagos ellenállás érzékenység definiálása után különböző telepes modellekre (szén, bauxit) számitott paraméterérzékenység függvényeket, majd ezek alapján a földalatti mérések néhány jellegzetességét mutatja be a dolgozat.

**ЧУВСТВИТЕЛЬНОСТЬ ПАРАМЕТРОВ ПЛАСТА ПРИ ЗОНДИРОВАНИЯХ
МЕТОДОМ ПОСТОЯННОГО ТОКА В ПОДЗЕМНЫХ УСЛОВИЯХ**

Акош ДЬЮЛАИ

Для сопоставления методов электроразведки постоянным током в подземных условиях, для планирования исследований необходимо введение и употребление понятия, так называемой, чувствительности параметров пласта. Наряду с определением чувствительности мощности (глубины) и удельного сопротивления приводятся зависимости чувствительности параметров пласта, рассчитанные на моделях различных залежей (угля, боксита), а также некоторые особенности зондирования в подземных условиях.



This page is waiting for you!